Interactions between titanium surfaces and biological components

PhD thesis Dissertation

Marta Pegueroles Neyra

Supervisors:
Professor Conrado José Aparicio Bádenas, PhD
Professor Francisco Javier Gil Mur, PhD

Departament de Ciència dels Materials i Enginyeria Metal.lúrgica
E.T.S. d'Enginyeria Industrial de Barcelona
Universitat Politècnica de Catalunya

July 2009

3. Kinetics and two-step competitive protein adsorption characterization on TiO$_2$ crystals using QCM-D

3.1. Introduction

The first event taking place at the implant-tissue interface is water molecules and salt ions interacting with the material surface. This aspect has been previously reported in Chapter 2. Wettability and surface energy characterization allowed gaining knowledge of the liquid/solid interaction of the studied system. Shortly after the formation of the hydration layer, blood proteins start to crowd the surface [1;2]. The adsorption of blood proteins influences cell behaviour. Then, when cells reach the implant site, they scan the protein layer covering the surface looking for activation factors to attach to. So, the protein adsorption plays a crucial role in the integration of an implant into the body. To this respect, the material properties have to elucidate appropriate responses for specific applications.

Understanding and eventually controlling the protein adsorption on the material used is essential to obtain a good integration of the implant. Proteins are a special, highly

complex, and important case of particles adsorbing at surfaces. Protein adsorption is a dynamic process involving non-covalent interactions such as hydrophobic interactions, electrostatic forces, hydrogen bonding and Van der Waals forces [3]. Moreover, protein parameters as well as surface properties such as surface energy, roughness and chemistry have been identified as key factors influencing the adsorption process [4-6]. Since the amount and structure of proteins at the interface as a function of time remains not well known, this chapter will be focused on the study of the protein adsorption on TiO₂ surfaces as a function of time.

Proteins interact on fundamental biochemical mechanisms of biological processes such as blood clotting and molecular recognition. There are several proteins in human blood plasma but, among them, fibrinogen, fibronectin and albumin have been chosen for our study. The three of them are well-known, thoroughly characterized, extensively described proteins. In addition, several studies have suggested that platelet adhesion and activation might be affected particularly by fibrinogen, a mediator of platelet activation via its direct interaction with the platelet receptors [7-9]. Fibronectin is a key component of the extracellular matrix (ECM), is a large dimeric glycoprotein triggering cell adhesion [10] and undergoes cell-driven assembly in supramolecular fibrils and furthermore provides specific binding sites for various ECM biopolymers [11]. Albumin is the most abundant component of many biofluids, serving as transport media for various metabolites and as regulator of osmotic pressure.

Different techniques have been used for protein adsorption characterization. They are mainly based on the labelling of the adsorbing molecules with a radioactive, fluorescent or other type of marker. But most of these techniques are laborious procedures with discrete and non-continuous values measurements. As said by Norde and Lylema, [12], since the proteins systems are so complex 'measurements with well-defined model systems carried out under well-controlled conditions' are essential to understand the underlying mechanisms. Following this criteria, this chapter has started by studying the simplest model, i.e., the study of a single protein system on a smooth TiO₂ surface to understand the essential adsorption mechanisms in real time. More complex systems with two proteins in solution, competing and interacting for adsorption on the TiO₂ surfaces, have been further analyzed.

Metal surfaces are, with few exceptions, covered by an oxide layer of a few to several nanometers thickness. As a consequence, interactions between metal implants, proteins and cells are governed by the physical-chemical properties of theirs corresponding metallic oxides. Titanium surfaces are mainly covered with the spontaneous formation of a TiO₂ layer. And so, TiO₂-covered sensor crystals have been used in the experiments of this chapter for their use in the quartz crystal microbalance with dissipation monitoring (QCM-D).

The use of QCM-D allows a reliable and sensitive real-time kinematics protein-adsorption study. QCM-D may be used to explore and analyze not only the amount of

protein adsorbed on the studied substrates but also the conformational changes of the proteins in play. These are significant parameters to understand the effect of the adsorbed protein layer on the biological performance of biocompatible surfaces. The adsorption kinetics on the studied surface and the conformational changes of the three working proteins -bovine serum albumin (BSA), fibrinogen (Fbg), and fibronectin (Fn)- was carried out with monoprotein solutions. The interaction, competition, displacement and/or co-adsorption of those proteins were also studied performing two-steps biprotein experiments.

The fact that significantly smooth surfaces have to be tested when using real time protein adsorption techniques, e.g, QCM-D, ellypsometry and optical waveguide lightmode spectroscopy (OWLS), is a known limitation of these characterization techniques. The effect of roughness on protein adsorption will be discussed on Chapter 4 carrying out experiments with traditional labelling techniques.

3.2. Objectives

The main objective of the present chapter is to evaluate and characterize protein adsorption processes on a titanium oxide surface using a quartz crystal microbalance with monitoring of dissipation (QCM-D). To do so, the following partial objectives where defined:

1. To characterize the morphology, chemistry, wettability and roughness of TiO$_2$-coated quartz crystals.

2. To determine the amount and rate of protein adsorbed on the tested surfaces for three different proteins with specific biological interest: fibronectin, albumin, and fibrinogen.

3. To study kinetics of adsorption and possible conformational changes of the three proteins (fibronectin, albumin, fibrinogen) on TiO$_2$ surfaces from monoprotein solutions.

4. To determine the interaction, competition, and displacement between the three relevant proteins by means of two-step biprotein adsorption experiments on TiO$_2$ surfaces.

3.3. Protein adsorption

Proteins are mainly in aqueous environments. Nevertheless, when a protein solution is in contact with another phase, proteins tend to accumulate spontaneously at interfacial regions, [13;14]. This occurrence can be an advantage or a disadvantage depending on the application of the biomaterial.

On one hand, for bone anchored implants, such as dental implants or artificial hip joints, the clinical goal is to obtain a long term secure anchoring of the implant. Achieving this function with the shortest possible healing-time is of relevance and can be favoured with a guided protein adsorption resulting in a beneficial induction of bone formation.

On the other side, the engineering of blood-compatible materials, e.g. artificial blood vessels or heart valves, has the main goal of suppressing blood coagulation on anti-fouling surfaces. Understanding and controlling the surface characteristics of these surfaces will also be crucial for controlling protein adsorption.

3.3.1.   Protein structure and functions

Proteins are essential parts of organisms and participate in many fundamental and essential processes within cells. Many functions are supported by proteins: (1) enzymatic catalysis of biochemical reactions that are vital to metabolism; (2) structural or mechanical support; forming the cytoskeleton or forming part of the extracellular matrix; (3) cell signaling; (4) immune responses; (5) cell adhesion and (6) cell cycle.

Proteins are large biological organic macromolecules built up from 20 different amino acids linked together by peptide bonds and forming highly organized polymers. Their molecular masses range from a few thousand to several hundred thousand kDa. All proteins considered in this study are water soluble and all adsorption studies have been performed in aqueous solutions.

Protein function depends on its third-dimensional arrangement, which in turn depends on its amino acid sequence. Each amino acid has the same fundamental structure (Figure 3-1 a), including an α carbon (C^α) to which an amino group, a carboxyl group, and a differing variable side chain are bonded.

The sequence of amino acids linked together by covalent bonds, also called peptide bonds, in the polypeptide chain determines the primary structure of a protein molecule. Two of the three bonds in the peptide unit are free to rotate (Figure 3-1 b). Amino acids are usually classified by the properties of the side chain -R group- into four groups. The side chain can provide the amino acid with different properties: acidity, basicity,

hydrophilicity if it is polar, and hydrophobicity if it is non-polar. The chemical structures of the 20 standard amino acids, along with their chemical properties, are catalogued [15].
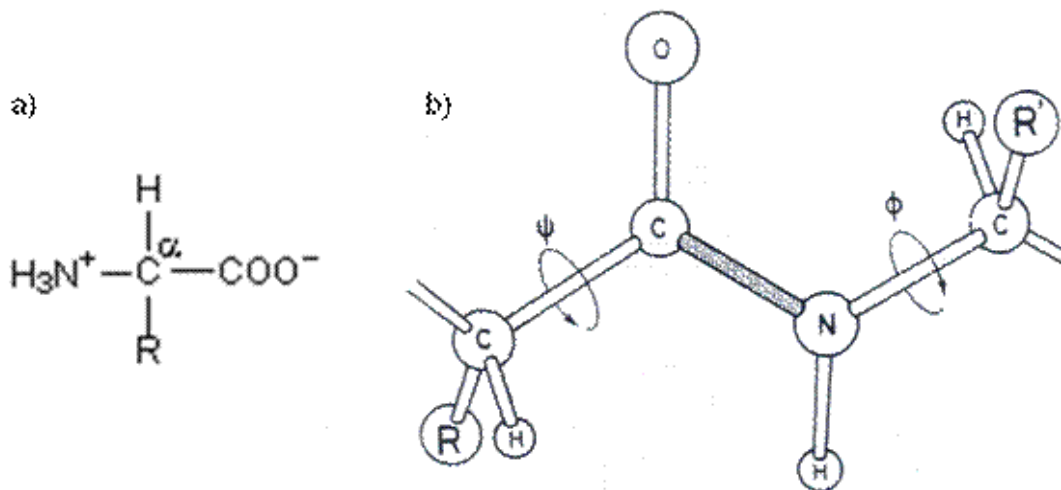

Figure 3-1 *a) Amino acid and b) Structure of a peptide unit in a polypeptide chain. Two of the three bonds are free to rotate, R and R' represent amino acid side-groups [14;16]*

The secondary structure refers to the folding of the polypeptide chain into periodic structure such as α-helix and β-sheet, this is a local structure stabilized by hydrogen bonds between amide and carboxyl groups.

The tertiary structure is referred to the way the folded segments of the polypeptide chain are arranged in space, [14], so the completed three dimensional folding of a protein. Stabilization of the tertiary structure of a protein may involve interactions between amino acids located far apart along the primary sequence. These may include:

- weak interactions such as hydrogen bonds and Van der Waals interactions

- ionic bonds involving negatively charged and positively charged amino acid side-chain groups

- disulfide bonds

Interactions with the aqueous solvent, known as the hydrophobic effect results in residues with non-polar side-chains, i.e. hydrophobic amino acid residues, typically in the interior of the molecule, [14]. Conversely, polar amino acid side-chains are predominantly found on the surface of a protein where they are exposed to the aqueous milieu [13]. There are, however, many exceptions in which polar residues are buried or non-polar residues exposed on the surface of a protein. This heterogeneity of protein surfaces, mixed polar (hydrophilic) and non-polar (hydrophobic) regions will affect protein/surface interactions.

The quaternary structure is the non-covalent association of independent tertiary structures to form a complex [13]. A multi-subunit protein may be composed of two or

more identical polypeptides, or it may include different polypeptides. It is unique combination of two or more polypeptide chains amino acids that determines the three dimensional structure of protein and thereby, its function. To perform their biological function, proteins may alter between several related structures, during these functional rearrangements the tertiary and quaternary structures are modified and this process is called conformational change [17].

3.3.2.   Proteins adsorption studies in TiO₂ surfaces

Fibronectin (Fn), bovine serum albumin (BSA), and fibrinogen (Fbg) are the three well-characterized proteins used in this work. The interpretation of an adsorption graph is presented before the presentation of the properties of the studied proteins.

Adsorption isotherms, i.e., amount of protein adsorbed (Γ) vs the protein concentration (c_p) plots, are commonly reported as a result of protein adsorption experiments. The initial part of the isotherm (Figure 3-2) reflects the affinity between the protein and the surface. Eventually, when saturation of protein adsorption on the tested surface is achieved the amount of protein adsorbed reaches a plateau. If a strong affinity between the surface and the protein exist, a) the complete coverage of the surface is reached earlier in time, and b) the adsorbed amount is usually higher, as shown on Figure 3-2. Adsorption and desorption processes have been reflected equally in terms of affinity at the graph, but both processes can act differently meaning that the system has two equilibrium states probably due to an irreversible physical change in the system [18].
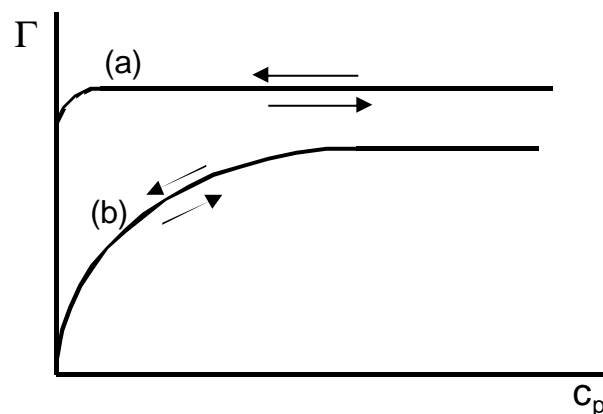

Figure 3-2 *Schematics of (a) strong-affinity protein adsorption isotherm, and (b)weak-affinity protein adsorption isotherm (adapted from [18])*

3.3.2.1. Fibronectin

Fibronectin (Fn) is an adhesive protein and a key component of the extracellular matrix (ECM). It promotes attachment of cells to the biomaterial surface through its central binding domain RGD sequence. Moreover Fn participates in complex interactions with other macromolecules by influencing cellular properties including morphology, migration, homeostasis and oncogenic transformation [1;19-21].

The formation of focal adhesions by osteoblasts on fibronectin-coated Ti surfaces is enhanced and the adhesion and spreading of fibroblasts is improved [22]. Osteoblast precursors could then adhere to these proteins, which provide a matrix for cell attachment, through integrin-mediated mechanisms.

Fn is a large and fibrillar protein composed of two 250kDa-subunits joined together by disulfide bonds and it has an isoelectric point (IEP) of 6,1 (MW~500 kDa) [20;23]. The concentration of Fn in blood plasma is 30 mg/100ml [24]. The different adsorption isotherms reported in the literature [1;23;25] show a high affinity of Fn onto titanium surfaces. In particular, Sousa et al. [23] adsorbed Fn in PBS at concentrations of 5, 10, 20, 100 and 200 μg/ml on c.p. Ti sheets and TiO₂ sputtered substrates and quantification was performed using ^{125}I labelled Fn (Figure 3-3). The adsorption isotherms showed that the amount adsorbed on both types of surfaces increased as the Fn concentration increased in solution and a plateau was never attained. Tamada et al. [26] referred that the minimum amount of Fn required for fibroblast cell adhesion was 500 μg/m². After elution, and for Fn concentration = 20 μg/ml for TiO₂ cp, and = 100 μg/ml for TiO₂ sp [23], surface retains more than the referred Fn amount for cell adhesion. Then a range from 20 up to 50 μg/ml will be the studied Fn concentrations for protein adsorption assays with the QCM-D technique.
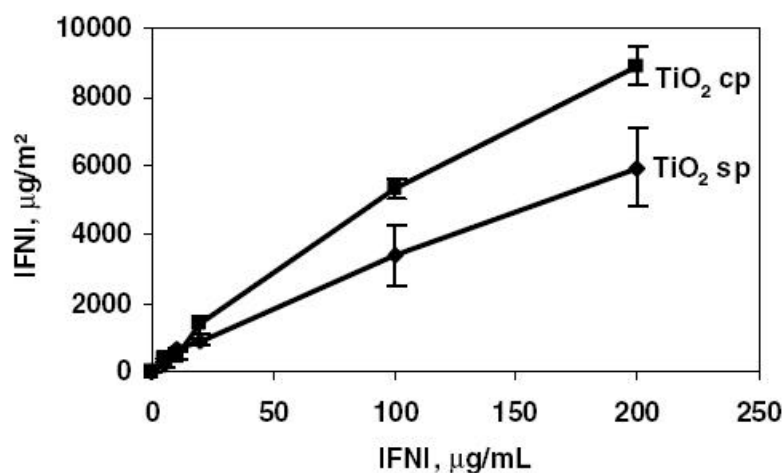

Figure 3-3 *Adsorption isotherm for human plasma fibronectin on c.p. TiO₂ and TiO₂ sputtered substrates after adsorption in solutions ranging from 5 mg/ml to 200 mg/ml at 25ºC [23]*

3.3.2.2. Fibrinogen

Fibrinogen (Fbg) is one of the main proteins involved in the blood coagulation cascade [27]. In some cases, Fbg layers formed at the liquid-solid implant interface have triggered an inflammatory response and have been a part of some of the process that may lead to acceptance or rejection of the implant [28].

Fbg is an ECM protein with a molecular weight of 340kDa [27;29] and a IEP value that can vary between 5,1 and 6,3. The concentration in human plasma is 300 mg/100ml [24;29]. Bai et al. [29] showed the adsorption isotherm data for fibrinogen on 316L stainless steel, nitinol and c.p. Ti after 1 h adsorption in PBS solutions ranging from 10 μg/ml to 5 mg/ml at 37ºC (Figure 3-4). Fbg adsorption results indicated that Fbg amount on Ti range from about 400 ng/cm² to 700 ng/cm² as the solution concentration varies from 80 μg/ml to 2 mg/ml after about 1 h adsorption. Then, in our work, studied Fbg concentrations will be 80 and 100 μg/ml for single protein adsorption assays with the QCM-D technique.
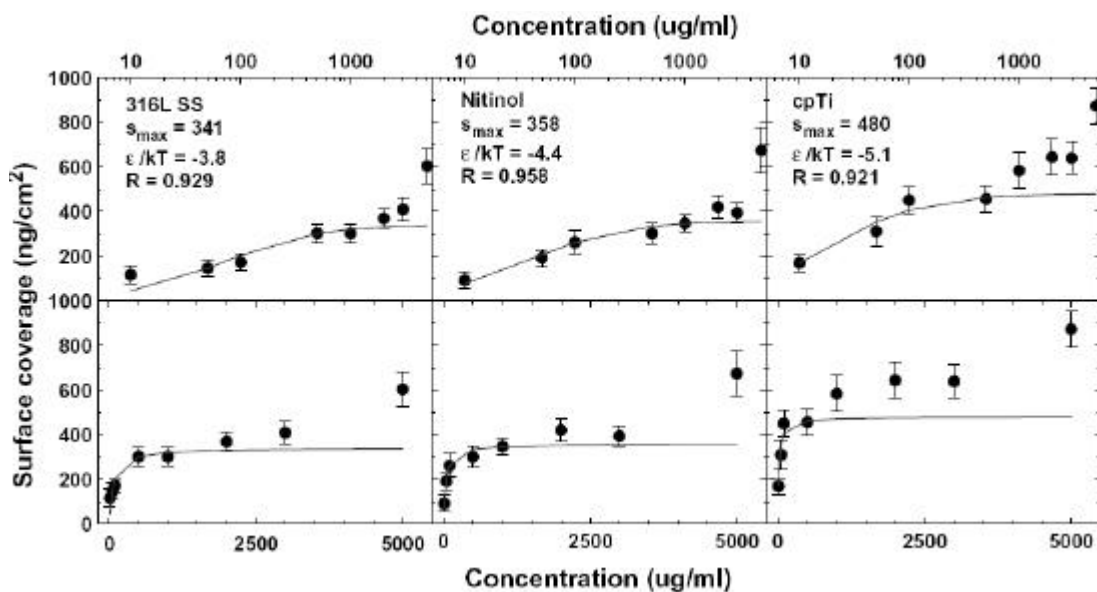

Figure 3-4 *Adsorption isotherms for fibrinogen on 316L stainless steel, nitinol and c.p. Ti after 1h adsorption in PBS solutions ranging from 10 ng/ml to 5 mg/ml at 37ºC [29]*

3.3.2.3. Bovine serum albumin

Bovine serum albumin (BSA) is a globular protein and the most abundant component of many biofluids serving the transport of various metabolites and the regulation of the osmotic pressure [11;30].

BSA is pretty much used for protein adsorption studies since its structure is close to the human serum albumin (HSA) structure [31]. The molecular weight of BSA is 66 kDa and 69 kDa for HSA [32]. HSA has an isoelectric point between 4,7-4,8 [32;33] , nearly coincident to the one for BSA, which is 4,7 [32]. In normal conditions, HSA concentration in human plasma is of 3,5-5 g/100ml [33].

Sousa et al. [34] quantified protein adsorption of HSA solutions in PBS at concentrations of 0,2; 0,4; 1; 4 and 10 mg/ml on TiO₂ surfaces using ^{125}I labelled albumin (Figure 3-5). Specifically, the adsorbed amount increased with HSA concentration and a plateau was reached for concentrations of ~1 mg/ml for TiO₂ c.p. Hughes et al. [35] studied the BSA adsorption on Ti powder and found that maximum adsorption was reached at 10min and 15 min for 100 and 500 µg/ml BSA, respectively (pH=6,8). Moreover, BSA is more tightly bound to the titanium surface at lower concentrations. Wassell et al., [36], also showed a saturation value of 100 µg/ml for BSA protein on TiO₂ surfaces at pH 7,2. Consequently, 100 µg/ml will be the BSA concentration used for single protein studies with the QCM-D technique.
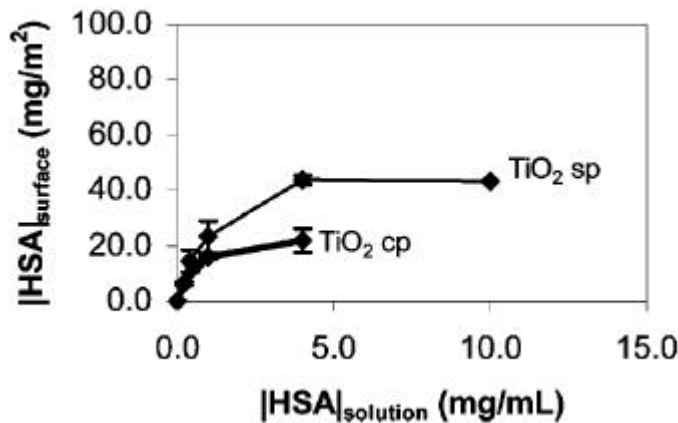

Figure 3-5 *Adsorption isotherm for human serum albumin on c.p. TiO₂ and TiO₂ sputtered substrates after 1 h adsorption in solutions ranging from 0,2 mg/ml to 10 mg/ml at 2 5ºC [34]*

3.3.3. Surfaces

When a surface is created, the bonds that hold the material together are broken and thus, generally represent an increase in energy, the surface energy. Since a surface contains a large number of unsaturated bonds; it is an energetically unfavourable system [37]. If there is a reactive environment such as air or water at a metal surface, the bonds react immediately and spontaneously to form new bonds and compounds, and consequently lowering its surface energy. Therefore, a material surface usually has a different chemical composition from its bulk, as for example the oxide overlayer on almost all metals.

The energy required to create a unit area of a surface in vacuum defines the surface energy (J/m^2). In general, the stronger the bonding within the atoms molecules of the material, the larger is its surface energy [13]. Many inorganic materials such as metals, oxides, semiconductors etc. have high surface free energies, while many organic materials, polymers, etc. have low surface energies [38].

When titanium, which is used for dental implants [39] and in orthopaedic devices [40], is exposed to air reacts rapidly/spontaneously with atmospheric oxygen to form a surface oxide layer which is typically a few nanometres thick. The oxide stoichiometry is close to TiO_2 [41;42] and the oxide interacts with the surrounding biofluids. It is amphoteric, i.e., it can react either as an acid or as a base. It is mechanically rigid and binds structural water in the outermost atomic layer, forming $-O^-$, $-OH$, and $-OH_2^+$ sites [43]. A very important consequence of all those properties of the oxide is that it is negatively charged at physiological pH. The oxide has surface free energy $\sim$ 40 mJ/m^2, as obtained and reported in the previous Chapter 2 of this work and in agreement with others [43]. Those properties are referred to the smooth and ordinary titanium surface onto which water, ions and proteins adsorb upon in contact with body fluids. Any surface treatment can alter the surface properties listed above.

As a consequence, the different properties of a surface will affect the protein adsorption response. Table 3-1 summarizes the surface properties of importance for the interactions between surfaces and proteins.

Table 3-1 *Main surfaces properties that determine protein adsorption. Adapted from [14;43]*

Surface properties	Protein properties
Chemistry	Bonding number
Surface topography	Quaternary, tertiary and secondary structure
Free energy	Overall hydrophobicity
Charge	Charge
Acid/Base properties	Isoelectric point (pI)
Surface impurities	Specific interacting residues

Since the properties of TiO_2 are significantly different from those of pure metal, it is necessary to gain knowledge about the properties of the surface to understand the interaction between the material and the biological entities.

3.3.4.   Interactions between proteins and surfaces

When an aqueous protein solution is exposed to a solid surface, spontaneous accumulation of protein molecules at the solid-liquid interface is generally observed. Proteins can adopt many and unplanned conformations since its charge/polarity irregular/regular distribution along the 3D molecules. They can be exposed to several sites that can interact with the surface, promoting dynamic protein adsorption/desorption processes. The large protein size compared to the single binding sites, the heterogeneous nature referred to local charge, polarity and proteins surface composition can cause a complex dynamic protein adsorption process onto a surface. This process can have a number of intermediate states, with changing conformation and/or orientation of the protein [13].

Protein adsorption is due to the interaction between the different components present in the system such as, the sorbent surface, the protein molecules and the solvent (water). In fact, during all the dynamic process, proteins expose several sites to reach its minimum free-energy state while approaching and adsorbing to the surface [14]. Figure 3-6 shows a schematic drawing of a protein molecule and a surface with the respectively different charged, polar and topographic regions.
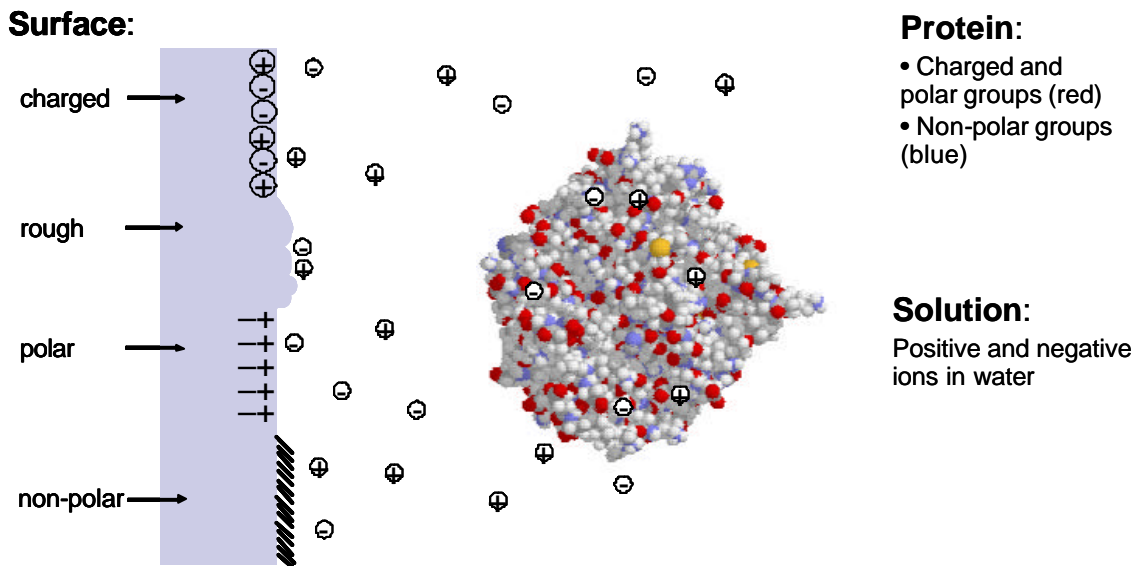

Figure 3-6 Schematic view of a protein and a well characterized surface [13]

For spontaneous adsorption, at constant pressure and temperature, the change in the Gibbs free energy (G) must be negative (Equation 3-1) [14;16-18;44;45]:

Equation 3-1 $$\Delta G_{ads} = \Delta H_{ads} - T \cdot \Delta S_{ads} < 0$$

where H, S and T are the enthalpy, entropy and temperature of the system, respectively, and Δ_{ads} indicates the variation resulting from the adsorption process. Then, according to Equation 3-1, Gibbs energy will be negative with the decrease in enthalpy and/or an increase in the entropy. Moreover, Equation 3-1 can be expressed in terms of interfacial energies as:

Equation 3-2 $$\Delta G_{ads} = \gamma_{sp} - \gamma_{pl} - \gamma_{sl} < 0$$

subscripts s, l and p refer to solid, liquid and protein, respectively.

Factors including bound ions, surface and protein characteristics have to be considered in defining the interaction at the solid-protein solution interface. The surface presents a heterogeneous nature with respect to the local charge, polarity, roughness and composition and the protein molecules are characterized by regions with different charge and polarity.

The number of protein conformations is also limited because, as mentioned in section 3.3.1, the rotation around the peptide bond is restricted. The final structure taken by the polypeptide is determined by the interactions that occur between the amino acids themselves and the surrounding water what will determinate the final Gibbs free energy. The protein stability, what will determine adsorption/desorption processes, is considering the change in free energy between the fully denatured and the fully assembled, native state, conformation [13].

The most important interactions determining protein structure are presented below [13;14;16;17;46]. Among them, distribution of charge and hydrophobic effects have a strong influence on the protein's structural stability [12].

i) Coulomb interaction, electrostatic interaction due to charges

Depending on the isoelectric point, coulomb interaction between charged groups can be attractive or repulsive. The isoelectric point (IEP) is the pH at which a molecule carries no net electrical charge. At a pH below the IEP, proteins carry a net positive charge while above the pI they carry a net negative charge. Around the IEP, the net intermolecular Coulomb interaction is attractive and favours the compact structure of proteins. Away from the IEP, the excess of either positive or negative charges lead to repulsion, promoting a more expanded protein structure.

ii) Hydrogen bonds

In proteins, each peptide group is capable of hydrogen bond formation. H bonding between peptide units does not stabilize a compact structure. However, it stabilizes helical and pleated sheet structures in the places where the polypeptide chain is shielded from water due to other interactions [17].

iii) Hydrophobic interaction

The hydrophobic interaction refers to the spontaneous dehydration and subsequent aggregation of non-polar components in an aqueous environment. Hydration layer has to be displaced in order to obtain a close contact between protein and surface. The interior of proteins mostly consists of non-polar amino acids. The reason for this is the hydrophobic interaction, which forces the non-polar amino acids away from water towards the interior of the protein molecule where they contact other non-polar molecules. Then, the polar side chains are therefore mainly found on the surface of the protein molecule, which can lower the free energy by interactions with the surrounding water and ions by forming hydrogen bonds. Mainly due to the entropy increase in water that is released from contact with hydrophobic components and a relative small enthalpy effect [17]. Then, the Gibbs energy of the system is lowered.

iv) Van der Waals interaction

Interactions between ionic groups, dipoles and induced dipoles, included in van der Waals bond, in a protein molecule is also influenced by the surrounding aqueous medium which also contains dipoles and ions. It is commonly referred as dispersive or London-van der Waals interactions and it is generally attractive [13].

v) Rotational mobility

Directive interactions, e.g. hydrogen bonds, limit the rotation along the polypeptide chain and the side chains.

Protein adsorption is not only affected by protein and surface interactions, proteins mutually compete for adsorption at any exposed surface. Initially, the surface will be mainly occupied by the smaller and more abundantly molecules. Then, the adsorbed molecules may be displaced by other molecules that have a stronger tendency to adsorb. Consequently, the protein layer changes, a dynamic process.

The protein adsorption process cannot be predicted by a single factor, however changes in hydration, redistribution of charged groups, and rearrangements in the protein structure are considered to be the dominant contribution [18].

3.3.4.1. Kinetics of protein adsorption

The adsorption of proteins can be divided into four steps [13;17;18]:

i) Transport towards the sorbent surface. The basic transport mechanisms are gradient diffusion and Brownian motion which explains the random movement of particles due to the collisions with molecules of the surrounding medium. The rate of transport of a protein molecule from solution towards an interface increases with increasing concentration of the protein solution and then, a higher degree of coverage is expected.

ii) Attachment at the interface. The initial protein-surface interaction, whose strength determines the residence time of the initial protein attachment.

iii) Structure rearrangements in the adsorbed state. Dynamic processes in the interfacial region including movements and conformational changes of the protein molecules.

iv) Detachment and transport away from the interface. Transport of desorbed protein molecules away from the interface, if the binding is not too strong.

Once a protein molecule has reached the surface, complex dynamic processes occur (Figure 3-7). First, the protein molecules approach the surface in random orientations. Since the protein molecule is irregular and heterogeneous with respect to surface polarity and charge, several orientations may occur with different strength. As the residence time at the surface increases, the number of contact points between the protein and the surface might increase. Over time this can lead to irreversible adsorption and conformational changes such that a larger area is occupied by each protein.
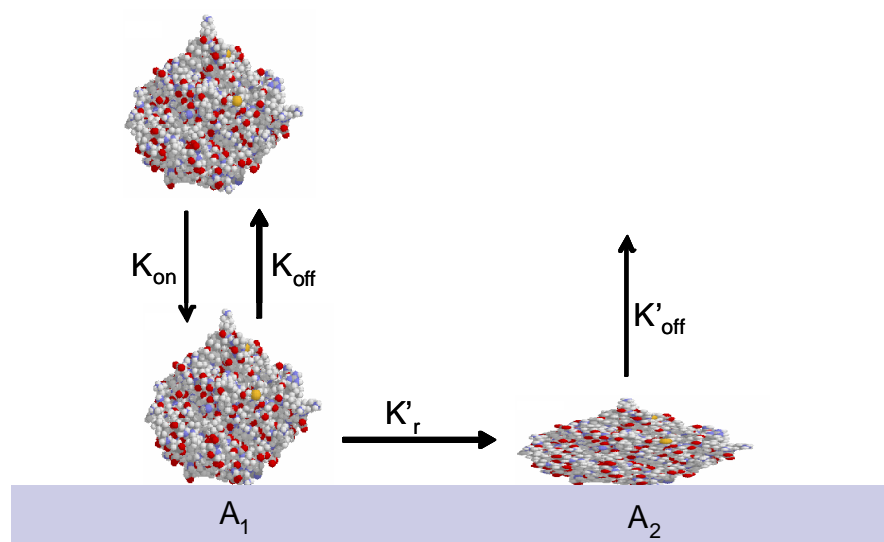

Figure 3-7 *Protein adsorption characterized by two states: A_1 is a reversible state but can lead to an irreversible state as A_2. The K_{on} and the K_{off} represent the probability of a protein molecule to attach or detach from the surface [13]*

3.4. The QCM-D technique

3.4.1. Introduction

Information about protein-adsorption kinetics can be achieved by using optical, electrical or labelling techniques, which mainly provide information about the amount of mass adsorbed [30].

The quartz crystal microbalance (QCM) has been used for a long time as a weighting device to monitor thin film deposition in vacuum or gas environment. In 1980 Nomura [47] showed that the QCM may be used in the liquid phase and in 1997 Hook [13;48] constructed an experimental setup to measure simultaneously the frequency and the dissipation of energy in vacuum, air and liquid which completed the name of the device to the quartz crystal microbalance with monitoring of dissipation (QCM-D). This technique, [49], represents an extension of the traditional QCM method and can provide unique and quantitative information on the viscoelastic properties of surface adsorbed layers [50]. The QCM-D allows a reliable protein adsorption study [51;52] as well as other surface-related processes [53].

3.4.2. Fundamental principles of the QCM-D technique

The quartz crystal microbalance consists of a piezoelectric quartz crystal sensor that is used to measure very small masses. The thin piezoelectric sensor crystal has gold electrodes evaporated on its two faces. When an AC-voltage is applied over the electrodes, the crystal can be made to oscillate at its resonant frequency, f. If a mass is adsorbed on the crystal, the resonant frequency decreases proportionally to the mass of the film, which also accounts for the adsorbed water from aqueous solutions. The contribution of water to the mass of the adsorbed layer can be elucidated from the dissipation factor, D.

The principle of QCM-D is based on the resonance frequency of the quartz crystal induced by applying an alternating electric field across the crystal [48;49;54;55]. Consequently, an oscillating electric field will induce mechanical shear waves in the crystal. Resonance will occur when the thickness of the plate (t_q) is an odd integer of half wavelengths of the induced wave ($t_q = n \cdot \lambda/2$) [13]. The resonant frequency, f, is thus given by:

Equation 3-3
$$f = n \cdot \frac{v_q}{2 \cdot t_q} = n \cdot f_0$$

where v_q is the wave velocity in the quartz plate and t_q is the thickness of the quartz plate [13]. The resonant frequency for n=1 is called the fundamental resonant frequency, $f_0(=v_q/2 \cdot t_q)$, n=3 the third overtone, etc.

An increase in mass (Δm) bound to the quartz surface causes the crystal oscillation frequency to decrease, obtaining a negative shift of the resonance frequency ($-\Delta f$). The linear relation between Δm and Δf was demonstrated in 1959 by Sauerbrey [27;56].

Equation 3-4 $$df = \Delta f = -\frac{f}{t_q \cdot \rho_q} \cdot \Delta m = -n \frac{2 \cdot f_0^2}{v_q \cdot \rho_q} = -n \cdot \frac{1}{C} \cdot \Delta m$$

where C is the mass sensitivity constant (C=17,7 $ng \cdot cm^{-2} \cdot Hz^{-1}$ at 5MHz) and n is the overtone number (n=1, 3,…).

Sauerbrey equation (Equation 3-4) holds if the adsorbed layer is rigid, if the added mass is small compared to the weight of the crystal, if there is no slip in the metal/layer interface, and if the layer is homogeneously distributed on the surface. The Sauerbrey relation concludes that the change in resonance frequency is proportional to the change in the adsorbed mass if the adsorbed is much smaller than the mass of the crystal [27].

3.4.2.1.   The dissipation factor

The QCM is a very sensitive tool to study protein adsorption kinetics in aqueous solutions, with sensitivity in the ng/cm^2 regime [48;52;54]. In other situations, where the layer is not rigid and/or thicker the response of the QCM is more complex because the Sauerbrey relation is not accomplished. Most surface-adsorbed protein layers are hydrated, and so they are highly viscous and cause significant energy dissipation. In those cases the dissipation factor, D, calculated when using the QCM must also be taken into consideration [27;48]. The dissipation factor is inversely proportional to the Q-factor of the oscillator [57], which is an adimensional parameter that compares the time or decay of an oscillating physical system's amplitude to its oscillation period as defined by:

Equation 3-5 $$D = \frac{1}{Q} = \frac{E_{dissipated}}{2 \cdot \pi \cdot E_{stored}}$$

where $E_{dissipated}$ is the energy dissipated during one period of oscillation, and E_{stored} is the energy stored in the oscillating system.

The technique to measure the dissipation factor is based on the fact that when the driving power to a piezoelectric crystal oscillator is switched off, the voltage over the

crystal, A(t), decays as an exponentially damped sinusoidal with time, t (Figure 3-8) [48;49]:

Equation 3-6
$$A(t) = A_0 \cdot e^{t/\tau} \cdot \sin(2\pi ft + \varphi)$$

where A_0 is the amplitude of oscillation before switching off the driving power, t is the decay time constant, f the frequency and f is the phase angle. The decay time constant is related to the dissipation factor:

Equation 3-7
$$D = \frac{1}{\pi \cdot f \cdot \tau}$$

The loss of energy in the system depends on the medium surrounding the crystal and on the properties of the mass added onto the crystal. To get information about changes in f and D during adsorption from liquid solutions, f and D are recorded as functions of time.
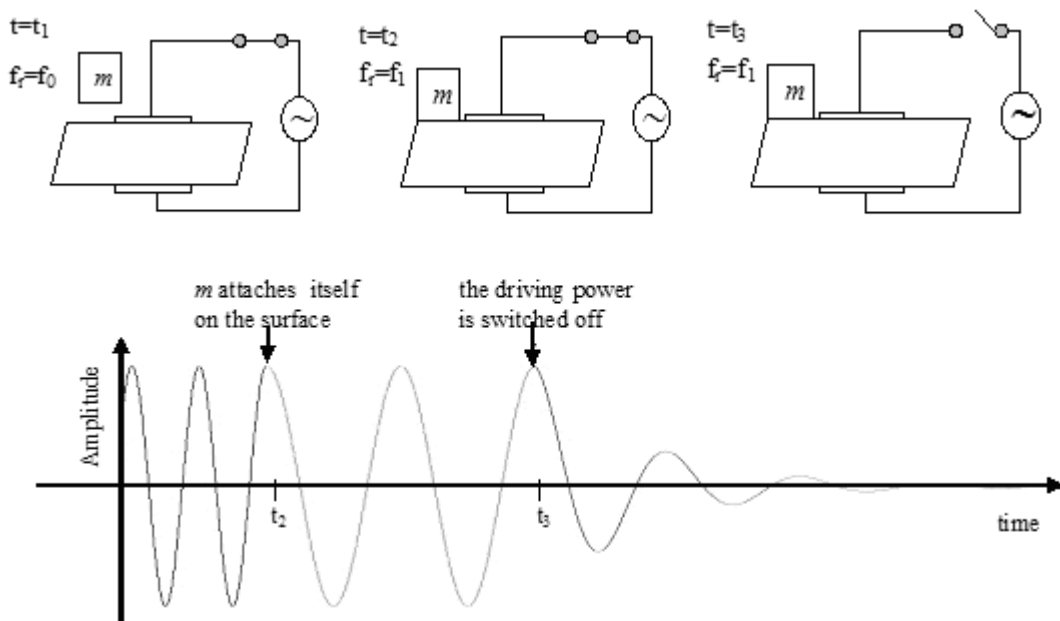

Figure 3-8 *Steps of adsorption of a mass m on the crystal surface and relative changes in the crystal oscillation. Initially the frequency is constant at its fundamental overtone; then, when the mass is added the frequency decreases but remains constant; finally, when the driving power is switched off, the frequency decays and the dissipation can be calculated [58]*

The possibility of the device to determine the dissipation shift induced by the protein adsorption in real-time gives additional valuable information about the protein layer formed. When proteins adsorb from the solution to the surface, the following interfaces have to be considered: the interface between the solid surface and the proteins and the

interface between the proteins and the liquid. Then, the changes of energy dissipation are localized

- at the protein-substrate interface

- at the protein-liquid interface

- within the protein layer

Different studies, [56;59;60], have shown that interfacial protein/liquid and protein/substrate processes are not the dominant mechanisms to increase dissipation and consequently, the observed dissipation shift must primarily be due to losses of energy within the protein layer. These changes in the dissipation are believed to arise from conformational changes of the protein layer and/or from the amount of water trapped inside the layer [27].

3.4.2.2. Viscoelastic properties of the adlayer

QCM-D can provide unique and quantitative information on the viscoelastic properties of surface-adsorbed layers including density, shear elastic modulus, and shear viscosity [61].

As seen in previous 3.4.1 section, the total amount of mass can be calculated from the frequency shift using the Sauerbrey equation (Equation 3-4) for rigid, nonporous, homogeneous adlayers [62]. Since protein layers are not rigid and may slip on the moving electrodes surface, the Sauerbrey equation hypothesis are not satisfied and the value of mass calculated with this method for a viscoelastic surface is expected to be underestimated than the real one since the film is not fully coupled to the motion of the sensor surface [63].
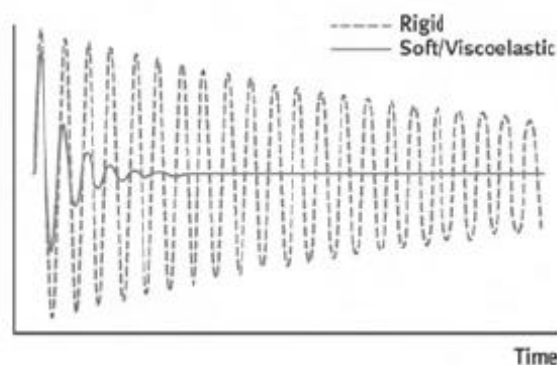

Figure 3-9 *The diagram illustrates the difference in dissipation signal generated by a rigid and soft molecular layer on the sensor crystal [58]*

Therefore, for no thin and no rigid films the Sauerbrey equation must be used cautiously. For viscoelastic films, the Sauerbrey equation can be applied without inducing a high error if the layer has the two following characteristics:

- the dissipation shift is less than $1?10^{-6}$ for a frequency shift of 10Hz [58;64]

- the layer is thinner than 250nm, which is the extinction depth into the aqueous protein solution of the shear waves excited by the QCM-D crystal [56]

The Sauerbrey mass value is not the real one but can be useful to give and idea of the total amount of mass on the crystal surface and to have a knowledge of the mass tendencies, which allows the comparison between different surfaces.

A Newtonian fluid flows like water – its stress at each point is linearly proportional to its strain rate at that point; the proportionality factor is the viscosity coefficient. In QCM-D measurements, this means that the fluid will have the same viscosity regardless of frequency. This allows for viscosity modelling at multiple overtones which gives more information about the system. A fluid that does not obey this rule is non-Newtonian, i.e. the viscosity changes with the applied strain rate. When using QCM-D, the fluid will have different viscosities at different harmonics.

Because the linear relation between the adsorbed mass and the change in frequency is not necessary valid for viscoelastic films, additional information in terms of energy dissipation and frequency (overtone)-dependent response is necessary. Therefore, to calculate the adsorbed mass and viscoelastic properties of such protein layers, theoretical modelling of the QCM-D response is necessary by introducing a shear viscosity coefficient ? and a shear elasticity modulus μ within one of two basic models (i) Maxwell and (ii) Voigt.

The Maxwell model is usually applied to polymer solutions which can demonstrate purely liquid-like behaviour at least for low shear rates, whereas the Voigt model is applicable for polymers which conserve their shape and do not flow [65]. For that reason, since we can not assure purely liquid-like behaviour in our systems, the Voigt model will be the used approach in our studies.

In the Voigt model (Equation 3-8), the viscoelastic element is described by complex shear modulus G, real part of which (the storage modulus G) is independent of frequency whereas its imaginary one (the loss modulus G") increases linearly with frequency [65;66].

Equation 3-8 $$G = G' + iG'' = \mu_f + i2\pi f\eta_f = \mu_f(1 + i2\pi f\tau_f)$$

where μ_f is the elastic shear (storage) modulus, η_f the shear viscosity (loss modulus), f the oscillation frequency, and τ_f the characteristic relaxation time of the film.

In this model, each protein film is represented by four unknown parameters (Figure 3-10): density (ρ_f), shear viscosity (η_f), shear elastic modulus (μ_f), and the thickness (t_f). Because viscous layers exhibit different penetration depths of harmonic acoustic frequencies, changes in frequency (Δf) and dissipation (ΔD) induced by adsorbed protein are measured simultaneously at different overtones. Then, up to eight experimental values are available (Δf and ΔD for 5, 15, 25 and 35 MHz), allowing the model to fit the data and to calculate the unknown parameters (η_f, μ_f, t_f) but certain assumptions have to be made such as ρ_f.

Liquid
(r_l, h_l)

f: frequency (Hz)
r: density (kg/m^3)
η: shear viscosity (G''/2pf), (kg/ms)
μ: elastic shear modulus (G'), (Pa)
t: thickness (m)

n=1
n=3

Adlayer
(r_f, h_f, μ_f)

t_f

Crystal
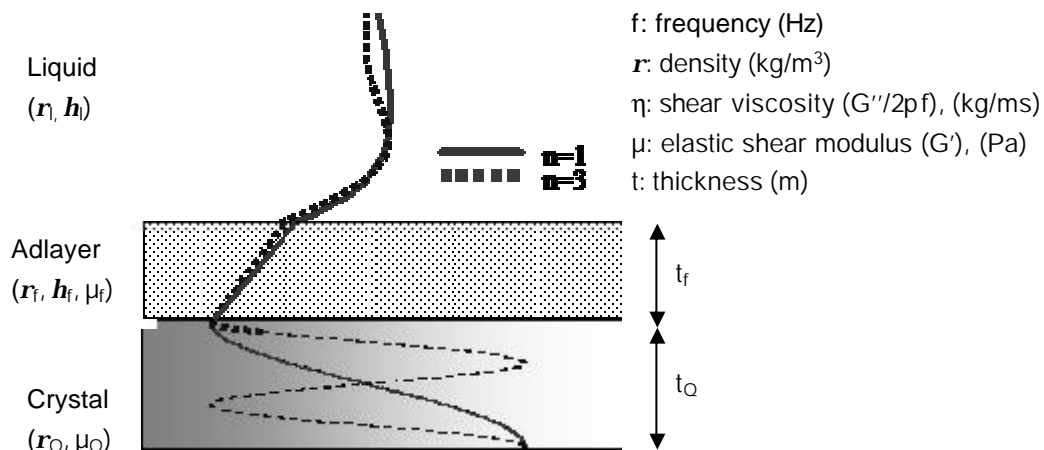(r_Q, μ_Q)

t_Q

Figure 3-10 *Schematic illustration of the geometry and the parameters of a quartz crystal covered with a viscoelastic protein film. The film is represented by density (r_f), viscosity (h_f), elastic shear modulus (μ_f), and thickness (t_f). The bulk liquid is represented by a density (r_l), and a viscosity (h_l). The crystal is represented by density (r_Q), elastic shear modulus (m_Q), and thickness (t_Q) [67].*

The no-slip boundary condition at the solid-overlayer interface corresponds to a continuous variation of the displacement and of the shear stress across the interface. Then if the adsorbed film is situated between the QCM crystal and a semi-infinite Newtonian liquid under no-slip conditions, changes in the resonant frequency and the dissipation shift are obtained from the imaginary and real parts of β-function [65;68]:

Equation 3-9
$$\Delta f = \frac{Im(\beta)}{2\pi\rho_Q t_Q}$$

Equation 3-10
$$\Delta D = -\frac{Re(\beta)}{\pi f \rho_Q t_Q}$$

Where

$$\beta = \xi_1 \frac{2\pi f \eta_f - i\mu_f}{2\pi f} \frac{1 - \alpha \exp(2\xi_1 t_f)}{1 + \alpha \exp(2\xi_1 t_f)},$$

$$\alpha = \frac{\dfrac{\xi_1}{\xi_2} \dfrac{2\pi f \eta_f - i\mu_f}{2\pi f \eta_l} + 1}{\dfrac{\xi_1}{\xi_2} \dfrac{2\pi f \eta_f - i\mu_f}{2\pi f \eta_l} - 1},$$

$$\xi_1 = \sqrt{-\frac{(2\pi f)^2 \rho_f}{\mu_f + i2\pi \eta_f}},$$

$$\xi_2 = \sqrt{i \frac{2\pi f \rho_l}{\eta_l}}$$

and where t_f is the thickness of the viscoelastic film, ρ_f and ρ_l the density of the film and the bulk liquid, respectively, η_f and η_l the viscosity of the film and the bulk liquid, respectively and μ_f is the elastic modulus of the film.

3.4.2.3. Overtone sensitivity

The QCM-D used allows simultaneous measurements of the resonance frequencies and the dissipation shift at the fundamental, third, fifth and seventh (n=1, 3, 5…; i.e., f=5 MHz, 15 MHz, 25 MHz…) up to n=7 with a repetition rate of 1 Hz. The third overtone of the QCM-D has been monitored during the adsorption of the three proteins and it is plotted in the next section for all the assays. This is because the fundamental mode is too sensitive to environmental fluctuation and because a higher overtone number is related to a lower penetration/detection depth (Figure 3-11). However, the third overtone data must be normalized to the fundamental resonant frequency of the quartz crystal. Therefore the values acquired were plotted divided for a factor of three.
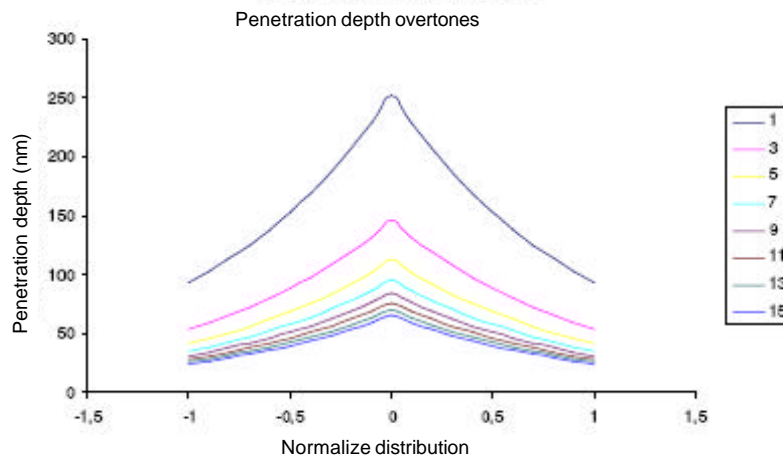

Figure 3-11 *Viscous penetration depth as function of the overtone number (Q-Sense reported data)*

Simultaneous measurement of multiple overtones is required to model viscoelastic properties and extract correct thickness for films outside the Sauerbrey region. With the Q-Sense D300 system, 8 incoming parameters (4 frequencies and 4 dissipation values) per sensor provide a well-determined model of the particular film properties. Moreover, the different overtones give information about the homogeneity of applied layers: as the detection range out from the crystal surface decreases with increasing overtone number, abnormal frequency behaviour suggests vertical variations in film properties. The fact that the detection range out from the crystal surface decreases with increasing frequency is also used by the modelling software to calculate accurate thickness of films that do not fully couple to the oscillation of the crystal. For rather soft films, containing much water (films made of large proteins for example), accurate thickness information can not be obtained without measuring at several frequencies.

3.4.2.4. Data interpretation

A typical protein measurement with the QCM-D will show that the adsorption causes an initial rapid frequency decrease (mass increase) followed by a slower frequency decrease as the surface coverage saturates. The D-shifts are positive and display kinetics similar to the f-shifts (Figure 3-12). The frequency (Δf) and dissipation shift (ΔD) plotted are calculated as the difference between the value at each instant of time and the initial value f_0, D_0 acquired when the crystal is surrounding of aqueous solution that contains no protein. Therefore, the data plotted shows only the changes due to the presence of protein on the surface and does not consider shift in frequency and dissipation induced by the fluid surrounding the crystal, such as liquid trapped in cavities or porous of the surface, that increase the mass value, and the loss of energy induced by the liquid during the oscillation of the crystal.
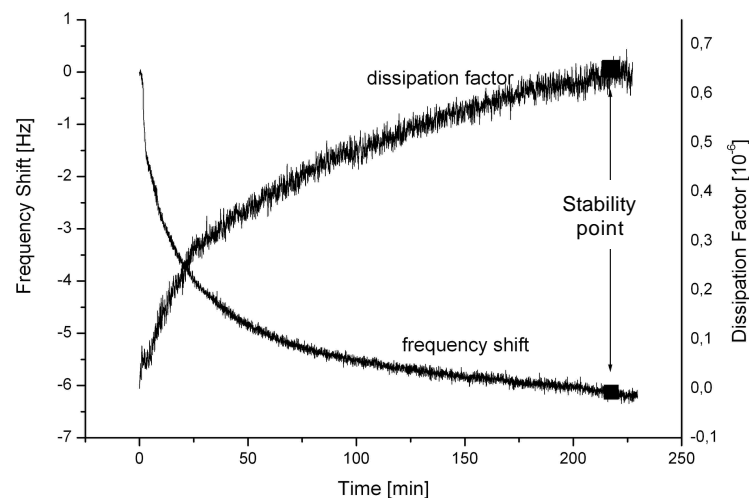

Figure 3-12 *Frequency shift and dissipation shift of a typical protein adsorption assay obtained as a preliminary result for this study.*

An important consideration is that the frequency shift measured by the device is due to the total mass added on the surface. Since proteins are in aqueous solution, it is possible to have a significantly increase in weight due to the bond water and, moreover, water trapped between the proteins adsorbed may be sensed as an additional mass. For this reason, the shift in frequency is related to the total amount of mass that is the sum between the mass of protein adsorbed and the mass of the water uptake. The amount of water influences the viscoelasticity of the adlayer and consequently the dissipation; in particular a high quantity of water induces a higher loss of energy. Many studies have been done in order to evaluate the overestimation of the protein adsorbed mass [57;63;69]. Comparison between QCM and optical or labelling techniques has demonstrated that the amount of hydrodynamically coupled water varies between 10 and 90% of the proteins mass, the exact amount depends on the type of protein and the structure of the protein layer formed at the sensor/liquid interface [13;56;57;69]. An elongated protein that adsorbs flat to the surface gives low dissipation while the very same molecule standing up on the surface gives high dissipation [58].

Generally, Δf and ΔD show different time dependencies. A useful and revealing way of exploring Δf-ΔD relationship is to plot ΔD vs. Δf (called the D-f plots) as shown in Figure 3-13, where time is eliminated as an explicit parameter. This plot is useful to evaluate the structural properties of the adlayer because it relates how much dissipation is caused per unit of frequency change (mass). Changes via slope suggest structural alterations within the individual proteins or within the protein layer as the adsorption proceeds [56]. In other words, this plots gives an estimate of how new mass added affects the structure on the surface: the higher the ΔD/Δf slope, the higher the dissipation per unit added mass, signalling an increasing water content in the protein film forming a less rigid protein layer [13;56;63].
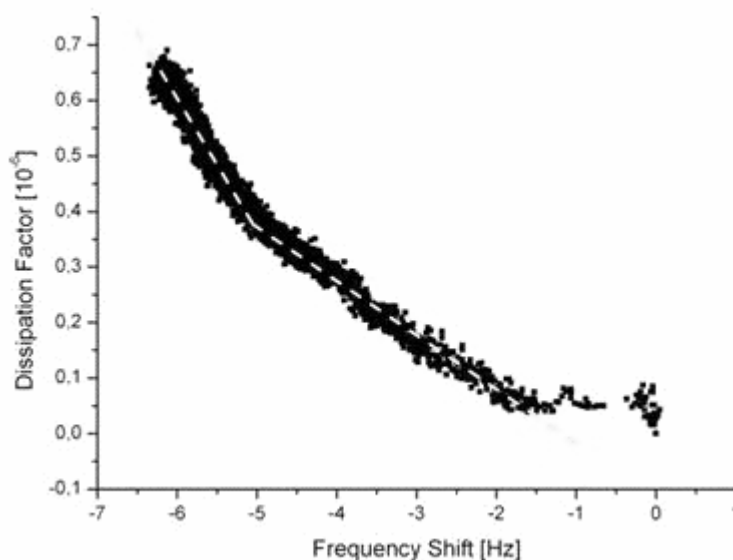

Figure 3-13 *Dissipation vs. frequency plot of a typical protein adsorption assay. Obtained as a preliminary result for this study*

3.4.2.5. Data analysis

In order to determine which approach, Sauerbrey or Voigt, should be applied to model the obtained results, the frequency and the dissipation shift vs. time of the different overtones should be plotted. Under normal conditions, the fundamental overtone should be disregarded, since it is too sensitive, and third, fifth and seventh overtone will be viewed. The data will require viscoelastic modelling if D values are not close to zero, or if D-shifts (in 1E-6) are higher than 5% of f shifts (in Hz). In addition, if the are significant differences between overtones viscoelastic modelling is suggested [58].

3.4.2.5.1. Rigid films, Sauerbrey's approximation

The frequency data from one-step surface adsorption process is fit to the Sauerbrey model where the areal mass (ng/cm^2), the thickness (m) and the density (kg/m^3) of the protein layer can be calculated by the QTools software (Q-Sense AB, Sweden). When calculating the thickness and the density one or the other needs to be held constant.

Only one frequency data from one overtone can be selected for the calculations.

3.4.2.5.2. Viscoelastic films, Voigt's approximation

Once experimental data are recorded, the protein layer viscosity, the layer shear elastic modulus and the layer thickness applying the appropriate model can be calculated. The software Qtools (Q-Sense AB, Sweden) is used to fit the model from the experimental data using some fixed parameters, as explained above. As the behaviour of the protein layer is unknown, a viscoelastic layer is assumed in all studied cases studied here, and calculations are performed applying the Voigt model. As a summary, the main steps for the analysis with the Qtools software are the following:

A. Model settings

The selected data obtained experimentally is introduced. The first harmonic is not chosen, since is too sensitive, but the 3rd, 5th and 7th harmonic data are introduced to the Voigt modelling.

B. Parameters

A certain range of floating (Table 3-2) and fix variables (Table 3-3) are used by Qtools to calculate the frequency and the dissipation of the studied system. Chi-square comparisons of the experimental and the calculated Δf and ΔD values are estimated.

Then the range values of the floating variables might be changed until the calculated Chi-square is minimized.

The parameters used an initial input for the calculations should be carefully chosen to be as close as possible to the real experimental system. The fixed parameters (fluid density, fluid viscosity) are those corresponding to water, which is a good estimation since the system includes a highly hydrated protein film. The value of the protein layer density, the third fix parameter, might vary between 1000 kg/m³ (water) and 1350 kg/m³ (protein) [57;62;70;71] depending on the protein coverage. 1200 kg/m³ was chosen on the basis of a saturated protein coverage is slightly above 50% [57;62;70]; then, the rest of the protein layer should be covered by water. The parameters to fit are those corresponding to the layer viscosity, layer shear elastic modulus and layer thickness. The software allows changes between fixed parameters and parameters to fit as desired.

Table 3-2 Parameters to fit for Voigt model calculations from Qtools software

Parameters to fit	Minimum estimation	Maximum estimation	Steps
Layer viscosity (kg/ms)	0,001	0,01	10
Layer shear elastic modulus (Pa)	1E5	1E9	10
Layer thickness (m)	1E-10	1E-6	10

Table 3-3 Fixed parameters for Voigt model calculations from Qtools software

Fixed parameters	Input
Fluid density (kg/m³)	1000
Fluid viscosity (kg/ms)	0,001
Layer density (kg/m³)	1200

C. Measured data

Once the measured data are introduced to start the calculation, the standard deviation of the noise is calculated. The nosiest data are excluded for further calculations.

D. Fit settings

Fit settings include the limitation and exclusion of data –establishment of the base line-, and the selection of the initial value and incremental direction for the model fitting. All fitting have been done starting the fitting with the last recorded value.

E. Refining the fit

Once the fit analysis is performed, the different fit parameters can be plotted vs. time. With this information, new input parameters can be used and so, get a refined fit. Refining the fit means that:

i. The total Chi-square is reduced

ii. The overlayer of the calculated values from the experimental values is ameliorated

3.4.2.6.   Other techniques for protein adsorption studies

There are other relevant techniques that have been applied to understand the protein-surface interactions. As a first group, the optical techniques can be considered. Ellipsometry [72-75], scanning angle reflectometry (SAR) [30] measure the thickness and the refractive index of the adsorbed layer based on the fact that the polarization of a light beam reflected at a planar surface changes due to changes in the dielectric properties of the interface, in this case, from proteins adsorbed. The optical waveguide lightmode spectroscopy (OWLS) [57] measures changes in phase velocity of transparent or semitransparent materials. All techniques are suitable to follow protein-surface and protein-antibody interactions in real-time and provide quantitative values of the adsorbed adlayer mass. QCM-D provides complementary information because the analysis of energy dissipation allows the characterization of mechanical/structural properties of the adlayer.

A second group of alternative methods for protein/surface interactions is formed with labelling techniques. Proteins are labelled with either a fluorescent or a radio dye for diagnostic purposes. The enzyme-linked-immunosorbent-assay (ELISA), the radio-labelling based systems and the total internal reflection fluorescence (TIRF) [72] are good examples. Only the later is able to measure kinetics of protein adsorption. An additional limitation of the labelling techniques is that labelling of protein molecules can alter the conformation and function of the protein and thereby also its adsorption behaviour.

A last group is formed with the techniques based on electrical properties, which take advantage of the fact that proteins are heterogeneous molecules with surfaces composed of hydrophobic, polar and charged regions. Then, the protein adsorption changes the electrical properties of the interfacial layer. Some examples of electrical techniques are (streaming) potential measurements [76] and impedance (capacitance) measurements.

Circular Dichroism [77], which can estimate the average loss of secondary structure of proteins due to the surface interaction; Fourier transform-attenuated total reflection-infrared spectroscopy (FT-ATR-IR), which can give information about the structure and the kinetics of the surface adsorbed proteins [78], and techniques based on ultraviolet-visible spectroscopy [79], which can determine the orientation and conformational changes of adsorbed protein, are useful complementary optical and spectroscopic techniques.

Scanning tunnelling microscopy (STM) and transmission electron microscopy (TEM) require a dry protein film [69]. Atomic Force Microscopy (AFM) [73] can be used for imaging protein adlayers also in the aqueous phase [80] and has benn used as the most popular technique to visualize and complement information of results obtained with QCM-D.

3.4.3. The QCM-D system

The QCM-D that has been used for the assays in this work is the D300 model by Q-Sense, Sweden. This machine consists of four parts (Figure 3-14):

1. The sensor crystal.

2. The measurement chamber, in which the sensor crystal is mounted. This chamber provides a temperature-controlled environment for the crystal during the measurement.

3. The electronics unit, which allows the QCM-D measurements and contains the temperature control system.

4. The data acquisition software, Q-soft 301 (Q-Sense, Sweden), and data analysis software, Q-tool (Q-Sense, Sweden).
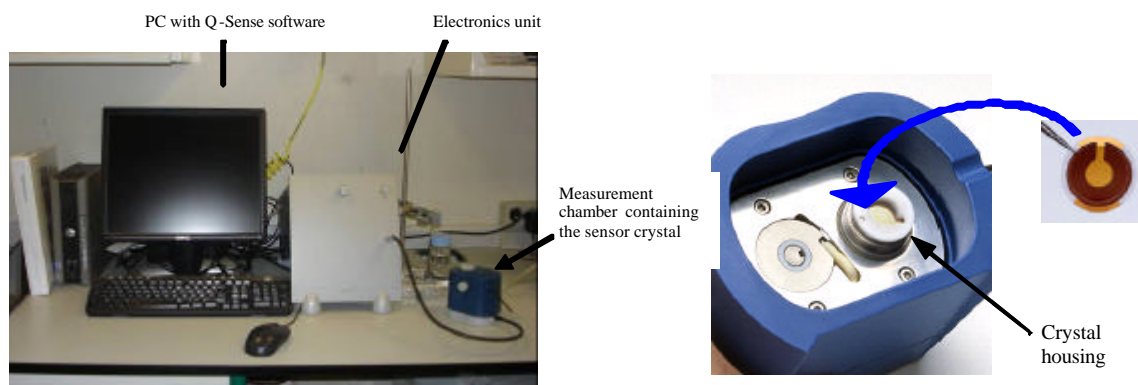

Figure 3-14 *General view of Q-Sense D300 system (Q-Sense, Sweden) and the axial-flow measurement chamber (QAFC 302, Q-Sense, Sweden)*

The axial flow chamber (QAFC 302, Q-Sense, Sweden) allows measuring the adsorption and desorption of molecules and particles from solution, such as proteins, lipids and surfactants. The chamber consists of two parts: the T-loop, to thermally equilibrate the fluid, and the sensor (Figure 3-15).
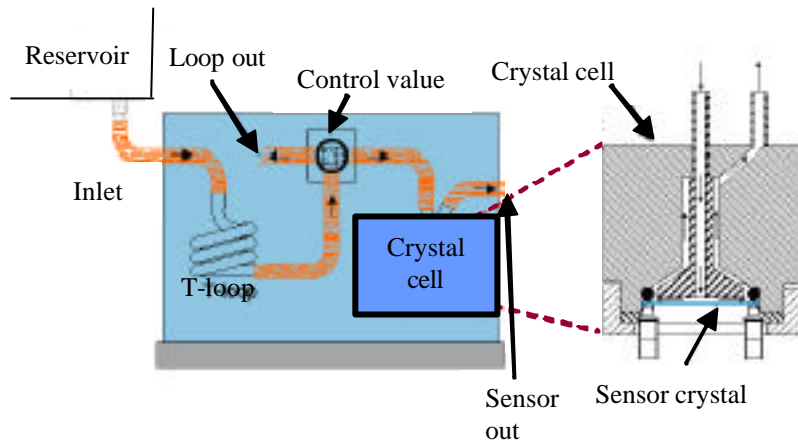
Figure 3-15 *Schematics of the axial flow chamber. The solution is placed in the reservoir and introduced into the T-loop where it is warmed. Finally, the soiution is introduced into the crystal cell and exposed to the surface. The system is controlled within the control valve.*

3.4.4.   TiO₂-crystals

The crystal used in the QCM-D is a thin piezoelectric quartz disc with two different sides (Figure 3-16), supplied by Q-Sense (Sweden). One side is the contact side, which gold electrodes have been evaporated on and is connected to the electronic unit. The other side is the active part, which is in contact with the protein solution. Gold is usually chosen for the active side, but other materials can be sputtered on it too [11;54].
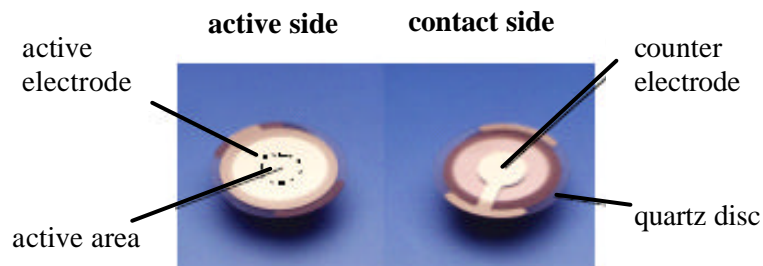

Figure 3-16 *Image of the two sides -and their corresponding parts- of the crystal: the active and the contact sides*

In this work, the crystal used (QSX 310 Q-Sense, Sweden) has the active side coated with titanium oxide by vapour deposition. Figure 3-17 schematically shows the vapour deposition process. Titanium ions are detached from the target by collision with argon gas. The presence of oxygen in the processing chamber allows titanium ions to react with

oxygen molecules and, consequently, form titanium oxide before being adhered on the crystal surface.

The crystals are 14mm in diameter. The coverage thickness is about 20nm and the ir fundamental mode is at 4.95 MHz.

The cleaning protocol used before starting the experiments was: (1) 10min sonication with ethanol; (2) 10min sonication with acetone; (3) 10min sonication with MilliQ ultrapure water; and (4) 10 min UV/ozone chamber (BioForce Nanosciences, Ames, USA). During the cleaning process the crystals where hold on a Teflon crystal.
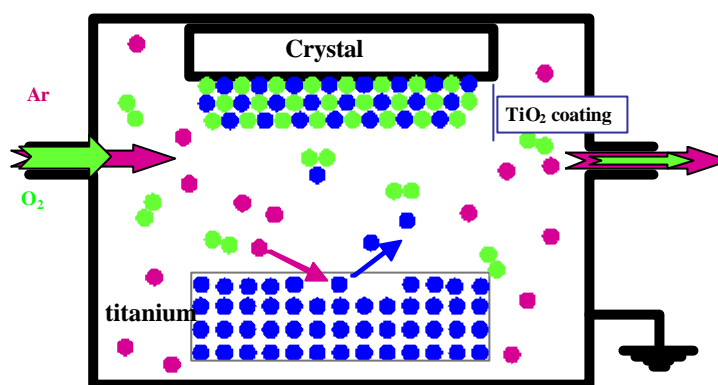

Figure 3-17 *Vapour deposition process to coat the gold crystal with titanium oxide*

After using the crystals, they were washed with Hellmanex 2% (Hellmanex II, Hellma GmbH&Co, Mullheim, Germany) during 20min at room temperature to eliminate all the organic substances and then washed with MilliQ water. Contact angle measurements were performed as a quality control to assess that all cleanings and measurements do not affect physical-chemical properties of the crystal for crystal reuse purposes, if needed.

3.4.5.   Characterization of TiO₂-crystals

Basic characterization was done to the crystals to gain valuable additional knowledge of the properties of the sensors provided by Q-Sense company. Roughness and wettability values were compared to the results obtained with a Ti c.p. grade II surface previously described at Chapter 2. The working surfaces were prepared as follows:

Surfaces	Preparation
Smooth c.p. Ti grade II	Polished c.p. Ti. The samples were abraded subsequently with 400, 600 and 1200 grit silicon carbide abrasive paper and finally polished with a water suspension of 1 μm

alumina powder.

| TiO$_2$-crystal | QCM-D titanium sensors (QSX 310 Q-Sense AB) |

3.4.5.1. Morphological and topographical characterization

The morphology and topography of the crystal surface was performed with an Environmental Scanning Electron Microscope (ESEM, Electroscan, USA).

The ESEM images show two different parts of the active side of a TiO$_2$-crystal (Figure 3-18). The inner part of the crystal reproduces a very smooth TiO$_2$-coated part, with some micrometric pores. The outer part of the crystal corresponds to a not TiO$_2$-coated part. The crystalline structure of the α-quartz is noticeable.

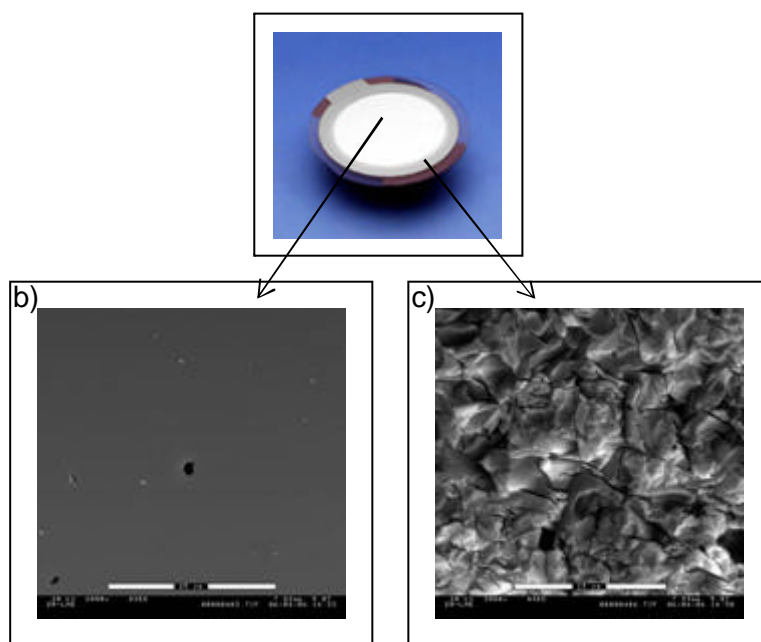**Figure 3-18** *General view of a TiO$_2$-crystal and ESEM images of its active side: b) TiO$_2$ inner part where the protein solution is in contact with (bar: 25μm); and c) α-quartz outer part (bar: 15 μm)*

3.4.5.2. Chemical characterization

The chemical analysis of the TiO$_2$-crystal surface was obtained by X-ray photoelectron spectroscopy (XPS) (PHI 5500 ESCA System, Perkin-Elmer Physical Electronics, USA).

The XPS spectra were obtained using a monochromatic X-ray source, with an Al anode and a K_a radiation energy of 1486,6 eV. The analyses were conducted at a take-off angle of 45°. The elements present on the surface were qualitatively evaluated by low-resolution (pass energy=187,85 eV) survey spectra, whereas high-resolution (pass energy=23,5 eV) spectra were taken to establish the binding energy and peak area for quantitative analysis. The positions of the peaks were referenced to the C 1s at 285,0±0.2 eV.

The determination of the atomic concentration provides the ratio (element/sum of all the elements) present in the acquired data. The calculation is based on the evaluation of the area of the peak, using the sensitivity factors provided by Perkin-Elmer. All data calculations (peak fitting, integration and background subtraction) were performed with appropriate software (Multipak 6.0, Perkin-Elmer Physical Electronics, USA).

XPS analysis revealed the presence of O, C, N and Ti at the crystal surface. The atomic ratios of the most significant elements respect to Ti on TiO₂ QCM-D crystals surfaces are shown in Figure 3-19. An important parameter is the O/Ti ratio; our work detected a value of 2,31 for TiO₂ crystals. As known, the cp Ti oxide film is mainly composed of the stable oxide TiO₂ then, the O/Ti ratio is around 2. The detected difference can be due to the XPS intrinsic uncertainness. The XPS technique has an inaccuracy of quantification around 5-10% for the three primary parameters [81]. This is mainly due to the lack of knowledge of the in-depth composition of the solid. The presence of carbon and nitrogen on the surface is probably contamination adsorbed from air.

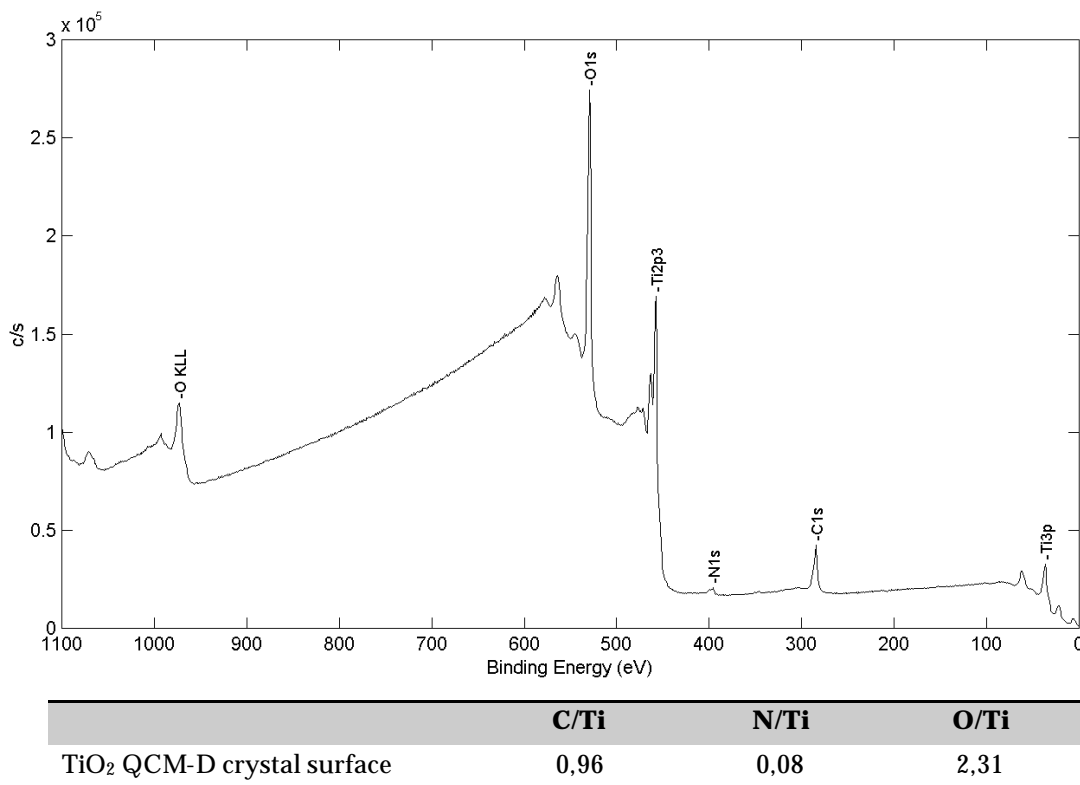|	C/Ti	N/Ti	O/Ti
TiO₂ QCM-D crystal surface	0,96	0,08	2,31

Figure 3-19 *XPS spectra and atomic percent with respect to Ti obtained for the more significant elements of TiO₂ QCM-D crystals surface. Values obtained by XPS-analysis*

3.4.5.3. Structure characterization

Grazing incidence X-ray diffraction (GIXD) (D8 Advance, Bruker® Axs) was carried out in order to evaluate the composition of the TiO_2 QCM-D crystals. The diffractometer was operated at 40 kV and 10 mA using a Ni filter, Cu Kα radiation, and was equipped with a 0,6 mm slit. The incidence angle was fixed at 1° thus limiting the X-ray beam penetration depth. A counting time of 8s per 0.01º step was set for each measurement. A range of 2θ angles of 10 to 80º were scanned.

Figure 3-20 and Figure 3-21 show de diffraction patterns obtained by grazing incidence X-ray diffraction (GIXD) on TiO_2 QCM-D crystals surface. The maximum peaks obtained are 26.64º and 38.22º. When it is marked out a range of 2θ angles between 25 to 45º the peaks 24.05º, 26.87º, and 34.42º are also detected.

The position and intensities of the diffraction peaks from TiO_2 QCM-D crystals and the powder diffraction peaks of relevant substances (according to the JCPDS-International Centre for Diffraction Data cards no. 21-1272 for anatase, no. 21-1276 for rutile, no. 44-1294 for titanium, and no. 46-1045 for SiO_2, quartz) are compared.

The GIXD pattern shows a maximum-intensity peak at 26.64º that corresponds to the quartz crystal where TiO_2 has been evaporated on. Titanium and anatase-TiO_2 phases were also detected and so, constitute the layer of material tested in the protein adsorption experiments. The prevalence of the SiO_2 signal prevented from a more accurate characterization of the deposited material.
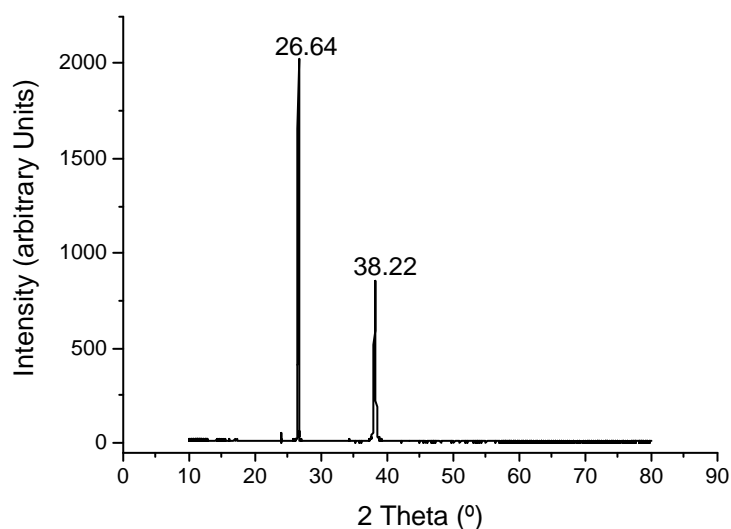

Figure 3-20 *General pattern of the grazing incidence X-ray diffraction performed on TiO₂ QCM-D crystals surface*
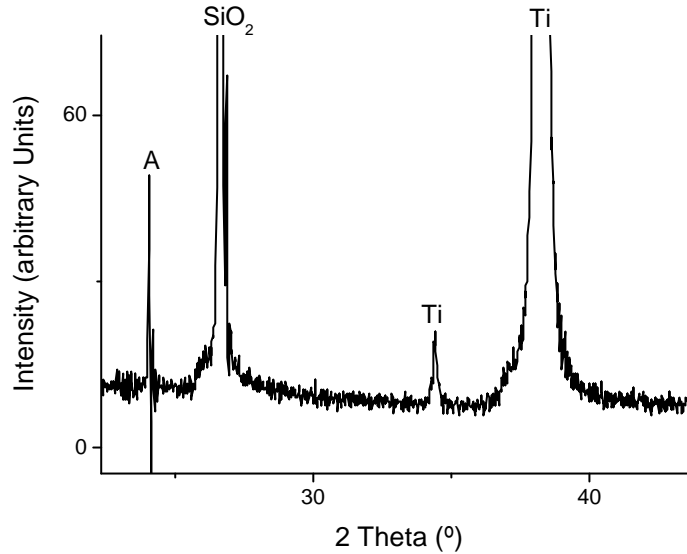
Figure 3-21 *2?=23-44º range of the grazing incidence X-ray diffraction pattern seen at Figure 3-20. A: titanium dioxide, anatase; Ti: titanium; SiO$_2$: silicon oxide, quartz.*

3.4.5.4. Roughness characterization

The roughness measurements were performed with an interferometer microscope (Optical Profiling System, Wyko NT1100, Veeco, USA). Images were taken using a 10X objective. A Gaussian filter was used to separate waviness and form from roughness of the surface by applying a cut-off value (λ_c) of 0,25 mm for smooth surfaces according to ISO 11562:1996 standard.

The selected parameters for the study were two amplitude ones (R_a: arithmetic average roughness, R_y: maximum peak-to-valley height) and two spacing factors (P_c: peak density and S_m: average mean line spacing); all of them explained in detail at Chapter 2 of this document (see section 2.3.4.2.2). Moreover, the results were compared to those obtained for c.p. Ti grade II surfaces at Chapter 2 (see section 2.3.5.2) and shown at Table 3-4.

Table 3-4 *Mean-values ± standard deviation of roughness parameters by interferometry for TiO$_2$-crystal sensors and smooth c.p. Ti grade II*

Surface	R_a (nm) ± SD	R_y (nm) ± SD	S_m (mm) ± SD	P_c (1/mm) ± SD
TiO$_2$-crystal	5,11 ± 0,31	182,03 ± 55,42	3,82 ± 0,09	80,58 ± 0,56
Smooth c.p. Ti grade II	34,83 ± 9,69	236,07 ± 63,65	9,48 ± 9,87	43,39 ± 18,72

Both types of surfaces are at the nano-level scale, but TiO$_2$-covered crystal surfaces are smoother than c.p. Ti grade II polished samples. The mean roughness, R_a, of smooth c.p. Ti grade II surfaces is ~7 times greater than the one for TiO$_2$ sensors crystals.

3.4.5.5. Wettability characterization

The measurement of the static contact angle (SCA) of the TiO_2-crystals with ultrapure distilled water (Millipore) was carried out with the sessile drop method. Drops were generated with a micrometric syringe and deposited on the substrate surface. The wettability studies were performed with a contact angle video based system (Contact Angle System OCA15plus, Dataphysics, Germany) and analysed with the SCA20 software (Dataphysics, Germany). The wettability of the coated TiO_2-crystal was compared to a Ti c.p. grade II surface described at Chapter 2 (see section 2.4.6.1). TiO_2-crystals were cleaned (described in section 3.4.4) to reuse them. Then, the influence of the cleaning protocol was also studied. A minimum of five measurements for three replicas were performed to obtain representative data.

Table 3-5 shows the wettability results of a pristine TiO_2-crystal and a c.p. Ti grade II dis. Additionally, representative images of the contact angle obtained are shown in Figure 3-22. Pristine TiO_2-crystals are more hydrophilic than smooth c.p. Ti grade II, differences are statistically significant (p-value < 0,05, Fisher test). The facts that, c.p. Ti grade II surfaces are rougher (at the nano-level scale) than the crystals may explain this difference.

Moreover, Table 3-6 and Figure 3-22 report the mean values of the contact angle measurement for a new and ten-times used and cleaned TiO_2-crystal. In that case, no statistical differences were found between the new and the cleaned samples. The cleaning process does not affect the roughness parameters of the crystal surface, which is probably the cause that no effect of the cleaning method is observed on the wettability of the TiO_2-crystals.

Table 3-5 *Contact angle values for a pristine TiO_2-crystal and a TiO_2 surface*

	Contact angle (º)
Smooth c.p. Ti grade II	66,29 ± 4.62
Pristine TiO_2-crystal	51,25 ± 2.87

Table 3-6 *Contact angle values for a pristine TiO_2-crystal and a ten-times used and cleaned TiO_2-crystal*

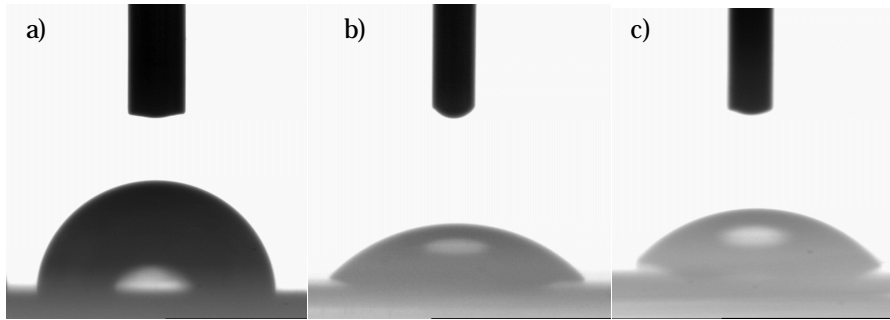|	Contact angle (º)
Ten-times used and cleaned TiO_2-crystal	55,00 ± 2.85
Pristine TiO_2-crystal	51,25 ± 2.87

Figure 3-22 *Contact angle images of: (a) a c.p. Ti grade II surface, (b) a new TiO$_2$-crystal, (c) a ten-times cleaned TiO$_2$ crystal*

3.4.5.6. Statistics

ANOVA tables with Fisher or Tukey multiple comparisons test were calculated to evaluate statistically significant differences between the average values of contact angle for the different surfaces analysed. Tukey's test was used to compare samples of different sizes, whereas Fisher test was applied when samples were of the same size. The level of significance was p-value<0.05. Statistical tests were carried out with Minitab ™ Release 14 (Minitab Inc.,USA) software.

3.4.6. Conclusions

❖ TiO$_2$ evaporated films on QCM-D crystals are homogeneous and smooth ($R_a \approx$ 5nm).

❖ The main component of the crystal surface is TiO$_2$.

❖ Titanium and anatase are the main phases detected on TiO$_2$ QCM-D crystals by grazing incidence X-ray diffraction.

❖ New TiO$_2$-crystal is more hydrophilic than smooth c.p. Ti grade II. No differences between new and re-used TiO$_2$-crystals have been found.

3.5. Single-protein adsorption

3.5.1. Materials

3.5.1.1. TiO$_2$ crystals

The QCM-D sensors (Q-Sense, Sweden) with gold electrode were polished crystals with a fundamental frequency of 5MHz. The gold-coated crystal (14mm) was covered with TiO$_2$ by vapour deposition as explained in section 3.4.4. The crystals were reused after cleaning (see section 3.4.4 for cleaning procedure protocol).

3.5.1.2. Protein solutions

Three different proteins were used in this work: human fibronectin (Fn), human fibrinogen (Fbg) and bovine serum albumin (BSA) all them purchased at Sigma (Sant Louis, USA). The concentrations used for each protein were different depending on the assay. The exact values will be explained bellow in section 3.5.2.1.

3.5.2. Methods

3.5.2.1. Solution concentration and temperature

Single adsorption studies of Fn, Fbg and BSA on a crystal coated with TiO$_2$ were performed. At monoprotein adsorption studies adsorption on TiO$_2$ surface from solutions containing only one protein are analyzed. The kinetics and conformation of the three studied proteins were studied at different protein concentrations and moreover, the effect of temperature on the protein adsorption was also studied.

- Concentration: Different protein concentrations were tested to determine their effect on the protein-adsorption kinetics. The selected protein concentrations, based on bibliography studies [23;26;29;34;35], were:

  a) Fibronectin: 20 µg/ml – 30 µg/ml – 40 µg/ml – 50 µg/ml

  b) Fibrinogen: 80 µg/ml – 100 µg/ml

  c) Bovine serum albumin: 100 µg/ml

- Temperature: The effect of temperature on protein kinetics and conformation was also studied. Tests at room, 25⁰C, and body, 37⁰C, temperature were performed.

3.5.2.2. The experimental assay

For single-protein experiments, the following protocol was applied (Figure 3-23):

(0) PBS 1X Baseline: A constant baseline is established with PBS 1X.

(1) Protein solution temperature setting: The protein solution of study is introduced from the reservoir to the Temperature-loop. The protein is then kept at the desired temperature.

(2) Protein solution introduction to the QCM-D sensor: The solution is transported into the crystal by opening the sensor part. The protein gets in contact with the crystal surface and then, the device suffers the frequency and dissipation changes due to protein adsorption.

(3) Δf and ΔD stability: The assay will be considered finished when the frequency and the dissipation shift reach a constant value by time, i.e. plateau, meaning that the a steady-state in the adsorption process has been obtained.

(4) Cleaning of non-attached proteins: To detach the non-adsorbed proteins, the crystal is cleaned with PBS 1X.
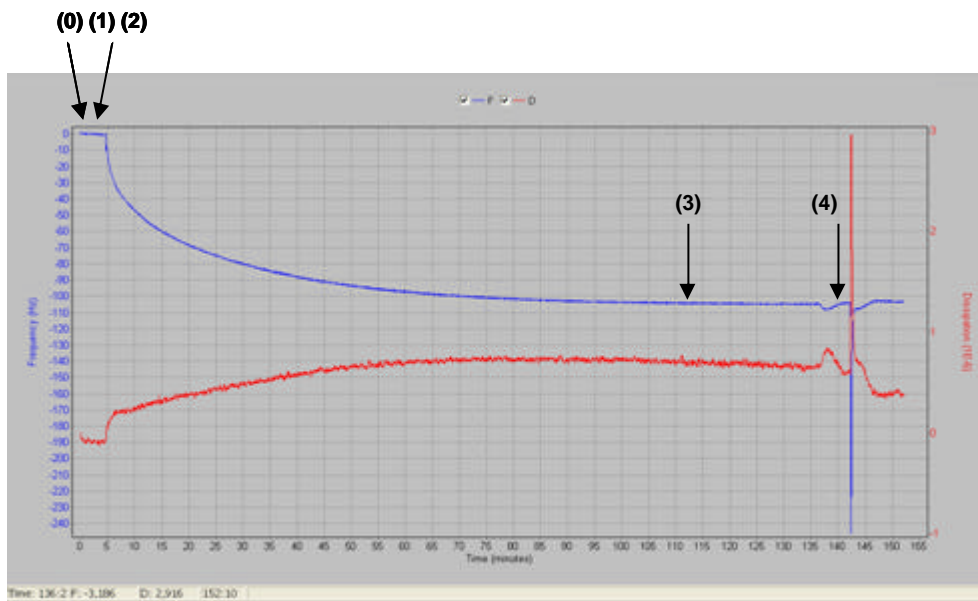

Figure 3-23 *Representative plot of a single-protein experiment with the corresponding steps: (0) PBS 1X baseline; (1) Protein solution temperature setting; (2) Protein solution introduction to the QCM-D sensor; (3) **D**f and **D**D stability, steady-state for protein coverage; (4) Cleaning of the non-attached proteins*

A minimum of three assays were performed for each protein solution (Fn, Fbg or BSA) at each concentration and temperature conditions.

3.5.3. Results

3.5.3.1. Fibronectin adsorption on TiO$_2$-crystals

Figure 3-24 and Figure 3-25 summarize the main results of Fn adsorption on TiO$_2$-crystals. Figure 3-24 show $\Delta f(t)$ and $\Delta D(t)$ vs time for adsorption of Fn at different concentrations in PBS 1X solution on TiO$_2$-crystals. All concentrations cause an initial rapid mass increase followed by a slower frequency decrease as the surface saturates its capacity of adsorbing proteins. The different studied concentrations (see 3.5.2.1) have shown different stable frequency values, i.e. constant frequency by time (Figure 3-24 left). As expected, the higher the protein concentration, the more negative frequency shifts with time and then, higher mass is adsorbed at the surface. Each increment of protein concentration also implies an increment of the frequency shift at the stable value. Specifically, the difference of frequency shift at the stable point, between the tests at 20 µg/ml and 30 µg/ml is around 7,5 Hz (an increment of 45%); a 13% between 30 and 40 µg/ml and a 2% between 40 and 50 µg/ml.

Concerning to the dissipation results (Figure 3-24, right), the higher the protein concentration, the higher the shift in energy dissipation is. This is true but in the case of the solution at 50µg/ml, which has a final dissipation shift lower than the obtained for the solution at 40µg/ml Fn-concentration.
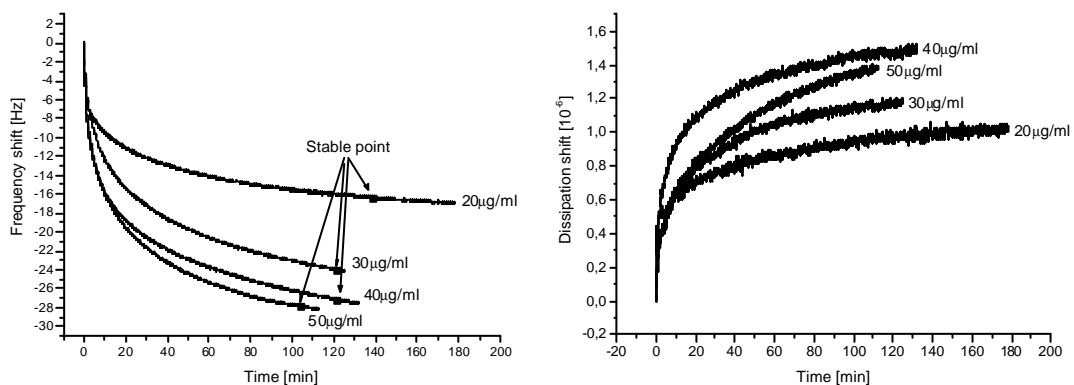

Figure 3-24 *Frequency shift (left) and dissipation shift (right) vs time plots of Fn adsorbed on TiO$_2$-crystals at different protein concentrations, 20, 30, 40 and 50 µg/ml, in PBS 1X*

The $\Delta D/\Delta f$ plots show almost equal type of slope response as well as slope value, which is around $-0,07.10^{-6}$/Hz, for all the studied Fn concentrations (Figure 3-25). Again, the

50µg/ml Fn-concentration assay is an exception because two slopes can be detected. The first slope is slightly less high compared to the other series, but at the end of the experimental time, the slope changes reaching values similar to the ones of the other series.
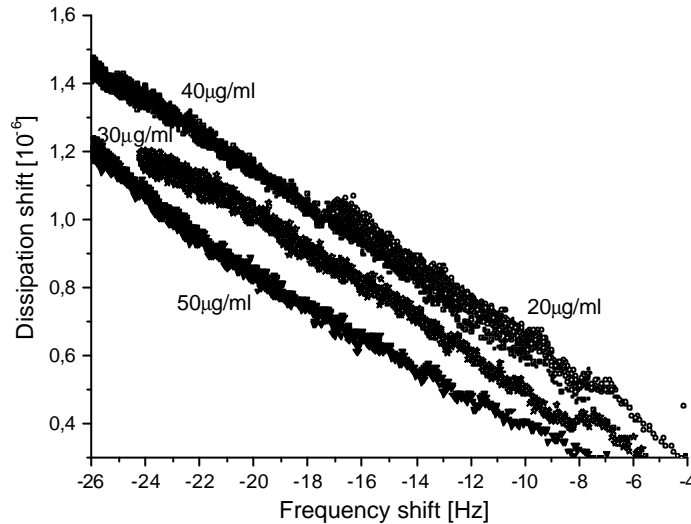

Figure 3-25 *DD vs Df plots of the Fn adsorbed layer on TiO$_2$-crystals for different protein concentrations 20, 30, 40 and 50 µg/ml in PBS 1X*

Sauerbrey and Voigt models have been used to obtain the thickness of the protein adsorbed layer on TiO$_2$-crystals. Results on Figure 3-26, left column, show differences between both approximations, which means that the use of the Sauerbrey equation is not appropriate for the tested system.

Surface mass density was also calculated from the Voigt model when multiplying the Voigt calculated thickness by the protein density and so, assuming a homogeneous distribution of the proteins on the surface of the crystals. The higher the protein concentration in solution, the higher the calculated thickness and the surface mass density (Table 3-7). For all the studied Fn concentrations, Sauerbrey model underestimates the thickness and the surface mass density of the protein layer.

Viscosity remained constant during time for all the working concentrations, and the obtained value, around 0,0036 kg/ms, was statistically the same for all cases. Shear elastic modulus changed depending on the studied protein concentration between 6 and 7×10^5 Pa; and fluctuated with time in 30 µg/ml Fn-concentration solutions (Figure 3-26, right column).
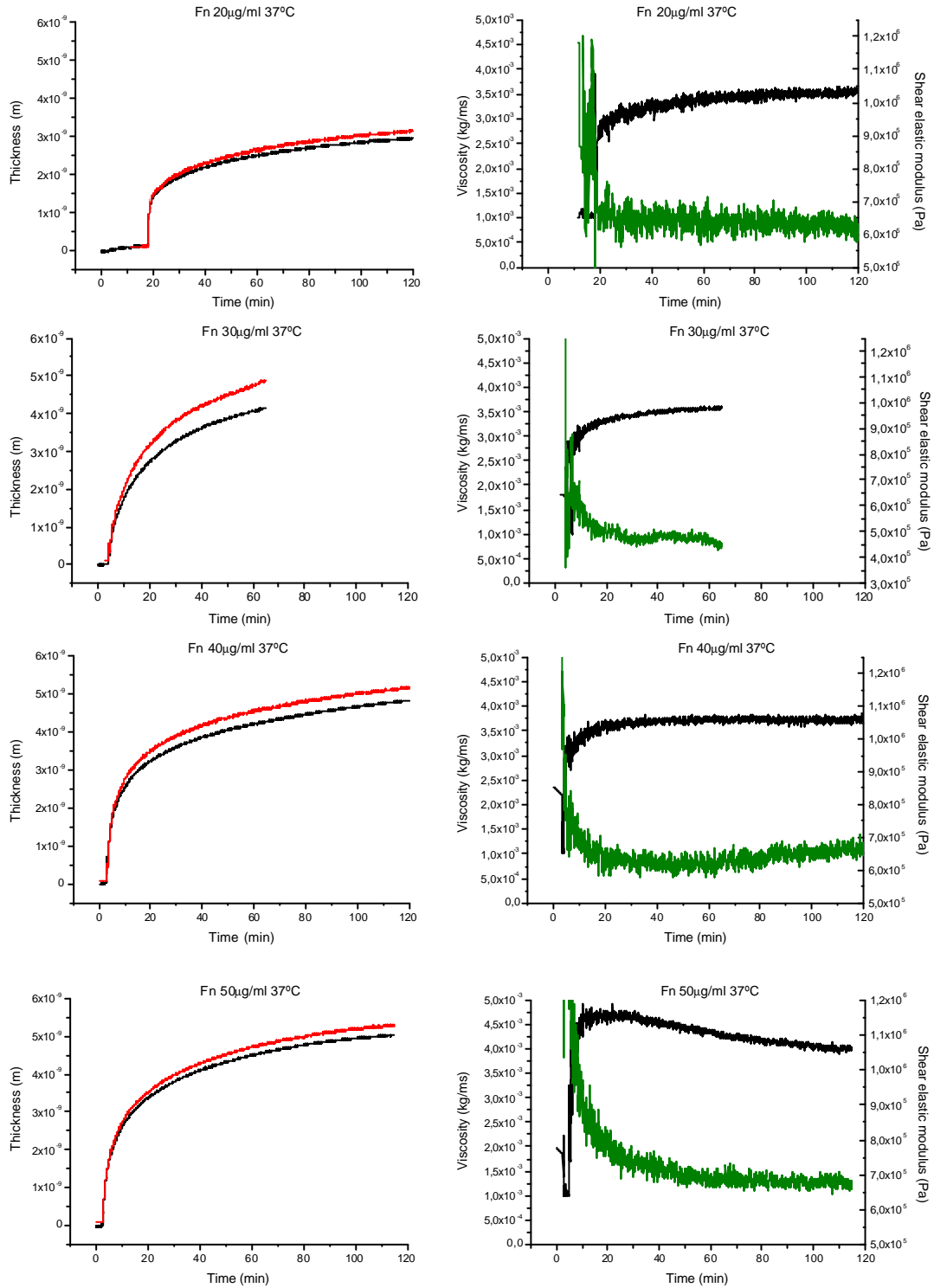
Figure 3-26 *Protein layer parameters obtained after Fn adsorption, on TiO₂ crystals, at different protein concentrations in PBS 1X solution. Left column corresponds to the protein adsorbed layer thickness calculated with Voigt (red) or Sauerbrey (black) models. Right column shows the viscosity (black) and the shear elastic modulus (green) calculated using Voigt model. All the experiments were performed at 37ºC and at different Fn concentrations (20, 30, 40, and 50 mg/ml graphs, from top to bottom). Results were obtained using QTools software from QCM-D experimental results*

Table 3-7 *Thickness, surface mass density, viscosity and shear elastic modulus obtained by using Voigt model of the absorbed Fn protein layer on TiO₂ crystals at different protein concentrations in PBS 1X solution after 60min of adsorption*

Fn concentration	Thickness (nm)	Surface mass density (ng/cm²)	Viscosity (kg/ms)	Shear elastic modulus (MPa)
20 µg/ml	2,60 ± 0,2	312,0 ± 3	0,0035 ± 0,000	0,48 ± 0,1
30 µg/ml	4,75 ± 0,1	570,0 ± 2	0,0036 ± 0,000	0,46 ± 0,1
40 µg/ml	4,83 ± 0,3	579,6 ± 4	0,0037 ± 0,001	0, 62 ± 0,2
50 µg/ml	4,90± 0, 6	588,0 ± 7	0,0049 ± 0,001	0, 68 ± 0,1

3.5.3.2.   Fibrinogen adsorption on TiO₂-crystals

The results obtained for the fibrinogen adsorption (Figure 3-27); illustrate that the higher the concentration, the higher the frequency shifts. In particular, the difference of frequency shift at the stable point for the two studied protein concentrations is near 25%. Furthermore, the higher the Fbg concentration, the higher the dissipation shifts.
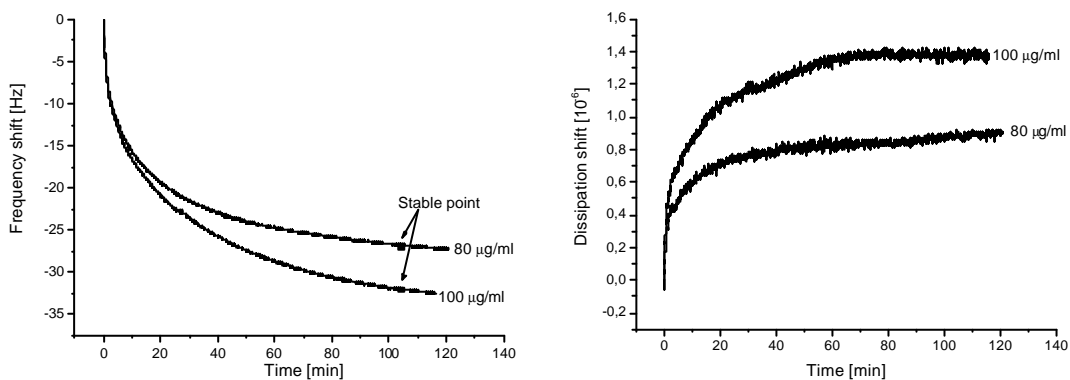
Figure 3-27 *Frequency shift (left) and dissipation shift (right) vs time plots of Fbg adsorption on TiO₂-crystals at 80 and 100 **m**g/ml protein concentration in PBS 1X*

The frequency shift versus dissipation shift plot (Figure 3-28) shows a single slope during protein adsorption on titanium but a slight change is detected at the end of the adsorption time. The slope value tends to zero indicating an increase of the rigidity of the protein layer with the added mass. This response is more evident for the higher in 100 µg/ml protein-concentration solution in PBS 1X.
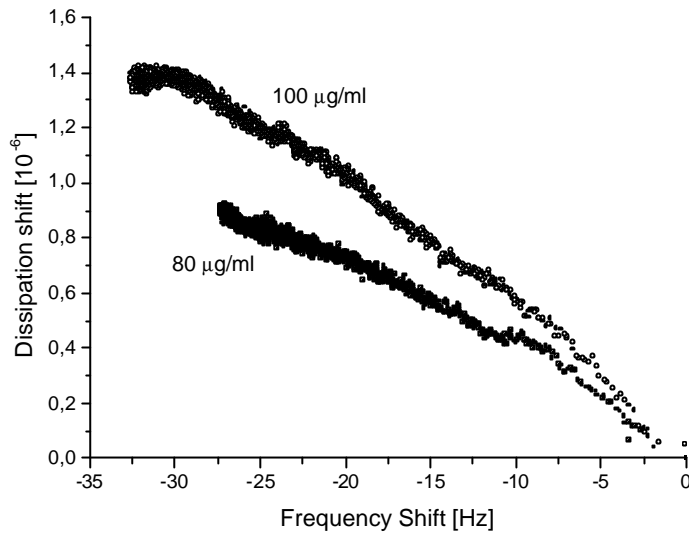
Figure 3-28 *DD vs Df plots of the Fbg adsorbed layer on TiO₂-crystals for 80 and 100 mg/ml protein concentration in PBS 1X*

Thickness of the fibrinogen-adsorbed layer, calculated using Voigt and Sauerbrey models, increases with the protein concentration in solution (Figure 3-29, left column; and Table 3-8). As expected, the Sauerbrey equation underestimates the protein layer thickness. The thickness curves for both protein concentrations show a rapid increase during the early stage of adsorption and subsequently, a moderate steady increase. Surface mass density, calculated with the Voigt model, after 60min of adsorption, is higher for 100 µg/ml concentration (697,2 ng/cm²) than 80 µg/ml (567,6 ng/cm²).

The viscosity of the Fbg protein layer increases very rapid during the first 30min of adsorption, (Figure 3-29, right column). This may indicate an increase of the protein layer rigidity. After 30min of adsorption the viscosity of the adlayer decrease when testing the solution with 80 µg/ml Fbg-concentration, but stays constant with a sudden increase after 60 min of adsorption when testing the solution with higher protein concentration. Shear elastic modulus, after a slight decrease, stabilizes its value to $5,3 \times 10^5$ and $4,6 \times 10^5$ Pa for 80 and 100 µg/ml protein concentration in PBS, respectively, after 1 hour of adsorption.
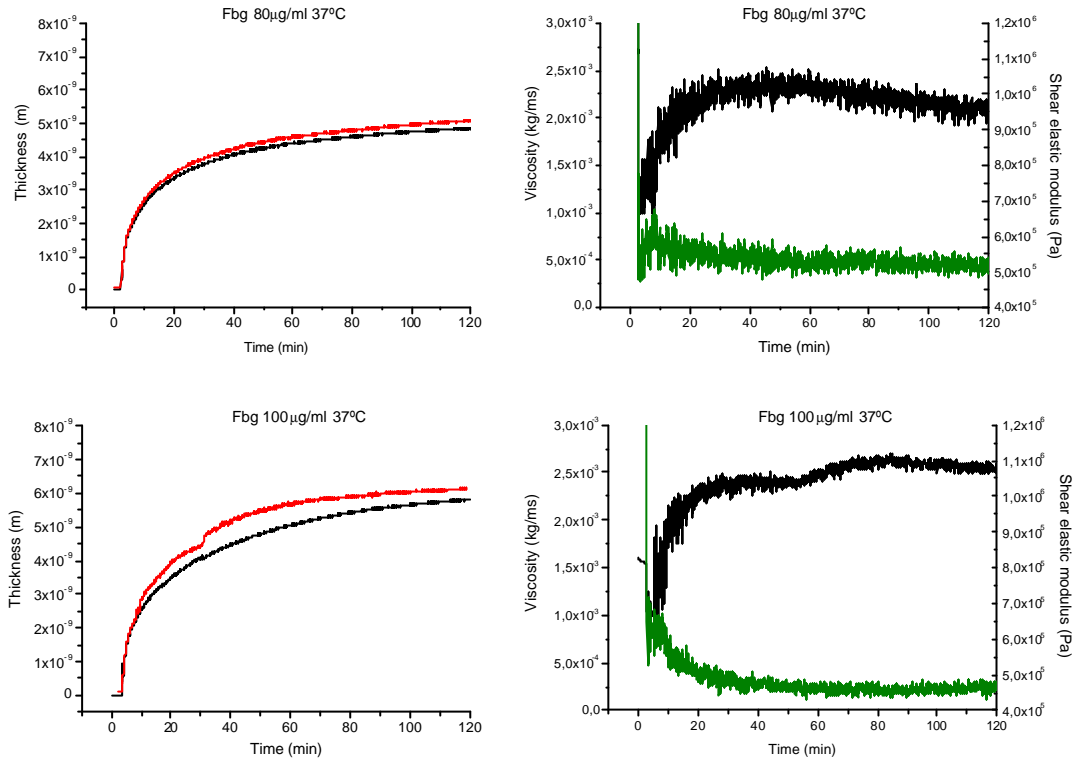
Figure 3-29 *Protein layer parameters obtained after Fbg adsorption on TiO₂-crystals, at different protein concentrations in PBS 1X solution. Left column shows the evolution with time of the thickness of the protein-adsorbed layer calculated using Voigt (red) and Sauerbrey (black) models. Right column shows the viscosity (black) and the shear elastic modulus (green) calculated with the Voigt model. All the experiments were performed at 37ºC and at different Fbg concentrations (80 and 100 mg/ml, from top to bottom). Results were obtained using QTools software from QCM-D experimental results*

Table 3-8 *Thickness, surface mass density, viscosity and shear elastic modulus calculated using Voigt model of the absorbed Fbg protein layer on TiO₂-crystals at different protein concentrations in PBS 1X solution after 60min of adsorption*

Fbg concentration	Thickness (nm)	Surface mass density (ng/cm²)	Viscosity (kg/ms)	Shear elastic modulus (MPa)
80 µg/ml	4,73 ± 0,3	567,6 ± 4	0,0022 ± 0,001	0,53 ± 0,1
100 µg/ml	5,81 ± 0,3	697,2 ± 4	0,0025 ± 0,002	0,46 ± 0,2

3.5.3.3. Bovine serum albumin adsorption on TiO₂-crystals

Figure 3-30 shows the frequency shift and dissipation vs. time plots of BSA adsorption on TiO₂ crystal surfaces for the studied protein concentration, 100 µg/ml. The f-shift and the D-factor shift decrease and increase, respectively, with time; rapidly during the first 30 min.
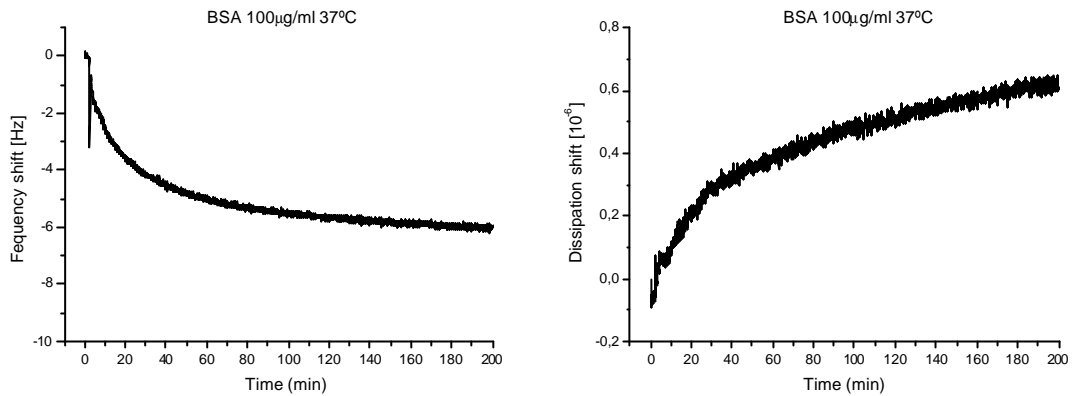
Figure 3-30 *Frequency shift (left) and Dissipation shift (right) vs time plots of BSA adsorption on TiO$_2$-crystals for 100 μg/ml protein concentration in PBS 1X*

Figure 3-31 presents the ΔD vs Δf plot of the BSA adsorbed layer on TiO$_2$-crystals. Three well-defined different slopes during the BSA protein adsorption assay can be detected. The slope increases while the frequency shift increases in module, which indicates a decrease of the rigidity of the BSA adsorbed protein layer when more mass is adsorbed on the crystal during the protein adsorption experiment.
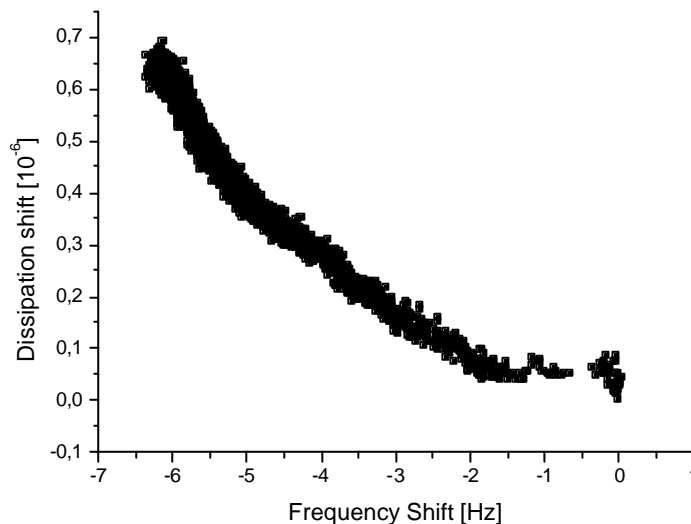
Figure 3-31 **DD vs Df** *plot of the BSA adsorbed layer on TiO$_2$-crystals for a concentration of 100 μg/ml in PBS 1X*

Figure 3-32 and Table 3-9 show the thickness of the adsorbed protein layer using Voigt and Sauerbrey models. The thickness steadily increases with time. Initially, the two curves overlap, but after 40min, the Sauerbrey curve underestimates the adsorbed mass, as in Fn- and Fbg adsorption experiments. The viscosity slightly decreases during the assay, from 0,003 kg/ms down to 0,0023 kg/ms. This is accompanied with a decrease in

its rigidity. The shear elastic modulus decreases, then, with time. It reaches a final value around 0,26 MPa.
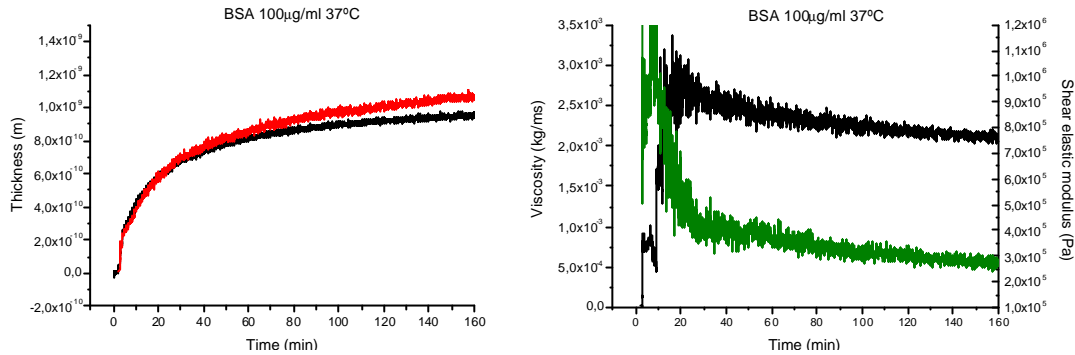
Figure 3-32 *Protein layer parameters obtained after BSA adsorption on TiO₂-crystals, at a concentration of 100 mg/ml in PBS 1X. Left column corresponds to the protein layer thickness calculated using Voigt (red) and Sauerbrey (black) models. Right column shows the viscosity (green) and the shear elastic modulus (black) calculated with Voigt model. All the experiments were performed at 37 °C. Results were obtained using QTools software from QCM-D experimental results*

Table 3-9 *Thickness, surface mass density, viscosity and shear elastic modulus obtained using Voigt model of the absorbed BSA protein layer on TiO₂-crystals after 60 min of adsorption*

BSA concentration	Thickness (nm)	Surface mass density (ng/cm²)	Viscosity (kg/ms)	Shear elastic modulus (MPa)
100 µg/ml	0,85 ± 0,2	102,0 ± 2	0,0024 ± 0,003	0,30 ± 0,1

3.5.3.4. Comparison of Fn, Fbg and BSA protein adsorption on TiO₂-crystals

Dissipation shift versus frequency shift of the different studied proteins with Fn at 40µg/ml, Fbg at 100µg/ml and BSA at 100µg/ml concentration in solution is shown in Figure 3-33. A unique slope is detected for Fn; while two phases are detected for Fbg, the second one starts at higher values of frequency shift (higher mass). Finally, BSA shows three phases, all of them have a higher slope compared to the rest of proteins. The lower slope ΔD/Δf value is found for Fbg series.

Viscosity, thickness, elastic shear modulus, and surface mass density of the adlayer calculated using the Voigt model for the protein-adsorption experiments shown in Figure 3-33 are shown and compared in in Figure 3-34.

Fbg adsorption yields the thickest layer and the highest surface mass density under these specific experimental conditions. BSA yields a noticeable thinner and less dense layer compared to the obtained with the other working proteins (Figure 3-34, a) and b)).

Adsorption of Fn gives a more rigid and viscous adlayer on the TiO_2-crystals than the other tested proteins.
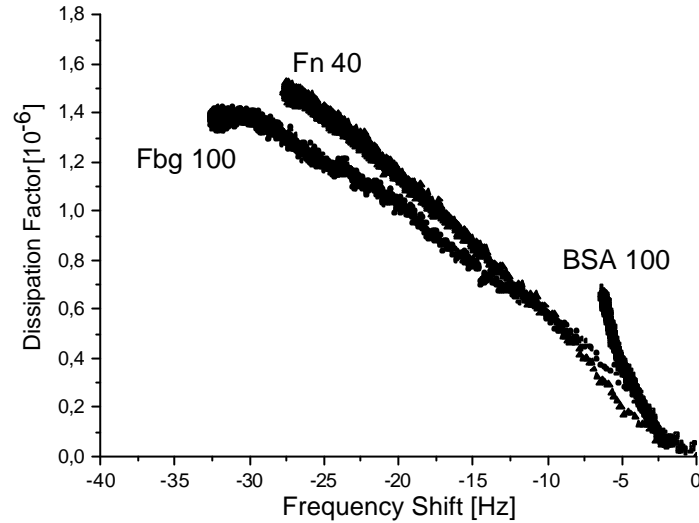
Figure 3-33 *DD vs Df plots of the Fn (40 mg/ml), Fbg (100 mg/ml) and BSA (100mg/ml) adsorbed layer on TiO_2-crystals*
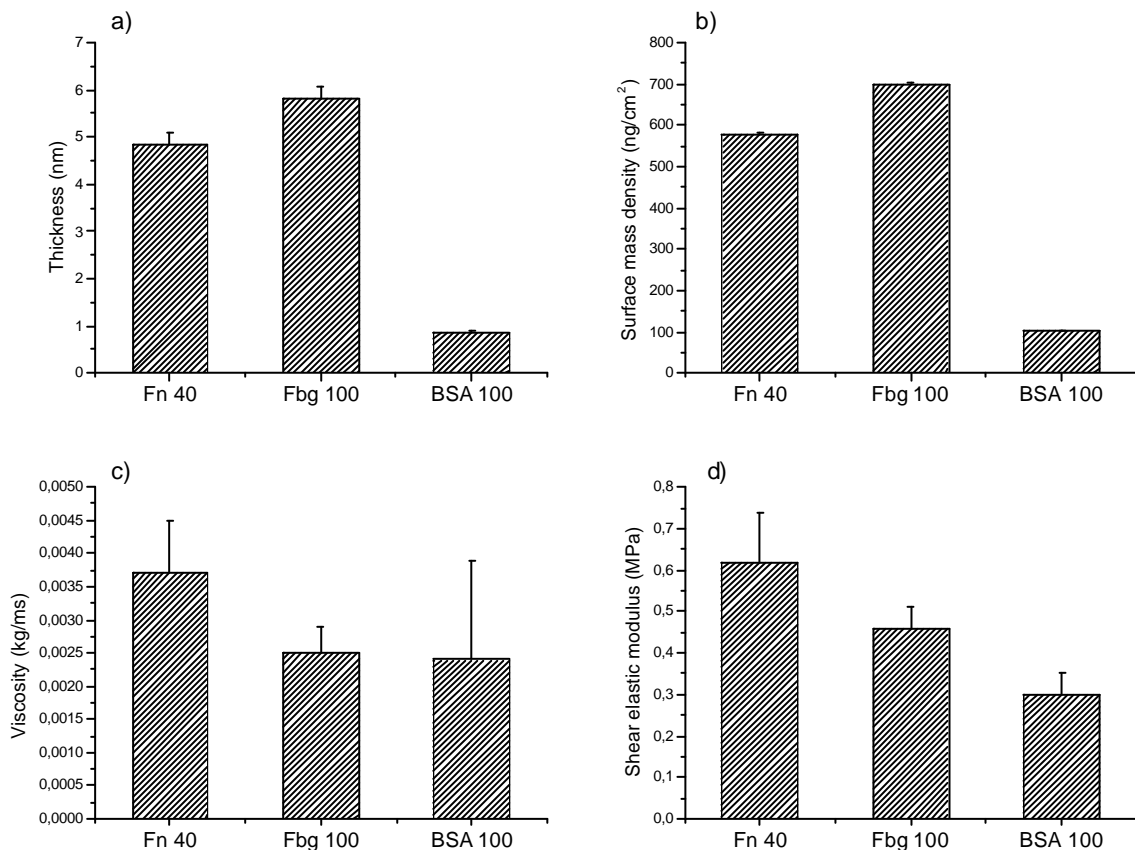
Figure 3-34 *Comparison of a) thickness, b) surface mass density, c) viscosity and d) shear elastic modulus of different protein adsorbed on TiO_2-crystal calculated suing Voigt model. Calculations were performed after 60min of adsorption using 40mg/ml Fn, 100mg/ml Fbg, and 100mg/ml BSA solutions in PBS.*

3.5.3.5. Effect of temperature

Figure 3-35 shows the frequency shift (left) and the dissipation shift (right) vs time at two studied temperatures, 25 ºC and 37 ºC, for 100 µg/ml BSA, 40 µg/ml Fn and 80 µg/ml Fbg solutions in PBS. The higher the protein solution temperature, the higher is the module of the frequency shift for all tested proteins. The higher of the protein solution temperature, the higher the dissipation shift, i.e., of the higher the viscosity of the adsorbed protein layer on the TiO$_2$-crystals.
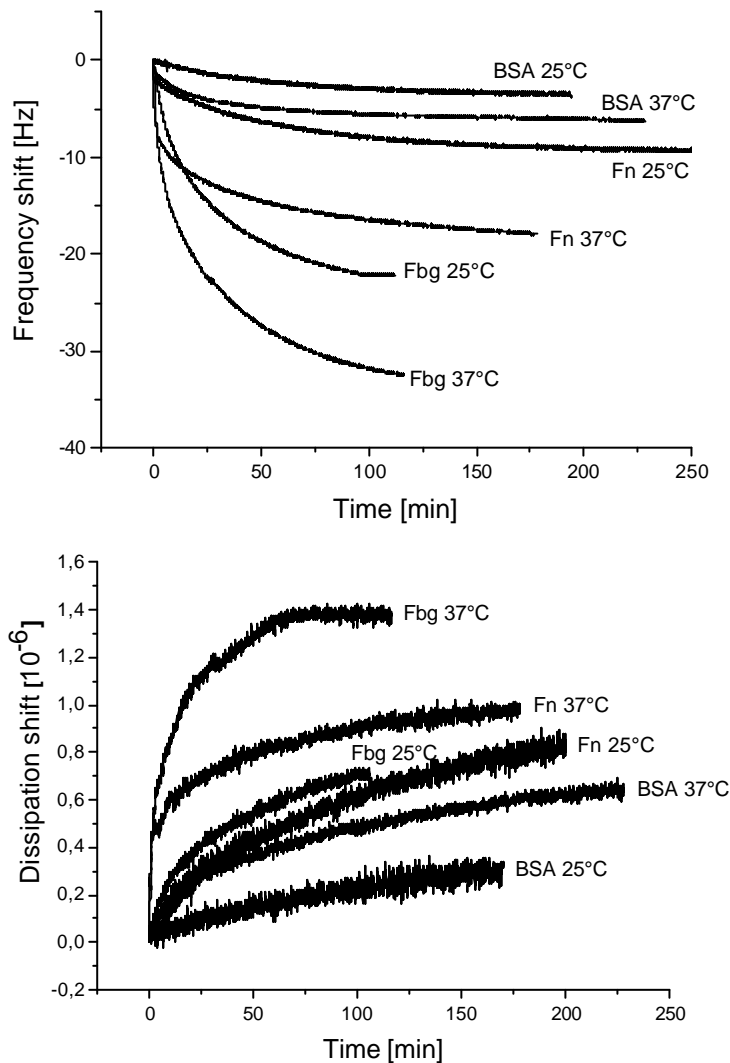
Figure 3-35 *?f vs. time (top) and ?D vs. time (bottom) for BSA [100 µg/ml], Fn [40 µg/ml] and Fbg [80 µg/ml] in PBS at 25 ºC and 37 ºC*

3.5.4. Discussion

In the present study, the initial adsorption behaviour of fibronectin, fibrinogen and albumin at different concentration in PBS, on titania surfaces was monitored by the QCM-D technique. The Sauerbrey equation gives a good estimation of the adsorbed mass only when the adsorbed protein layer on the studied surface is rigid. By measuring the dissipation, it is possible to determine if the relation is valid or not for the studied protein films. In all the studied cases, both Sauerbrey and Voigt models have been investigated to determine the valid description for our studied different protein layers. From the results obtained is possible to conclude that the Sauerbrey equation is not appropriate to describe the investigated system since significant values of dissipation shift have been recorded and subsequently, thickness of the layer is underestimated when this model is used. Then, for the following discussion and for comparison purposes, only the parameters calculated (protein layer thickness, viscosity and shear elastic modulus) using the Voigt model will be considered. In addition, surface mass density has been calculated from thickness values obtained applying the Voigt model, too.

Fibronectin and fibrinogen adsorbed from solutions at different concentrations onto TiO_2-crystals have been studied. One concentration for each protein has been chosen to do the comparison of the overall adsorption behaviour between proteins; specifically 40 µg/ml Fn, 100 µg/ml Fbg and 100 µg/ml BSA in PBS. The previous values have been selected in terms of protein adsorption saturation on the titanium surfaces as explained below.

3.5.4.1. Fibronectin adsorption on TiO_2-crystals

Fibronectin, a cell adhesive protein, plays an important role in governing the interactions of implants with their surrounding biological entities [20;82]. It is predicted that the attachment of Fn to titanium biomaterials will improve the connection of implants to the surrounding host hard-tissues [83].

The effect of Fn concentration in PBS solution on the adsorption response of the protein on TiO_2-crystals has been investigated. The increase of frequency shift when increasing protein concentration is an expected result (Figure 3-24). However, it is worth noting that the increase of frequency shift and so, the increase of the amount of protein adsorbed on TiO_2 is not linear with the protein concentration. For the lower protein concentrations the effects on the frequency shift when increasing protein concentration is higher than for the higher concentrations. In fact, when protein concentration is increased from 40 µg/ml (Fn 40) to 50 µg/ml (Fn50) a slight 2% increase in frequency

shift is recorded, which translates in a 9 ng/cm² increase in surface mass density (Table 3-7).

This result can indicate that the solution at 40 µg/ml of protein concentration saturates the available space for adsorption of proteins on the TiO_2-surfaces. The small quantity of more molecules that are added in the adlayer are probably displacing water molecules and competing for a few available spaces. This is yielding a more compact layer of adsorbed proteins layer.

The displacement of water molecules by protein molecules would be accompanied with a decrease in ΔD, and an increase in the viscosity and elastic shear modulus of the layer. The results obtained support this hypothesis (Table 3-7). This includes the change in the slope of the curve for Fn50 in the ΔD vs Δf plot (Figure 3-25). In fact, ΔD vs Δf plot gives an estimate of how new mass added affects the protein structure of the formed layer. For almost all the time of adsorption during the experiment the slope of the curve is slightly lower than for the rest of the protein-concentration solutions, indicating, again, a more rigid adlayer. The fact that the $\Delta D/\Delta f$ slope is almost invariable ($\approx 0,07?10^{-6}$/Hz) for all the rest of the adlayers obtained with other protein-concentration solutions indicates that the proteins does not change their conformation in the layer if the concentration of the solution is changed.

Thickness measured by the QCM-D technique was derived from the frequency shift using the Sauerbrey equation and was also calculated with Voigt model. The Sauerbrey equation is strictly valid for rigid, nonporous, homogeneous adlayers and it has been shown that taking the viscoelastic properties of the adsorbed layer into account adds a correction to the Sauerbrey thickness. This correction depends on the dissipation factor. For thin layers it is always positive and in our case is around 10% as confirmed by different authors [62;84]. The thickness of a protein layer is continuously increasing until reaching a value which is characteristic of the protein, the surface, and the experimental conditions. This corresponds to the random sequential model where the adsorbing molecules sequentially occupy the available surface [30].

Protein layer thickness was calculated using Sauerbrey and Voigt models (Figure 3-26, left column). For all studied concentrations, during the firsts 10 min of contact between the protein solution and the surface, both thickness curves overlap indicating that the protein layer is rigid or not significantly thick to make the viscoelastic properties of it a relevant mechanical feature. During further adsorption the two models differ due to the significant effect of the viscoelastic properties of the layer of proteins adsorb on the TiO_2-crystals. It is worth noting that after 60 min of adsorption, the thickness of the protein layer on the surface is very similar, around 4,80 nm, when testing solution at 30, 40 and 50 µg/ml of Fn-concentration (Table 3-7). This can be due to the fact that when the layer is near 5,00 nm thick, the quantity of adsorbed protein reaches a steady state because there are not more sites on the surface available for Fn to attach to. Conversely, for lower concentration, 20µg/ml, the obtained thickness was 2,60 nm (Table 3-7). This result

correlates with the obtained values, ~2,5 nm by MacDonald et al [20] with AFM; which is in accordance with the reported value of 2nm for the diameter of the Fn molecule based on electron microscopic analysis on mica [85]. The highest thickness, ~4.80 nm, obtained with adsorption of higher protein concentration solutions could be attributed to a more extended Fn form, which depends on the substrate and solution conditions [86].

The conformation of human plasma fibronectin will vary depending on whether or not the molecule is in solution or is surface bound. Moreover factors such as temperature, pH, and ionic strength of the local environment also will play a role in determining the molecular shape of fibronectin. In solution under normal physiologic conditions, Fn has been reported to assume a globular compact form [87]. This compact form of Fn is stabilised by interdomain electrostatic interactions [88]. At temperatures above 40 ⁰C, extreme pH levels, or increased ionic strength, fibronectin assumes a more extended form [88;89]. Based on the mentioned considerations, it can be assumed that our experimental conditions of pH 7,4 and a temperature 37 ⁰C would favour Fn in a globular-like conformation when in solution at least for concentration of 20 μg/ml; while a more extended form is obtained for higher concentrations.

Information of the Fn conformation from the thickness results can also been extracted. The theoretical values for Fn adsorbed on TiO_2 surface knowing the size and molecular weight of the protein [23]; indicates, for closely packed monolayers formed by side-on and end-on adsorption the concentrations are 175 ng/cm^2 and 4100 ng/cm^2, respectively. Demonstrating that the maximum adsorbed amount determined in this work by QCM-D technique, 588 ng/cm^2, may correspond to more than one monolayer in the side-on position for all the studied concentrations. Besides to conformation, a minimum Fn concentration seems to be necessary to achieve for cell adhesion. Tamada et al, [26], considered 50 ng/cm^2 the minimum amount for fibroblast cell adhesion. This goal was achieved for all the working concentrations since the minimum Fn mass density obtained in our work was 312 ng/cm^2 with Fn 20 series.

All these results can be used to design strategies to effectively coat implants with physisorbed layers of this very important protein for cell recruitment and adhesion.

3.5.4.2. Fibrinogen adsorption on TiO_2-crystals

It is widely accepted that the plasma protein fibrinogen (Fbg) plays a predominant role in mediating the adhesion and activation of platelets triggering a clotting reaction [70]. Fibrinogen is an anisotropic large protein meaning that one of the three dimensions is very different from the others; for this reason, depending on the protein orientation at the layer, the quantity of molecules adsorbed can be significantly different.

Both, Δf and ΔD vs. time increase when Fbg concentration in the solution increases during all the time of adsorption of the tests, which is an expected result (Figure 3-27). This is confirmed by the fact that thickness of the adsorbed layer and, therefore, its surface mass density, is higher when the concentration of Fbg in solution is also higher (Table 3-8).

The ΔD vs Δf plots for the two solutions at different protein concentrations show a common pattern of steadily decrease in the $\Delta D/\Delta f$ slope up to frequency shifts around 25 Hz (Figure 3-28). This indicates a continuous compactation/rigiditation of the layer along the experiment. This is possibly a consequence either of the appropriate and overall orderly occupation of the spaces in the layer by the added new protein molecules or of the continuous dehydration of when water molecules are replaced by protein molecules in the layer.

The more significant change in the slope for the experiments performed using solutions at the highest protein concentration at the latest part of the experiment can be related to the sudden increased in the calculated thickness after $\approx$ 30 min of adsorption (Figure 3-29, left-bottom). The change in the thickness could indicate a change in the conformation of the proteins adsorbed on the crystals more than a sudden gain of water or protein because a) no sudden change/gain of weight is detected in the shift of frequency vs time curve; and b) a final combined significantly more viscous adlayer and similar elastic shear elastic modulus is obtained, a combination that is not expected in case of more water would be trapped into the adsorbed layer.

One could expect a similar response if the experiment with Fn 80 lasts enough to reached the appropriate surface mass density to produce the conformational changes.

Using Sauerbrey and Voigt models, the calculated values reveal that, again, the use of Sauerbrey equation underestimates the adsorbed thickness of viscoelastic Fbg layers in a 8-13% range. When testing the higher protein concentration solutions, the calculated thickness layer using the Voigt model is 5,81nm, and the corresponding surface mass density is 0,70 μg/ml=700 ng/cm² (Table 3-8). Bai et al. [29] reviewed the fibrinogen adsorption on Ti performed by different studies with different techniques such as optical waveguide spectroscopy, electrochemical and radiolabelling methods and the quantified Fbg amount range from about 400 ng/cm² to 700 ng/cm² as the solution concentration varies from 80 μg/ml to 2 mg/ml after 1 h adsorption. Our results are within this range. But a much higher value of surface mass density, 1,8 μg/cm², was obtained by Rechendorff et al., [90] when testing. 1mg/ml Fbg-concentration in HEPES solution and mass calculated from the 7th overtone. Weber et al., [70], obtained an even higher range, 0,2 and 3,1μg/cm² for other different test surfaces and even higher concentrations of protein (3mg/ml). In their study data was extracted only from the 7th overtone. A direct comparison between the results presented here and those from the literature cannot be made mainly because of the noticeable difference between the protein concentrations in solution that was tested. Moreover the information given by a single overtone such as

the 7th is not enough to obtain reliable protein layer parameters. As explained in section 3.4.2.3, the measurement of multiple overtones is required to model viscoelastic properties and extract correct thickness for films outside the Sauerbrey region. If one of the overtones should be chosen as the representative one, it has to be considered that the higher overtone number is related to a lower penetration/detection depth in the adsorbed protein layer.

3.5.4.3.   BSA adsorption on TiO$_2$-crystals

BSA is a globular, extracellular protein and the main component of the blood transport system and it provides the transport of a range of physiologically compounds like calcium.

Typical frequency shifts and dissipation shifts vs. time curves are observed in Figure 3-30. The shifts are of lower value (in module) than in the case of Fbg and Fn. BSA is a significantly lower molecular-weight protein than the other two, which explains the differences in those lower values in frequency shift.

To obtain further insight into the adsorption of BSA on Ti surfaces, the dissipation shift per frequency shift $\Delta D/\Delta f$-values is explored. If any changes in the slope of the curve occurs during the adsorption process, such changes indicate that the protein binding to the surface undergo structural rearrangements during the adsorption process [91;92]. It has been previously shown at the results section that BSA adsorption on Ti crystals shows a complex behavior, reflected in that the slope of $\Delta D/\Delta f$ changed as a function of the frequency shift during the adsorption process (Figure 3-31). Three distinctive phases on the adsorption process were detected with an increasing $\Delta D/\Delta f$-slope with time. This indicates that the average structural conformation of the protein layer is altered during the adsorption process leading to a less compact and softer protein layer.

Others [93], have showed different BSA adsorption response from 1mg/ml BSA-concentration solutions in Tris buffer on platinum surfaces depending on the surface roughness for, root-mean-square values of 1,49 and 4,62nm. A single phase and two phases during adsorption were detected on flat and rough samples, respectively -root-mean-square=1,49 and 4,62 nm. The results reported here, in agreement with other reported works in the literature [34;93-95], show that surface chemistry, roughness and protein concentration and solvent, strongly affects the protein adsorption response. Specifically, Dolatshaki-Pirouz et al. [93] and our study coincide that a more opened structure with more water content and less stiff protein film is obtained if working at low concentrations such as 50 and 100 μg/ml BSA in solution, respectively. Other studies [93;94;96] have found that with increased protein concentration, around 1

mg/ml, structural rearrangements in the protein film occurs resulting in a stiffer protein layer.

When using Voigt model for viscoelastic materials, the adhered film can be characterized in detail: viscosity, elasticity and thickness of the layer can be more accurately calculated. The results obtained for BSA adsorption on TiO_2-crystals, Figure 3-32, confirm those obtained from the $\Delta D/\Delta f$ analysis, i.e, layer probably hydrates with time, which produces a softer and less viscous adlayer.

Höök et al., [57], determined a surface albumin density of 333 ng/cm² on TiO_2-coated substrates at 22 ⁰C. The lower values 102 ng/cm² reported here can be attributed to the different type of specific albumin used (human serum albumin vs bovine serum albumin).

3.5.4.4. Comparison of Fn, Fbg and BSA protein adsorption on TiO_2-crystals

Among the different properties that can influence on the mass and thickness of the adlayers obtained with different types of proteins, protein concentration in solution and molecular weight of the molecule tested are probably the most influencing ones. Other properties, such as protein conformation when adsorbed on the surface and amount of trapped water into the adlayer may have an important effect on the specific characteristics of the layer of proteins obtained, too.

The results report here confirm previous findings by others because the amount of adsorbed proteins is higher when the protein concentration of the solution is higher, although no detailed theoretical explanation of this phenomenon has been given to date [62].

Fn is a big protein with a molecular weight of 450-500 kDa, which is higher than the one of Fbg, 340 kDa. Consequently, one would expect that surface mass density for the adsorbed layers from Fn solutions would be higher than those obtained for Fbg layers. This is not the case as shown in Table 3-7 and Table 3-8. The fact that the mass surface density from Fbg solutions was higher than from Fn solutions can be due to the higher protein concentration used, 40 and 100 μg/ml, respectively. However, a different effect of the protein conformation adopted as well as the amount of trapped water by the proteins can be hypothesized. Fbg rearranges during the time of the adsorption test, as previously discussed (Figure 3-28). This arrangement could lead to a significant increase in the quantity of water associated to the adlayer. As a consequence, thickness of the layer of Fbg and its surface mass density were higher, but viscosity and shear elastic modulus lower than those for the Fn-adsorbed layer (Table 3-7 and Table 3-8). This hypothesis can be further confirmed by the fact that the shear elastic modulus of the

layer of Fbg adsorbed from the low concentration solution, 80 µg/ml, is higher than the one from the high concentration solution, 100 µg/ml (see Table 3-8).

A complex relationship between all this properties can be speculated. For BSA adsorption results, water is continuously being trapped in the layer during the time of the experiment, as demonstrated in Figure 3-31 and Figure 3-32 as well as with the low values of shear elastic modulus calculated (Table 3-9). However, the thickness and surface mass density obtained for the BSA-adsorbed layer are significantly lower than in the case of the Fn- and Fbg-adsorbed layers. A dominant influence of the molecular weight, size, and globular shape of the protein can be assessed from those results when comparing with other types of proteins.

Taking into consideration that BSA-adsorbed layers incorporated a high quantity of water; a lower viscosity for the BSA-adsorbed layers than the one obtained for the Fbg-adsorbed layers could be expected, too. One possible explanation for the similar values of these those two viscosities is the occurrence of the very thin layer of BSA on the TiO_2-crystals, which can change the energy dissipation of as well as the mobility of the molecules in the layer.

It is also important or relevant value the comparison of the results obtained using the QCM-D with those obtained using other already-established techniques for protein adsorption analysis, such as ellipsometry (ELM) and optical waveguide light mode spectroscopy (OWLS). Höök et al., [57], performed a comparative study between the aforementioned techniques and they found surface mass densities of adsorbed Fbg of $0,39 µg/cm^2$ measured with ELM, $0,45 µg/cm^2$ measured with OWLS, and $1,18 µg/cm^2$ measured with QCM-D, using the Sauerbrey equation at 22ºC. The discrepancy between the different techniques and the differences between the surface mass density reported here and that reported by Höök et al. and Vörös, [57;62]; can be mostly attributed can be explained by the fact that ELM and OWLS are based on optical principles and detect the adsorbed dry mass, while QCM-D detects hydrodynamically coupled water in addition to the protein mass.

Figure 3-34 c) and d) show the viscosity and the shear elastic modulus for the three working proteins. BSA is the protein which adsorbs obtaining the softer layer, since both modulus are low and $\Delta D/\Delta f$ relation is very high compared to Fn and Fbg. Fn 40 has a high shear elastic modulus and viscosity compared to BSA and Fbg, which means a more rigid layer contrasted to the rest of working proteins. Fbg has a similar viscosity as BSA but a higher elastic modulus, its $\Delta D/\Delta f$ relation is the lower indicating the more rigid layer from the three studied systems. The quantity of protein adsorbed depends strongly on the spatial organization of these big molecules.

3.5.4.5. Temperature

The influence of the protein solution temperature in contact with Ti surfaces has been studied at room temperature (25 ºC) and body temperature (37 ºC). As expected, the higher the temperature, the higher of the amount of adsorbed protein on the surface (Figure 3-35). This result agreed with those obtained by others [12;17;97;98]. However, a few other works concluded that protein adsorption decreased when increasing temperature of the protein solution [99;100].

On the one hand, as explained previously in section 3.3.4, only when the Gibbs free energy (Equation 3-1) is negative, spontaneous protein adsorption can occur. If temperature of the solution increases, the Gibbs free energy decreases which may favour spontaneous protein adsorption on Ti surfaces. On the other hand, the diffusion rates of the studied proteins in solution increases with temperature, if no conformational changes occur, and consequently, the number of molecules reaching the surface increases and so the amount of adsorbed protein.

3.5.5. Conclusions

❖ Fibronectin adsorbed on TiO₂-crystals in a one step adsorption process, i.e., Fn did not change its structure and properties once adsorbed on the surface. The same response was absorbed when testing different Fn concentrations in PBS.

❖ Fibrinogen adsorbed on TiO₂-crystals showed two different structures/conformations. The second step of adsorption was characterized by a significant increase in the rigidity of the adlayer. A different conformation of Fbg on the surface in two different steps is speculated.

❖ Bovine serum albumin adsorbed on TiO₂-crystals showed three different structures/conformations. As increasing the adsorbed mass, the increasing steps of adsorption were characterized by a decrease in rigidity of the adlayer. Protein layer probably hydrates with time, which produces a softer and less viscous adlayer.

❖ For Fbg and Fn solution in PBS adsorbed on TiO₂ surfaces, the higher the initial protein concentration in solution, the higher the protein adsorption. This indicates a more favourable protein adsorption when more protein molecules are available in solution leading to an optimized spatial organization of these molecules.

❖ At a given protein concentration, the adsorption on TiO₂ surfaces was higher in response to the increase in temperature.

3.6. Two-step protein adsorption studies

3.6.1. Materials

3.6.1.1. TiO$_2$-crystal

The QCM-D sensors (Q-Sense, Sweden) with gold electrode were polished crystals with a fundamental frequency of 5MHz. The gold-coated crystal (14mm) was covered with TiO$_2$ by vapour deposition as explained in section 3.4.4. The crystals were reused after cleaning (see section 3.4.4 for cleaning procedure protocol).

3.6.1.2. Protein solutions

Three different proteins were used in this work: human fibronectin (Fn), human fibrinogen (Fbg) and bovine serum albumin (BSA) (Sigma, Sant Louis, USA). Each concentration for each protein was different depending on the specific test; the exact values will be explained at the section 3.6.2.2.

3.6.2. Methods

3.6.2.1. Test conditions

Two-step adsorption studies of Fn, Fbg and BSA on a crystal coated with TiO$_2$ have been performed. At two-step adsorption studies two different protein solutions are introduced sequentially at the QCM-D system; these experiments allow studying the interaction/competition between the two proteins and the different affinity of these proteins for the studied surface. The studied protein adsorption sequences have been: BSA/Fn, BSA/Fbg, Fn/BSA and Fbg/BSA.

- Protein concentration: Protein concentration was decided taking into consideration their ratios in human blood plasma [24;29;33]

  i. Fn concentration in human blood plasma: 30 mg/100ml

  ii. Fbg concentration in human blood plasma: 300 mg/100ml

  iii. BSA concentration in human blood plasma: 3,5-5 g/100ml

Finally the working concentrations in PBS 1X solutions for the studied systems were:

    a) BSA/Fbg: 500 µg/ml for BSA and 50 µg/ml for Fbg in PBS

    b) Fbg/BSA: 50 µg/ml for Fn and 500 µg/ml for BSA in PBS

    c) BSA/Fn: 2 mg/ml for BSA and 20 µg/ml for Fn in PBS

    d) Fn/BSA: 50 µg/ml for Fn and 5 mg/ml for BSA in PBS

Different values of protein concentration were considered to select the most appropriate one for BSA/Fn and Fn/BSA systems. This was since a starting concentration of 5 mg/ml for BSA in PBS when evaluating the BSA/Fn resulted in a too high BSA concentration that interfered and even masked any Fn effect.

- Temperature: Tests were performed at body temperature, i.e., 37 °C.

3.6.2.2. QCM-D tests

For two-step protein experiments, the protocol followed is described below (Figure 3-36):

(0) PBS 1X Baseline: A constant baseline is established with PBS 1X.

(1) First protein solution temperature setting: The first protein solution of study is introduced from the reservoir to the Temperature-loop where it is maintained at the desired temperature.

(2) First protein solution introduction to the QCM-D sensor chamber: The solution is transported to the crystal by opening the sensor chamber. The protein gets in contact with the crystal surface and then, the device acquires the frequency and dissipation changes due to protein adsorption.

(3) ?f and ?D stability: The assay will be considered finished when the frequency and the dissipation shift reach a constant value by time, i.e. plateau, meaning that proteins are not significantly further adsorbed on the TiO₂-surface or that the dynamic adsorption/desorption process has reached an stabilized rate.

(4) PBS buffer temperature setting: When considered, a certain quantity of PBS 1X is introduced into the Temperature-loop to be warmed.

(5) PBS buffer introduction to the QCM-D sensor: PBS is introduced to the crystal to remove the non-permanently adsorbed proteins on the surface.

(6) Second protein solution temperature setting.

(7) Second protein solution introduction to the QCM-D sensor chamber.

(8)   ?f and ?D stability: The assay will be considered finished when the frequency and the dissipation shift reach a constant value with time after the second protein has been in contact with the first-protein-coated surface.

(9)   Cleaning of non-attached proteins: To detach the non-adsorbed proteins, the crystal is cleaned with PBS 1X.
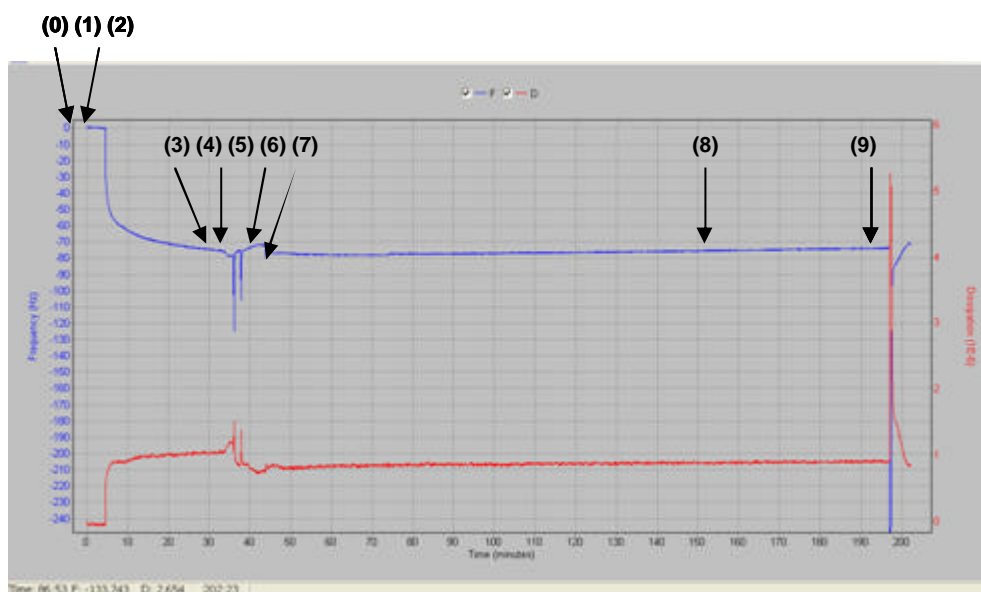
Figure 3-36 *Representative two-step protein : (0) PBS 1X baseline; (1) First protein solution temperature setting; (2) First protein solution introduction to the QCM-D sensor chamber; (3) ?f and ?D stability for the first protein; (4) PBS buffer temperature setting; (5) PBS buffer introduction to the QCM-D sensor-chamber; (6) Second protein solution temperature setting; (7) Second protein solution introduction to the QCM-D sensor chamber; (8) ?f and ?D stability for the second protein; (9) Cleaning of non-attached proteins with PBS 1X.*

A minimum of three assays have been performed for each two-step adsorption protein solutions at each concentration and temperature conditions.

3.6.3.   Results

To perform two-step adsorption studies on Ti surfaces, two different protein solutions were introduced sequentially in the QCM-D device. The main objective was to find out the competitive processes of adsorption and interactions between the studied proteins influenced by the substrate properties. Tests with an alternate order of introduction in the sensor chamber for each set of two proteins were performed to study the specific effect of surface/specific first protein interactions in the competitive process of adsorption.

3.6.3.1.   Interaction between BSA, fibrinogen, and TiO$_2$-crystals

3.6.3.1.1.   First protein BSA-Second protein fibrinogen

Figure 3-37 shows the frequency shift and the dissipation shift vs time during the two-step protein adsorption process of BSA/Fbg solutions in PBS. BSA adsorption causes a Δf of -12 Hz; then, the addition of Fbg increases the frequency shift of the studied system to a value of -18 Hz. Considering the dissipation, BSA causes a ΔD of $0,22 \times 10^{-6}$ and when the second protein is introduced, Fbg, and dissipation increases up to $0,55 \times 10^{-6}$ and remains constant with time indicating that the surface is saturated and nearly no more proteins are attaching on the substrate.
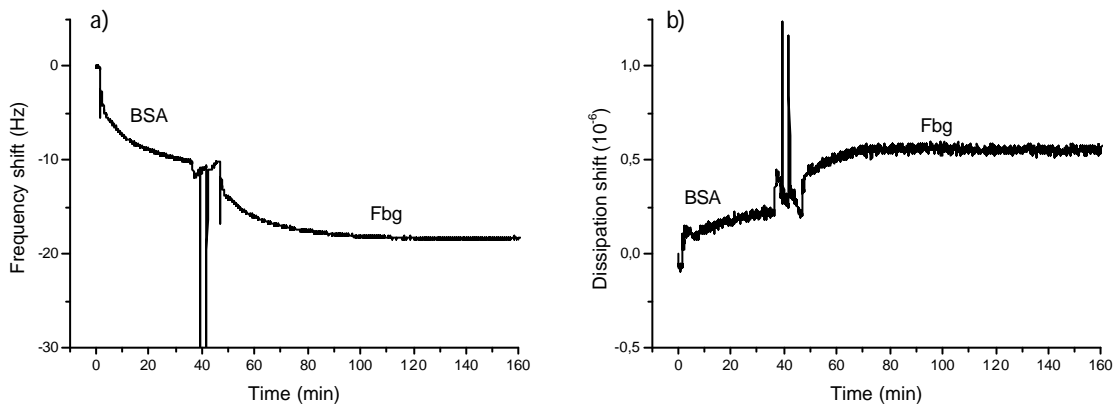
Figure 3-37 *a)* ***D****f and b)* ***D****D vs. time plots of first, BSA 500* ***ng****/ml and second, Fbg 50* ***ng****/ml in PBS on TiO₂-crystal. Peaks correspond to the PBS 1X cleanings and then, the introduction of the second protein*

The first part of the ΔD vs. Δf adsorption plot, Figure 3-38, corresponds to BSA adsorption and the second one to Fbg adsorption on TiO$_2$-crystals. Initially, the adsorbed BSA layer shows a similar plot as the one obtained for the one-step protein study, section 3.5.3.3, where three phases are detected. Each of these phases has a higher $\Delta D/\Delta f$ slope when ΔD increases. This indicates that the shear elastic modulus of the adlayer significantly decreases during the process of BSA adsorption on TiO$_2$-crystals, as shown in Figure 3-39 c). Secondly, the Fbg adsorbed on the BSA layer has the same behaviour as adsorbed on bear TiO$_2$-crystals, see 3.5.3.2, where two phases were identified and the $\Delta D/\Delta f$ slope reaches a value near zero by the end of the experiment. This is reflected in the calculated results for the viscosity of the adlayer because an increase of their values is observed at the end of the assay (Figure 3-39 c).

When calculating the thickness using Voigt and Sauerbrey models, Figure 3-39 a), the calculated curves overlap as occurred for one-step protein studies during the first 40 min of adsorption time. This effect was independently of the higher working concentration.

Surface mass density calculated by Voigt at the end of the two-step adsorption study was 329,9 ng/cm².
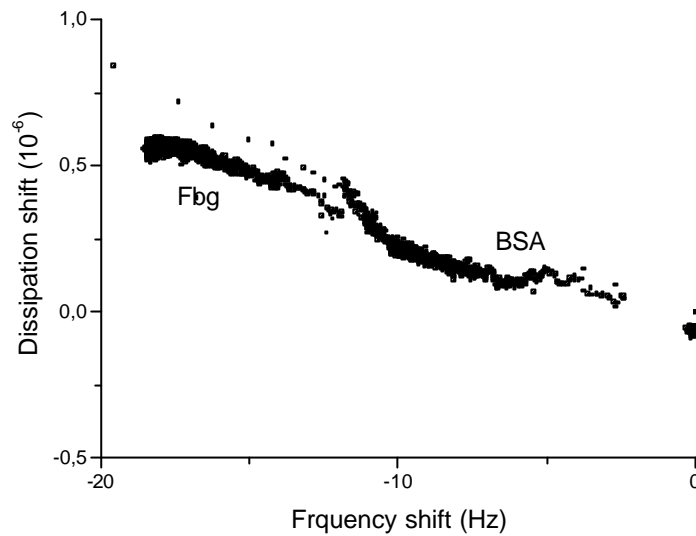
Figure 3-38 *?D vs. ?f plot of first, BSA 500 mg/ml adsorption, and second, Fbg 50 mg/ml adsorption from PBS 1X solutions on TiO₂-crystals*

Figure 3-39 *Protein layer parameters obtained after adsorption of first, BSA 500 mg/ml and second, Fbg 50 mg/ml in PBS 1X solutions on TiO₂-crystals a) protein-adsorbed-layer thickness calculated using Voigt (red) and Sauerbrey (black) models; b) surface mass density calculated using Voigt model ; and c) viscosity (black) and shear elastic modulus (green) calculated using Voigt model. All the experiments were performed at 37 ºC. Values were acquired using QTools software from QCM-D experimental data*

3.6.3.1.2. *First protein fibrinogen - Second protein BSA*

Figure 3-40 reports the frequency shift and the dissipation shift versus time of sequential protein adsorption of first, fibrinogen and second, BSA on TiO₂-surfaces. As expected, the adsorption of Fbg on TiO₂-crystals causes a rapid decrease of the frequency and a rapid increase of the dissipation shift. The further introduction of the BSA on the sensor chamber leads to an increase of the Δf and a decrease of the ΔD indicating that some of the Fbg adsorbed mass has been desorbed.
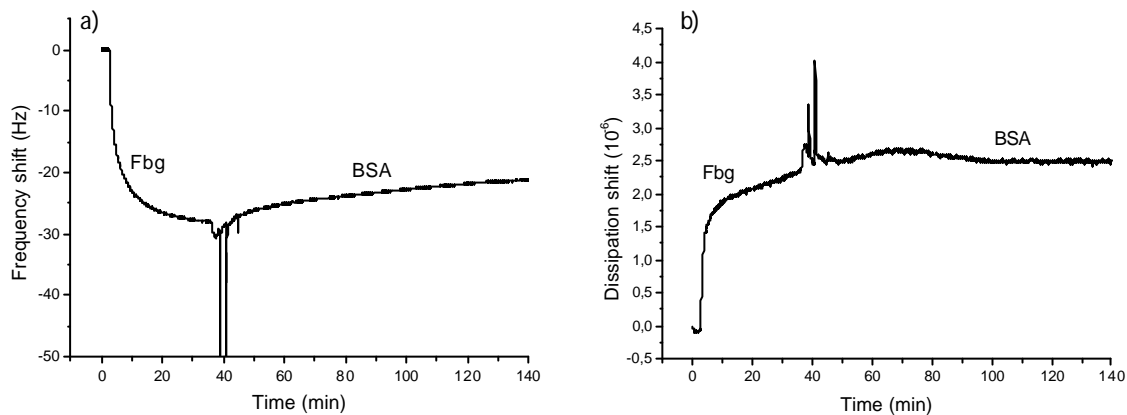
Figure 3-40 *a) **Δf** and b) **ΔD** vs. time plots of first, Fbg 50* **ng**/ml *and second, BSA 500* **ng**/ml *adsorption in PBS solutions on TiO₂-crystal. Peaks correspond to the PBS 1X cleanings and then, the introduction of the second protein*

The first part of the ΔD vs. Δf adsorption plot, Figure 3-41, shows the already explained behaviour of Fbg when monoprotein adsorption studies were reported in see section 3.5.3.2. This behaviour is mainly characterized by a decrease in the $\Delta D/\Delta f$ in the final part of the adsorption process. During washing a noticeable increase in $\Delta D/\Delta f$ slope is recorded, which may be related either to a protein rearrangement/desorption process or to a hydration process of the protein layer. Finally, when BSA solution is put into contact with the Fbg-coated TiO₂-crystals, four different steps in the adsorption process can be distinguished. But overall no major changes in the $\Delta D/\Delta f$ slope are produced when BSA is adsorbed.
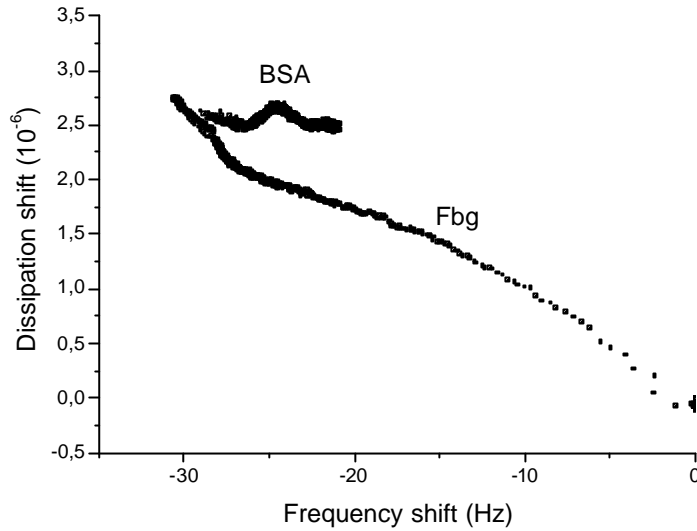
Figure 3-41 *DD vs. Df plot of first, Fbg 50 mg/ml adsorption and second, BSA 500 mg/ml adsorption from PBS 1X solutions on TiO₂-crystals*
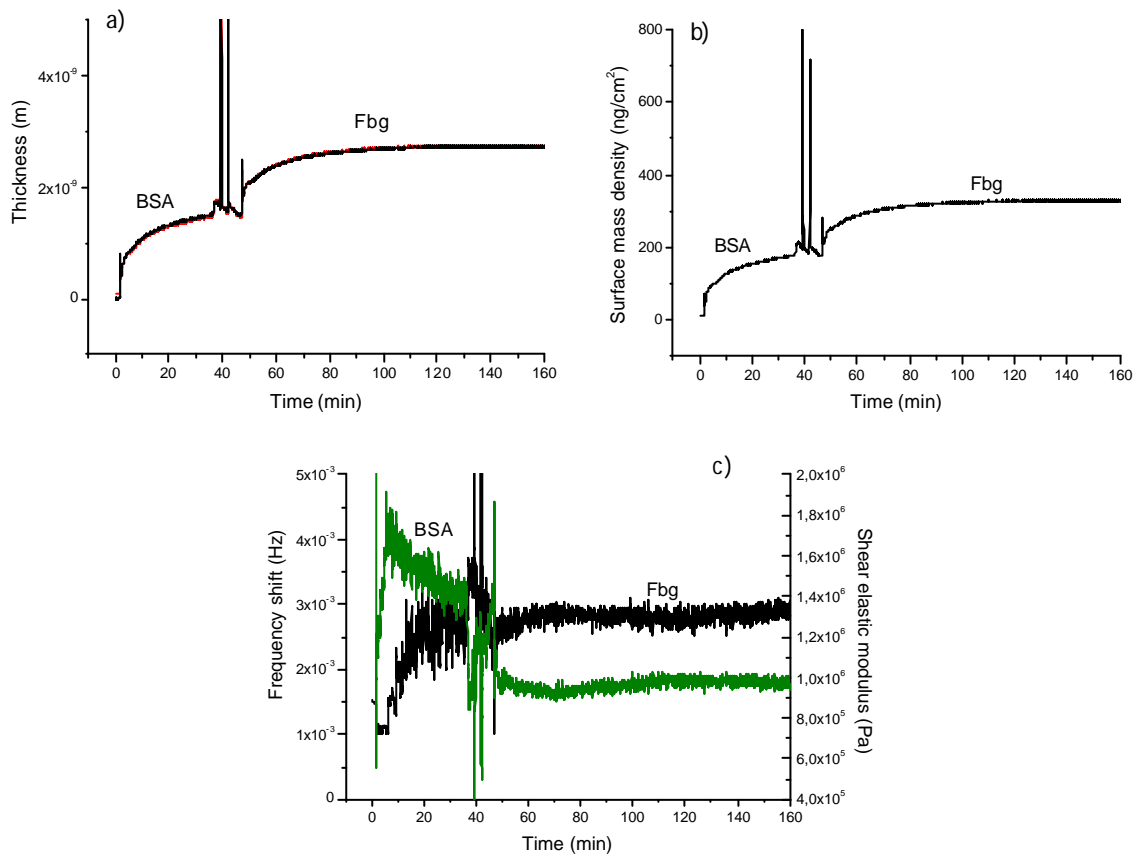
Concerning to protein layer parameters, it is observed a considerable difference between the Sauerbrey and Voigt calculated thickness parameters. After 5min of adsorption time, protein layer behaves viscoelastic probably due to the initial Fbg working concentration; 50 μg/ml. An interesting and relevant result is the calculated parameters using the Voigt model, Figure 3-42 a) (in red), indicates a decrease of thickness, from 5,21 down to 4,49 nm and surface mass density, from 626,10 down to 539,71 ng/cm². Values were measured at 40min, after the first protein Fbg is adsorbed and at 140min, after the second protein BSA is introduced and adsorbed, respectively. Viscosity, Figure 3-42 c), increases during Fbg adsorption. After that, a significant decrease in frequency shift during the washings between the two protein solutions was detected. Finally, this parameter remained stable while BSA is adsorbed. This can indicate that the proteins adsorbed in the last part of the Fbg adsorption step are weakly adsorbed to the adlayer. Proteins could be easily removed either with washing or by interaction with the BSA solution. In the latter case, this is indicative of some desorption process triggered and continuously induced by the smaller BSA molecules.
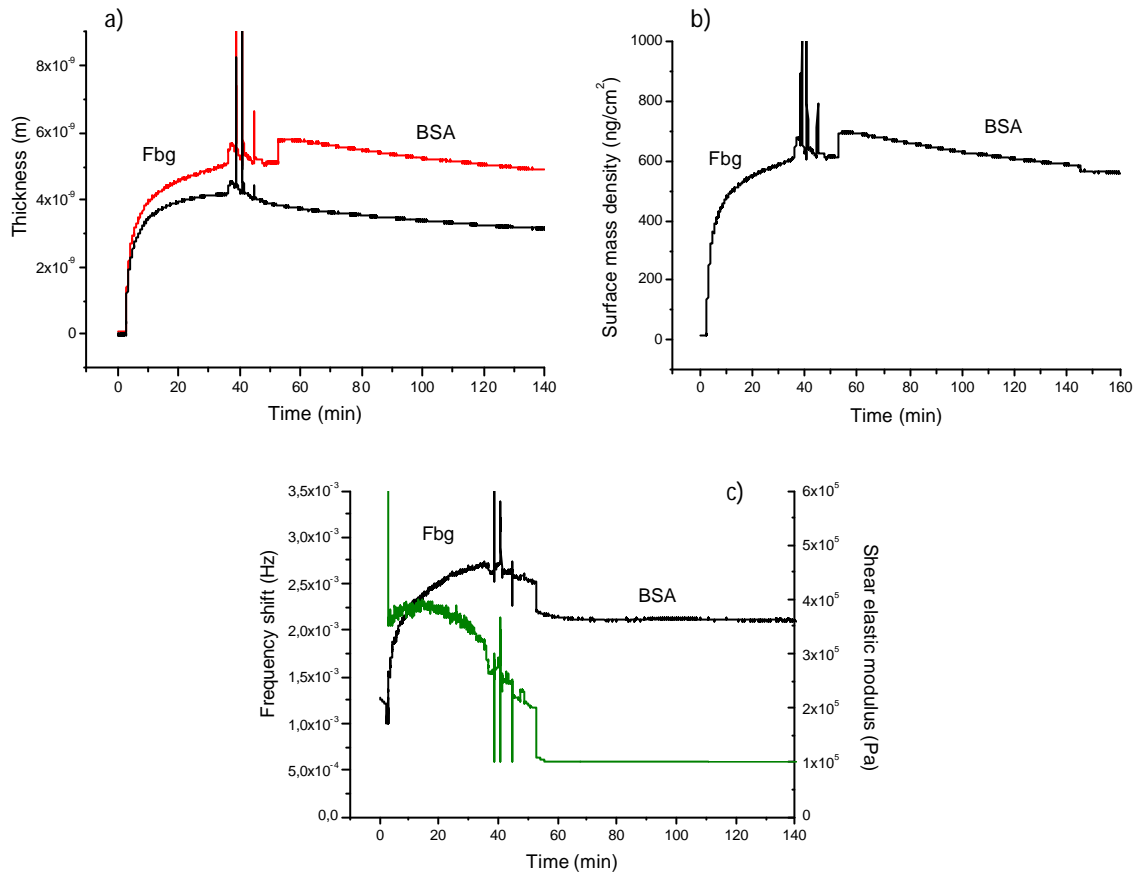
Figure 3-42 *Protein layer parameters obtained after adsorption of first, Fbg 50 mg/ml and second, BSA 500mg/ml in PBS 1X solution on TiO₂-crystals. a) protein-adsorbed-layer thickness calculated using Voigt (red) and Sauerbrey (black) models; b) surface mass density calculated using Voigt model ; and c) viscosity (black) and shear elastic modulus (green) calculated using Voigt model. All the experiments were performed at 37 ºC. Values were acquired using QTools software from QCM-D experimental data*

3.6.3.2. Interaction between BSA and fibronectin

3.6.3.2.1. First protein BSA-Second protein fibronectin

When BSA is first introduced, the frequency decreases rapidly (Figure 3-43 a)). During PBS 1X cleanings, a certain quantity of BSA is detached as showed by the slight frequency increase. When Fn is introduced, an almost negligible decrease of 1Hz in frequency is measured during the total Fn-adsorption time. Dissipation shift vs time, Figure 3-43 b), shows that once BSA adsorbed, PBS cleanings significantly decreased dissipation values. Then Fn is introduced, and dissipation values slowly increased again until they reached values similar to the ones recorded in the final part of the BSA adsorption process on TiO₂-crystals.
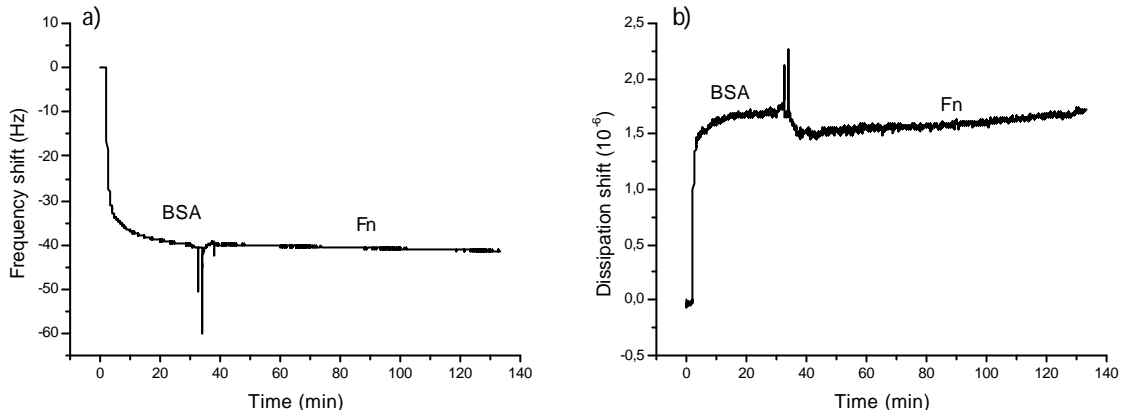
Figure 3-43 *a) **D**f and b) **D**D vs. time plots of first, BSA 2 mg/ml adsorption and second, Fn 2 0mg/ml adsorption from PBS solutions on TiO₂-crystasl. Peaks correspond to the PBS 1X cleanings and then, the introduction of the second protein*

The first part of the ΔD vs. Δf plot (Figure 3-44) corresponds to the first BSA-adsorption step. Again the $\Delta D/\Delta f$ slope increases with time as previously reported for monoprotein experiments. Then, the exposure to the second-protein Fn-solution abruptly increased the $\Delta D/\Delta f$ slope of the adlayer. This is accompanied with an slight increase of the thickness of the layer (from 6,58 nm up to 6,65 nm) as well as of the surface mass density (from 789,75 up to 798,68 ng/cm²) (Figure 3-45 a) and b)). Viscosity of the adlayer remains almost constant and shear elastic modulus slightly decreases during the time Fbg is being adsorbed on the BSA-coated TiO₂-crystals. Consequently, the interaction and adsorption of Fn after the BSA adsorption does not significantly affect mechanical properties of the adlayer.

Differences between Sauerbrey and Voigt approximations after 5 min of protein adsorption are noticeable. At the beginning, BSA protein layer is rigid. After 5 min of adsorptionthe adlayer acquires viscoelastic properties. Afterwards differences between the Sauerbrey and Voigt approximations are also observed.
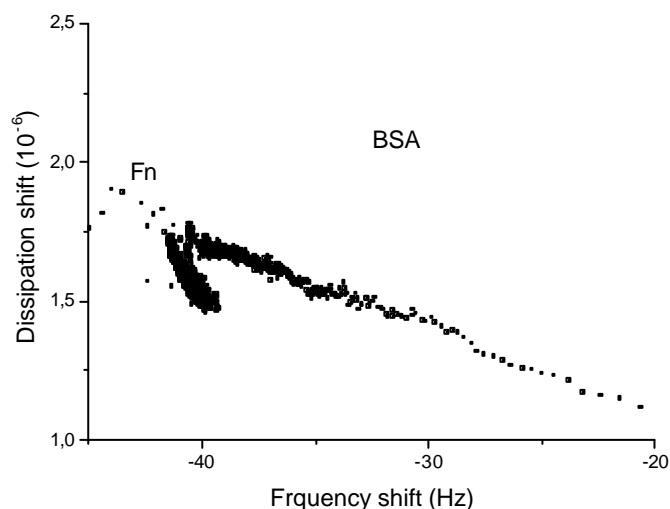
Figure 3-44 ***D**D vs. **D**f plot of first, BSA 2mg/ml adsorbed and second, Fn 20mg/ml adsorbed from PBS 1X solutions on TiO₂-crystals*

193

Figure 3-45 *Protein layer parameters obtained after adsorption of first, BSA 2 mg/ml and second, Fn 20 mg/ml solutions in PBS 1X on TiO₂-crystals a) protein-adsorbed-layer thickness calculated using Voigt (red) and Sauerbrey (black) model; b) surface mass density calculated using Voigt model; and c) viscosity (black) and shear elastic modulus (green) calculated using Voigt model. All the experiments were performed at 37ºC. Values were acquired using QTools software from QCM-D experimental data*

3.6.3.2.2.   First protein fibronectin -Second protein BSA

Figure 3-46 corresponds to the Δf and ΔD vs. time two-step adsorption plot of first Fn and second BSA solutions on TiO₂-crystals. The adsorption of BSA after Fn adsorption caused an increase of 2Hz in the frequency, which is probably an indication of the desorption of some mass from the Fn-coated surfaces. The dissipation shift continuously and slightly decreased when BSA was being adsorbed on the Fn-coated surface.

Figure 3-47 reports the ΔD vs Δf plot. Fn adsorption in the first step showed the same reponse than that obtained when monoprotein solutions were tested (section 3.5.3.1), i.e., a constant ΔD/Δf slope was recorded during the Fn adsorption. The second step of BSA adsorption slightly increased the ΔD/Δf slope.
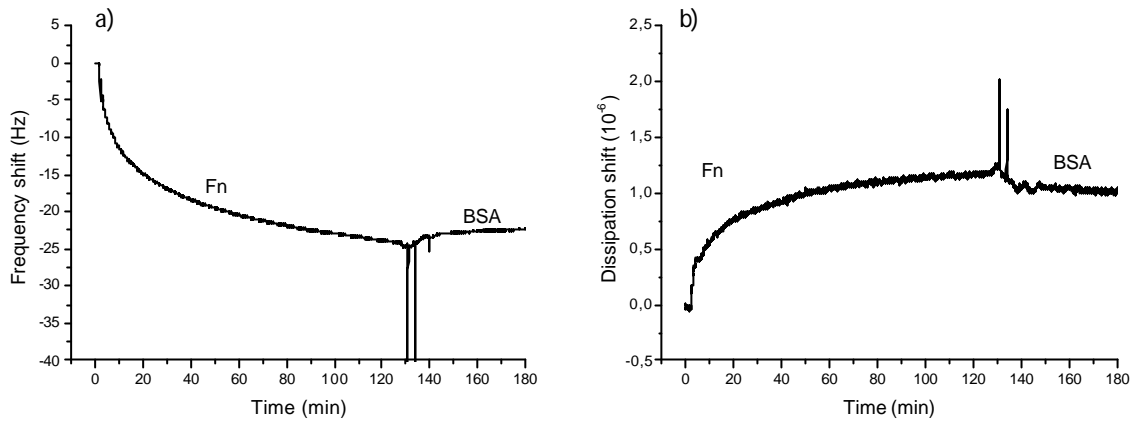
Figure 3-46 a) **D**f and b) **D**D vs. time plots of first, Fn 50 **mg**/ml adsorption and second, BSA 5 mg/ml adsorption from PBS solutions on TiO₂-crystals. Peaks correspond to the PBS 1X cleanings and then, the introduction of the second protein
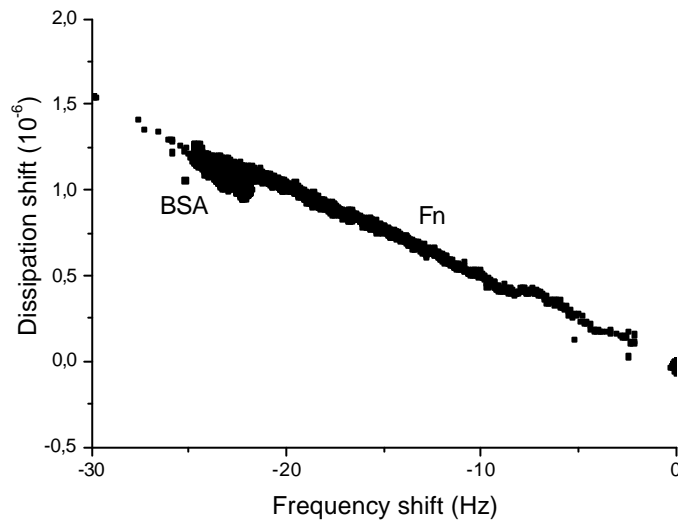
Figure 3-47 DD vs. Df plots of protein adsorbed sequence: first, Fn 50 **mg**/ml and second, BSA 5 mg/ml in PBS 1X on Ti crystals

The calculation of the protein layer parameters using the Voigt model (Figure 3-48) confirmed the trend of the structural characteristics of the adlayer suggested by the ΔD vs. Δf plot. Consequently, a decrease in the thickness of the layer when BSA is adsorbed was calculated (from 3,87 down to 3,36 nm) as well as in the surface mass density (from 464,80 down to 403,78 ng/cm²). Viscosity, Figure 3-48 c), decreased during Fbg and BSA adsorption, whereas the calculated shear elastic modulus increased during the adsorbed protein layer on the TiO₂-surfaces is formed in the two-steps of the process.
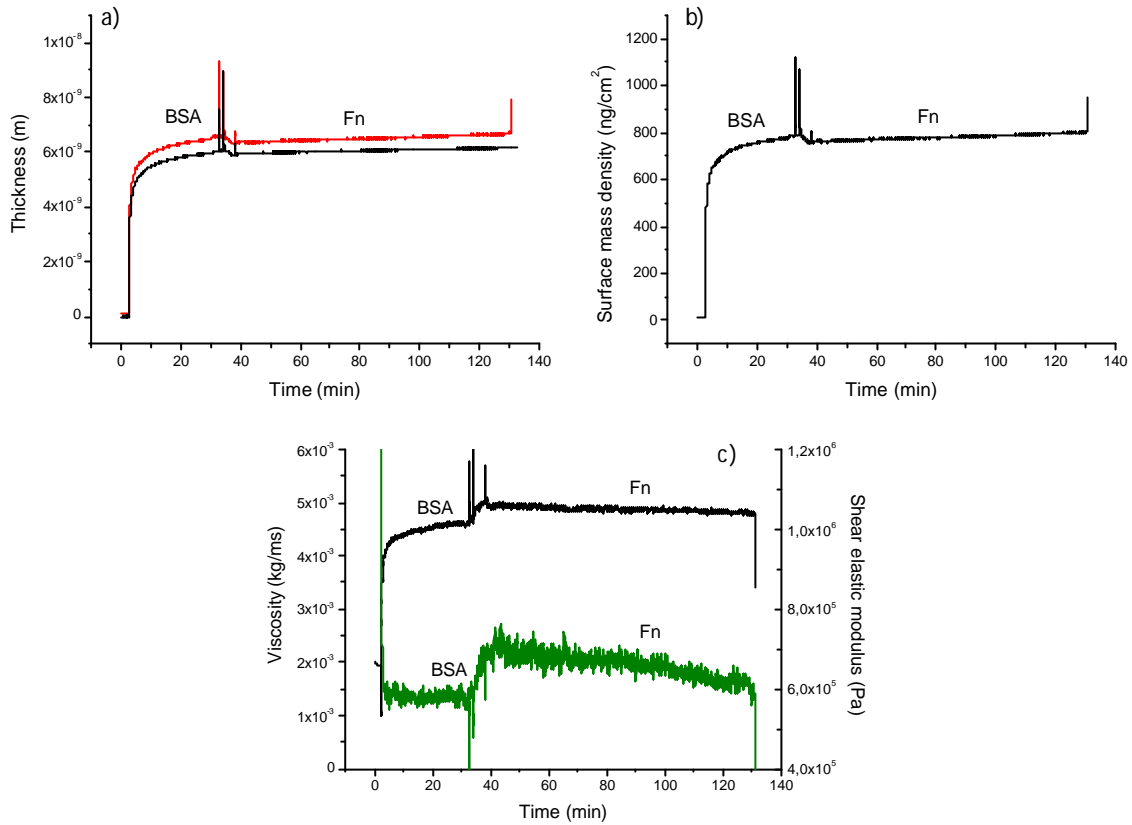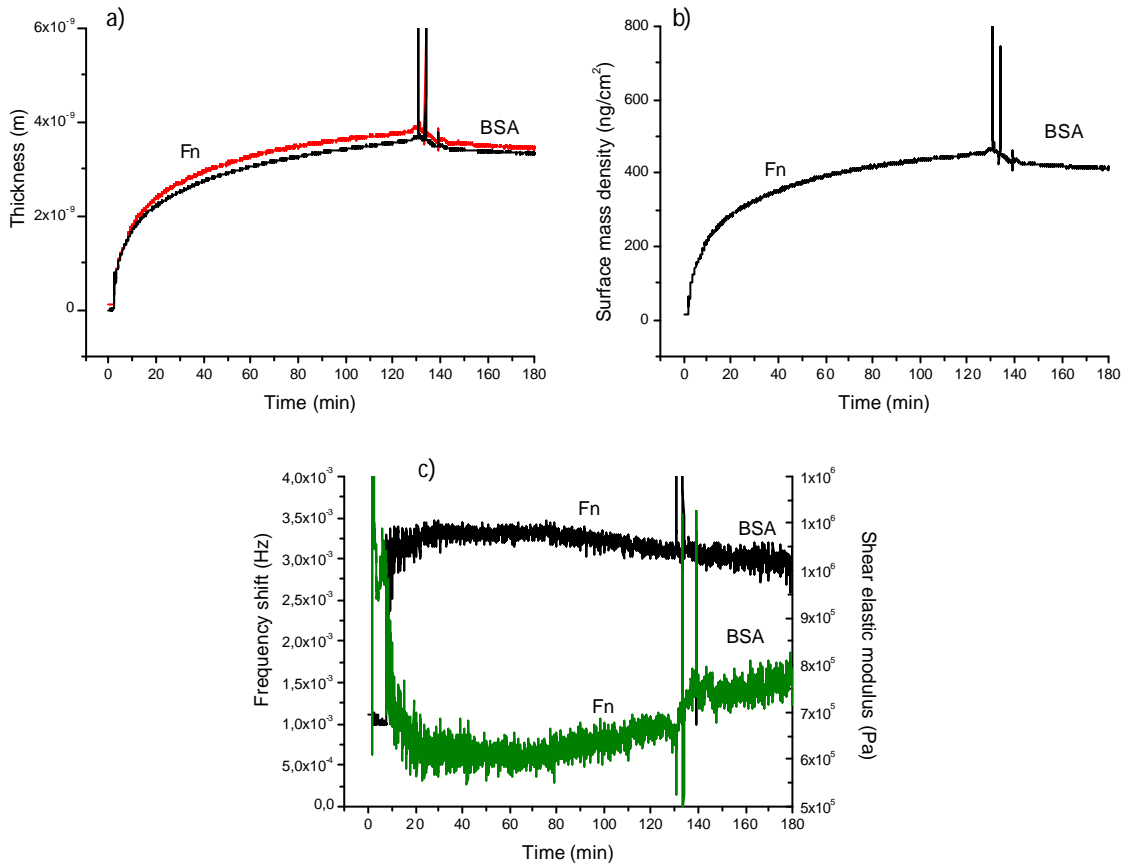
Figure 3-48 *Protein layer parameters obtained after adsorption of first, Fn 50 mg/ml and second, BSA 5 mg/ml solutions in PBS 1X on TiO₂-crystals. a) protein-adsorbed-layer thickness calculated using Voigt (red) and Sauerbrey (black) models; b) surface mass density calculated using Voigt model; and c) viscosity (black) and shear elastic modulus (green) calculated using Voigt model. All the experiments were performed at 37ºC. Values were acquired using QTools software from QCM-D experimental data*

3.6.4.   Discussion

Adsorption of plasma proteins to surfaces is one of the first and most important events before the initiation of key cellular activities such as cell attachment, migration, proliferation and differentiation. In particular, effects of adsorption time scales, interfacial competition, and extent of adsorption irreversibility are among some key issues of interest. The present study focuses on the sequential and competitive adsorption of fibronectin, fibrinogen and bovine serum albumin on titanium surfaces.

For all the sequential adsorption systems, the adsorption response of the proteins for the first solution introduced in the system is similar to that reported in previous sections of this work where one-step studies with a single protein solution was tested on TiO₂-surfaces. Differences were mainly due to the first protein concentration of the two-step studies compared to protein concentrations of single protein studies. Macromolecules adsorbed can use several adsorption sites depending on their structure and molecular

mass. At low concentrations, adsorbed proteins are in an unfolded state with more located binding sites to adsorption [101]. Protein adsorption such as Fn and HAS [23;102], are related to structural rearrangements in the molecules that enable them to overcome the unfavourable conditions offered by an electrostatic repelling surface. At higher protein concentrations the adsorption layer becomes more compressed and molecules with different degrees of unfolding will coexist at the interface [103], being more difficult for some molecules to overcome the unfavourable conditions to adsorption. This fact can explain the higher rigidity of the protein layer obtained for the lowest Fn and BSA concentrations since protein molecules are more tightly bound to the surface. The contrary occurs when working at higher protein concentration, such as 2mg/ml BSA concentration from two-step studies (BSA-Fn), where a more viscoelastic protein layer compared to BSA 500 µg/ml (BSA-Fbg) and 100 µg/ml concentrations from single protein studies was obtained.

Of relevant interest in this part of the study is the discussion about the interaction and competition of the secondly introduced protein with the previously adsorbed protein layer.

For the BSA-Fbg system, after the initial adsorption of BSA, fibrinogen is put in contact with TiO$_2$-crystals, Figure 3-37, and the frequency decreases indicating the adsorption of Fbg. The frequency shift is lower, around -10Hz, compared to the frequency shift recorded during the previously reported Fbg-adsorption measurements from monoprotein solutions. BSA has a high affinity for the TiO$_2$-crystal surface and that certainly can induce adsorption of Fbg either on top of BSA-layer or on the few BSA-free available spaces on those crystals. This can be responsible for the diminished adsorption of Fbg on the surface compare to the adsorption directly on top of the TiO$_2$-crystals. However, the way of Fbg adsorbs and the type of Fbg layer obtained does not be significantly influenced by the previous BSA adsorbed layer, according to results in Figure 3-37, Figure 3-38 and Figure 3-39. The Fbg-layer is being added on top of the BSA layer and the mechanical and structural characteristics of it are comparable to the results obtained with Fbg solutions during the single-step monoprotein experiments. The fact that the final adlayer on TiO$_2$-crystals when studying the BSA-Fbg system is mainly composed by BSA molecules, is also confirmed by the Voigt calculated thickness, 2,76 nm, and surface mass density, 329,95 ng/cm^2. Those values are noticeably lower than those calculated for Fbg adsorption from monoprotein solutions, Table 3-8, but similar to those calculated for BSA adsorption from monoprotein, Table 3-9. Numbers are not expected to be the same because the protein concentrations used for single and two-step experiments are not the same. ΔD-Δf plot confirms that a similar effect on the structure of the adlayer is obtained for both proteins than the one obtained when each individual protein solution was tested separately.

Considerably differences are found with the inverted studied system, Fbg-BSA, Figure 3-40, Figure 3-41 and Figure 3-42. The main difference is that frequency increases after the introduction of BSA solution in the system and its interaction with the already formed Fbg-layer on TiO₂-crystals. This result indicates that BSA is able to displace some of the Fbg molecules still adsorbed on the crystal surfaces. In fact, some previously reported works have concluded that some proteins can displace pre-adsorbed molecules because they have a superior affinity and they are able to bind strongly with the analyzed surface [104]. In this respect, the small size of BSA can favour this molecule to reach some of the non-covered surface points as well as to compete with Fbg molecules for the already occupied positions on the on the crystals. If this is the case, this means that BSA molecules showed a higher affinity of for TiO₂ surfaces than Fbg molecules, which in turn can also be a plausible explanation of the results discussed in the previous paragraph. This hypothesis was further confirmed by analyzing the calculated thickness and surface mass density using the Voigt model. Both values decrease when the second-step of BSA adsorption is on going, and so the displacement/replacement of Fbg molecules by BSA molecules results in a thinner adlayer. The transition state while some Fbg molecules detach when performing PBS washing is visualized by the increased ΔD/Δf slope, which could indicate a less dense Fbg adlayer. This is also a clear indication of the somehow weak affinity of some of the adsorbed Fbg molecules on the crystals. After BSA is putted in contact with the Fbg-adsorbed layer, the resulting adlayer fluctuate its rigidity to finally decrease as the adsorbed protein amount is increased. Some structural rearrangements occur, as shown in Figure 3-41 but they don't affect the viscosity and the shear elastic modulus, Figure 3-42 c). The significant softening of the adlayer when BSA is in contact with the surface may indicate the displacement of Fbg by BSA molecules because BSA-layers showed their low-rigidity properties from the single protein results as well as from the BSA-Fbg system results.

The two-step sequential protein adsorption in the BSA-Fn system shows a rapid decrease in frequency when BSA is introduced in the system, mainly due to its high concentration in PBS. Note that the concentration is 4 times the one used for the BSA-Fbg system. Since the solution has an elevated concentration many protein molecules were attached immediately on the surface. Ramsden et al., [30] stated that, depending on the protein, and surface and solution conditions, the area per molecules is inversely proportional to the rate of arrival of proteins at the surface. Then, probably, the rapid BSA adsorption caused a nearly non-spreading of the molecules onto the surface. This can also confirmed because of the significant desorption of BSA molecules when washing with PBS is performed. This is an occurrence that did not happen when tested the BSA-Fbg system, either. When Fn solution is put in contact with the BSA-layer adsorbed on TiO₂-crystals a slight decreased in the frequency shift is recorded, i.e., Fn is being adsorbed on top of the surface but in a small quantity. In fact, an almost negligible 1%-increase in both thickness and surface mass density of the adlayer was calculated. Again, the BSA adsorption process is similar to that reported for single-protein adsorption studies; independently of

the difference in the protein concentration of the solution. The protein layer becomes less rigid when BSA adsorbs during the experiment. The adsorption of Fn also results in a less rigid, less viscous layer. This is not what was calculated when Fn adsorbed and saturated the surface of the TiO_2-crystals during the single protein one-step experiments. This can be an indication of the weak interaction of the Fn molecules adsorbed on top of the BSA adlayer, which would lead to a decrease of the shear modulus of the combined BSA-Fn layer.

For the Fn-BSA two-step sequential adsorption study, the Fn adsorption follows the same pattern found at single-step adsorption studies showing one single phase during the adsorption process. But the introduction of BSA solution in PBS in the system leads to an increase of frequency, i.e. decrease in mass, and decrease of dissipation shift. Some of Fn molecules are displaced by BSA reducing the thickness and the surface mass density of the protein adsorbed layer around a 13%. This is a similar behaviour to the one obtained with the Fbg-BSA system. BSA is able to displace some of the previously bigger proteins adsorbed on the TiO_2-crystals. However, the structural and mechanical implications of the BSA adsorption and replacement/displacement of the bigger molecules is different in the case of Fn compared to Fbg. When BSA is putted in contact with Fn-adsorbed layer and interact, an increase in shear modulus, a decrease in viscosity and a decrease in the ΔD are recorded. All these results confirm that the resulted adlayer is more rigid after BSA is adsorbed. One possible explanation for this response may be the introduction and interaction of BSA molecules into the adsorbed Fn-layer. But the surface mass density calculated values does not support this hypothesis.

From the obtained results in sections 3.6.3.1.1, 3.6.3.1.2, 3.6.3.2.1 and 3.6.3.2.2, and as discussed previously, a difference is found when BSA is the first adsorbing molecule or when it is the second one from the two-step sequential adsorption on TiO_2-crystals.

The 'Vroman effect' relates to the competition between two or more proteins for the same adsorbent surface. The generalized Vroman effect, [105], demonstrated that adsorption from blood plasma involves a complex series of adsorption and displacement steps in which low molecular weight, MW, proteins arriving first at surface are displaced by relatively higher MW proteins arriving later. Literature has not consistently support the Vroman effect theory. Brash and Lyman proposed that in protein mixtures, such as blood, the proteins would simply adsorb in proportion to their concentrations in solution [106]. Noh et al. [107] concluded Brash and Lyman's idea that proteins adsorb in proportion to solution concentration is basically correct, except that mass balance forces a discrimination, a Vroman-like effect, leading to the selective adsorption of smaller proteins from a mixture of smaller and larger proteins on hydrophobic octyl sepharose adsorbent particles.

Concerning to our results, the studied Fbg/BSA and Fn/BSA systems show that BSA displaces larger proteins such as Fn and Fbg. Probably, the adopted conformation by Fbg and Fn leaves enough free binding sites to BSA to adsorb on the Ti surface. Moreover, the smaller MW, the higher concentration in proportion to the other working protein and its high affinity for Ti surfaces, explains the displacement effect founded when BSA is adsorbed onto a pre-adsorbed Fbg or Fn protein layer on TiO$_2$.

For the BSA/Fn and BSA/Fbg systems, where BSA is the first adsorbed protein, the Vroman effect and Brash and Lyman theory are in competition. From our results, the bigger molecules adsorb on the top of the BSA layer, but a significant displacement of the BSA molecules can not be confirmed. Moreover, BSA is typically used as a blocking agent for the elimination of non-specific adsorption; then the BSA protein layer enables most of the fibrinogen and fibronectin adsorption on TiO$_2$. After that, prevalence of the Brash and Lyman effect on the Vroman effect may explain the protein layer behavior, since a lower molecular weight and more concentrated protein in solution adsorb preferentially to Ti surfaces.

3.6.5. Conclusions

❖ Fbg/BSA and Fn/BSA systems showed that BSA displaces larger proteins such as Fn and Fbg since the high affinity of BSA for TiO$_2$ surfaces, its low molecular weight and size compared to the other working proteins and higher proportional concentration in solution.

❖ For the BSA/Fn and BSA/Fbg systems, where BSA is the first adsorbed protein, the bigger molecules adsorb on the top of the BSA layer. There is prevalence of the Brash and Lyman effect on the Vroman effect since a lower molecular weight and more concentrated protein in solution adsorb preferentially to Ti surfaces.

3.7. Bibliography

[1] MacDonald DE, Deo N, Markovic B, Stranick M, Somasundaran P. Adsorption and dissolution behavior of human plasma fibronectin on thermally and chemically modified titanium dioxide particles. Biomaterials 2002; 23: 1269-1279.

[2] Puleo DA, Nanci A. Understanding and controlling the bone-implant interface. Biomaterials 1999; 20: 2311-2321.

[3] Andrade JD, Hlady V. Protein adsorption and materials biocompatibility-a tutorial review and suggested hypotheses. Advances in Polymer Science 1986; 79: 1-63.

[4] Haynes CA, Sliwinsky E, Norde W. Structural and Electrostatic Properties of Globular-Proteins at A Polystyrene Water Interface. Journal of Colloid and Interface Science 1994; 164: 394-409.

[5] Deligianni DD, Katsala N, Ladas S, Sotiropoulou D, Amedee J, Missirlis YF. Effect of surface roughness of the titanium alloy Ti-6Al-4V on human bone marrow cell response and on protein adsorption. Biomaterials 2001; 22: 1241-1251.

[6] Michael K, Vernekar V, Keselowsky B, Meredith J, Latour R, García AJ. Adsorption-induced conformational changes in fibronectin due to interactions with well-defined surface chemistries. Langmuir 2003; 19: 8033-8040.

[7] Béguin S, Kumar R. Thrombin, fibrin and platelets, a resonance loop in which von Willebrand factor is a necessary link. Thrombosis and Haemostasis 1997; 78: 590-594.

[8] Kumar R, Béguin S, Hemker HC. The influence of fibrinogen and fibrin on thrombin generation–evidence for feedback activation of the clotting system by clot bound thrombin. Thrombosis and Haemostasis 1994; 72: 713-721.

[9] Tzoneva R, Heuchel M, Groth T, Altankov G, Albrecht W, Paul D. Fibrinogen adsorption and platelet interactions on polymer membranes. Journal of Biomaterials Science-Polymer Edition 2002; 13: 1033-1050.

[10] Scotchford CA, Ball M, Winkelmann M, Voros J, Csucs C, Brunette DM, Danuser G, Textor M. Chemically patterned, metal-oxide-based surfaces produced by photolithographic techniques for studying protein- and cell-interactions. II: Protein adsorption and early cell interactions. Biomaterials 2003; 24: 1147-1158.

[11] Renner L, Pompe T, Salchert K, Werner C. Fibronectin displacement at polymer surfaces. Langmuir 2005; 21: 4571-4577.

[12] Norde W, Lyklema J. The adsorption of human plasma albumin and bovine pancreas ribonuclease at negatively charged polystyrene surfaces : I. Adsorption isotherms. Effects of charge, ionic strength, and temperature. Journal of Colloid and Interface Science 1978; 66: 257-265.

[13] Höök F. Development of a novel QCM technique for protein adsorption studies. Chalmers University of Technology and Göteborg University, Sweden; 1997. Thesis.

[14] Norde W, Lyklema J. Why proteins prefer interfaces. Journal of Biomaterials Science Polymer edition 1991; 2: 183-202.

[15] Lodish H, Berk A, Zipursky S, Matsudaira P, Baltimore D, Darnell J. Biología celular y molecular. Editorial médica panamericana; 2002.

[16] Haynes CA, Norde W. Globular proteins at solid/liquid interfaces. Colloids and Surfaces B: Biointerfaces 1994; 2: 517-566.

[17]   Norde W. Adsorption of proteins from solution at the solid-liquid interface. Advances in Colloid and Interface Science 1986; 25: 267-340.

[18]   Norde W. Adsorption of proteins from solution at the solid-liquid interface. Cells and Materials 1995; 5: 97-112.

[19]   Grinnell F, Feld MK. Fibronectin Adsorption on Hydrophilic and Hydrophobic Surfaces Detected by Antibody-Binding and Analyzed During Cell-Adhesion in Serum-Containing Medium. Journal of Biological Chemistry 1982; 257: 4888-4893.

[20]   MacDonald DE, Markovic B, Allen M, Somasundaran P, Boskey AL. Surface analysis of human plasma fibronectin adsorbed to commercially pure titanium materials. Journal of Biomedical Materials Research 1998; 41: 120-130.

[21]   Pernodet N, Rafailovich M, Sokolov J, Xu D, Yang NL, McLeod K. Fibronectin fibrillogenesis on sulfonated polystyrene surfaces. Journal of Biomedical Materials Research Part A 2003; 64A: 684-692.

[22]   Rupp F, Scheideler L, Rehbein D, Axmann D, Gels-Gerstorfer J. Roughness induced dynamic changes of wettability of acid etched titanium implant modifications. Biomaterials 2004; 25: 1429-1438.

[23]   Sousa SR, Moradas-Ferreira P, Barbosa MA. TiO2 type influences fibronectin adsorption. Journal of Materials Science-Materials in Medicine 2005; 16: 1173-1178.

[24]   Grunkemeier JM, Tsai WB, McFarland CD, Horbett TA. The effect of adsorbed fibrinogen, fibronectin, von Willebrand factor and vitronectin on the procoagulant state of adherent platelets. Biomaterials 2000; 21: 2243-2252.

[25]   MacDonald DE, Markovic B, Boskey AL, Somasundaran P. Physico-chemical properties of human plasma fibronectin binding to well characterized titanium dioxide. Colloids and Surfaces B-Biointerfaces 1998; 11: 131-139.

[26]   Tamada Y, Ikada Y. Effect of preadsorbed proteins on cell adhesion to polymer surfaces. Journal of Colloid and Interface Science 1993; 155: 334-339.

[27]   Hemmersam AG, Foss M, Chevallier J, Besenbacher F. Adsorption of fibrinogen on tantalum oxide, titanium oxide and gold studied by the QCM-D technique. Colloids and Surfaces B-Biointerfaces 2005; 43: 208-215.

[28]   Yongli C, Xiufang Z, Yandao G, Nanming Z, Tingying Z, Xinqi S. Conformational Changes of Fibrinogen Adsorption onto Hydroxyapatite and Titanium Oxide Nanoparticles. Journal of Colloid and Interface Science 1999; 214: 38-45.

[29]   Bai Z, Filiaggi MJ, Dahn JR. Fibrinogen adsorption onto 316L stainless steel, nitinol and titanium. Surface Science 2009; 603: 839-846.

[30]   Ramsden JJ. Experimental Methods for Investigating Protein Adsorption-Kinetics at Surfaces. Quarterly Reviews of Biophysics 1994; 27: 41-105.

[31]   Annarelli CC, Fornazero J, Cohen R, Bert J, Besse JL. Colloidal protein solutions as a new standard sensor for adhesive wettability measurements. Journal of Colloid and Interface Science 1999; 213: 386-394.

[32]   Imamura K, Shimomura M, Nagai S, Akamatsu M, Nakanishi K. Adsorption characteristics of various proteins to titanium surface. Journal of Bioscience and Bioengineering 2008; 106: 273-278.

[33]   Oliva F, Avalle L, Cβmara O, De Pauli C. Adsorption of human serum albumin (HSA) onto colloidal TiO2 particles, Part I. Journal of Colloid and Interface Science 2003; 261: 299-311.

[34] Sousa SR, Moradas-Ferreira P, Saramago B, Melo LV, Barbosa MA. Human serum albumin adsorption on TiO2 from single protein solutions and from plasma. Langmuir 2004; 20: 9745-9754.

[35] Hughes DT, Embery G. Adsorption of bovine serum albumin on to titanium powder. Biomaterials 1996; 17: 859-864.

[36] Wassell D, Embery G. Adsorption of bovine serum albumin on to titanium powder. Biomaterials 1996; 17: 859-864.

[37] Kasemo B, Lausmaa J. Material-Tissue Interfaces - the Role of Surface-Properties and Processes. Environmental Health Perspectives 1994; 102: 41-45.

[38] Israelachvili JN. Intermolecular and surface forces. London: Academic Press; 1992.

[39] Branemark PI, Adell R, Albrektsson T, Lekholm U, Lundkvist S, Rockler B. Osseointegrated Titanium Fixtures in the Treatment of Edentulousness. Biomaterials 1983; 4: 25-28.

[40] Williams D.F. Titanium for medical applications. In: Brunette DM, Tengvall P, Textor M, Thomsen P (eds.), Titanium in Medicine. Springer; 2001: 14-23.

[41] Lausmaa J. Mechanical, thermal, chemical and electrochemical surface treatment of titanium. In: Brunette DM, Tengvall P, Textor M, Thomsen P (eds.), Titanium in Medicine. Springer; 2001: 232-258.

[42] Vöros J, Wieland M, Ruiz-Taylor L, Textor M, Brunette DM. Characterization of Titanium Surfaces. In: Brunette DM, Tengvall P, Textor M, Thomsen P (eds.), Titanium in Medicine. Ed.Springer; 2001: 87-144.

[43] Tengvall P. Proteins at titanium interfaces. In: Brunette DM, Tengvall P, Textor M, Thomsen P (eds.), Titanium in Medicine. Springer; 2001: 458-480.

[44] Norde W. Energy and entropy of protein adsorption. Journal of Dispersion Science and Technology, Biocolloids and Biosurfaces 1992; 13: 363-377.

[45] Norde W. Protein adsorption at solid surfaces: a thermodynamic approach. Pure and Applied Chemistry 1994; 66: 491-496.

[46] Rosengren A. Cell-protein-material interactions on bioceramics and model surfaces. Faculty of Science and Technology, Uppsala; 2004. Thesis.

[47] Nomura T, Hattori O. Determination of Micromolar Concentrations of Cyanide in Solution with A Piezoelectric Detector. Analytica Chimica Acta 1980; 115: 323-326.

[48] Rodahl M, Hook F, Krozer A, Brzezinski P, Kasemo B. Quartz-Crystal Microbalance Setup for Frequency and Q-Factor Measurements in Gaseous and Liquid Environments. Review of Scientific Instruments 1995; 66: 3924-3930.

[49] Rodahl M, Kasemo B. A simple setup to simultaneously measure the resonant frequency and the absolute dissipation factor of a quartz crystal microbalance. Review of Scientific Instruments 1996; 67: 3238-3241.

[50] Hook F, Kasemo B, Nylander T, Fant C, Sott K, Elwing H. Variations in Coupled Water, Viscoelastic Properties, and Film Thickness of a Mefp-1 Protein Film during Adsorption and Cross-Linking: A Quartz Crystal Microbalance with Dissipation Monitoring, Ellipsometry, and Surface Plasmon Resonance Study. Anal. Chem. 2001; 73: 5796-5804.

[51] Andersson M, Andersson J, Sellborn A, Berglin M, Nilsson B, Elwing H. Quartz crystal microbalance-with dissipation monitoring (QCM-D) for real time measurements of blood coagulation density and immune complement activation on artificial surfaces. Biosensors & Bioelectronics 2005; 21: 79-86.

[52] Thompson M, Arthur CL, Dhaliwal GK. Liquid-Phase Piezoelectric and Acoustic Transmission Studies of Interfacial Immunochemistry. Anal. Chem. 1986; 58: 1206-1209.

[53] Fredriksson C, Kihlman S, Rodahl M, Kasemo B. The piezoelectric quartz crystal mass and dissipation sensor: A means of studying cell adhesion. Langmuir 1998; 14: 248-251.

[54] Weber N, Wendel HP, Kohn J. Formation of viscoelastic protein layers on polymeric surf aces relevant to platelet adhesion. Journal of Biomedical Materials Research Part A 2005; 72A: 420-427.

[55] Rodahl M, Hook F, Kasemo B. QCM operation in liquids: An explanation of measured variations in frequency and Q factor with liquid conductivity. Anal. Chem. 1996; 68: 2219-2227.

[56] Hook F, Rodahl M, Brzezinski P, Kasemo B. Energy dissipation kinetics for protein and antibody-antigen adsorption under shear oscillation on a quartz crystal microbalance. Langmuir 1998; 14: 729-734.

[57] Hook F, Voros J, Rodahl M, Kurrat R, Boni P, Ramsden JJ, Textor M, Spencer ND, Tengvall P, Gold J, Kasemo B. A comparative study of protein adsorption on titanium oxide surfaces using in situ ellipsometry, optical waveguide lightmode spectroscopy, and quartz crystal microbalance/dissipation. Colloids and Surfaces BBiointerfaces 2002; 24: 155-170.

[58] Q-Sense. QCM-D. 2008.
Ref Type: Internet Communication

[59] Urbakh M, Daikhin L. Influence of the surface morphology on the quartz crystal microbalance response in a fluid. Langmuir 1994; 10: 2836-2841.

[60] Urbakh M, Daikhin L. Roughness effect on the frequency of a quartz-crystal resonateor in contact with a liquid. Physical review letters 1994; 649: 4866-4870.

[61] Hook F, Kasemo B, Nylander T, Fant C, Sott K, Elwing H. Variations in Coupled Water, Viscoelastic Properties, and Film Thickness of a Mefp-1 Protein Film during Adsorption and Cross-Linking: A Quartz Crystal Microbalance with Dissipation Monitoring, Ellipsometry, and Surface Plasmon Resonance Study. Anal. Chem. 2001; 73: 5796-5804.

[62] Vörös J. The density and refractive index of adsorbing protein layers. Biophysical journal 2004; 87: 553-561.

[63] Limson J, Odunuga OO, Green H, Hook F, Blatch GL. The use of a quartz crystal microbalance with dissipation for the measurement of protein-protein interactions: a qualitative and quantitative analysis of the interactions between molecular chaperones. South African Journal of Science 2004; 100: 678-682.

[64] Brewer SH, Glomm WR, Johnson MC, Knag MK, Franzen S. Probing BSA binding to citrate-coated gold nanoparticles and surfaces. Langmuir 2005; 21: 9303-9307.

[65] Voinova M, Rodahl M, Jonson M, Kasemo B. Viscoelastic acoustic response of layered polymer films at fluid-solid interfaces: continuum mechanics approach. Physica Scripta 1999; 59: 391-396.

[66] Hook F, Kasemo B, Nylander T, Fant C, Sott K, Elwing H. Variations in Coupled Water, Viscoelastic Properties, and Film Thickness of a Mefp-1 Protein Film during Adsorption and Cross-Linking: A Quartz Crystal Microbalance with Dissipation Monitoring, Ellipsometry, and Surface Plasmon Resonance Study. Anal. Chem. 2001; 73: 5796-5804.

[67] Hook F, Kasemo B, Nylander T, Fant C, Sott K, Elwing H. Variations in Coupled Water, Viscoelastic Properties, and Film Thickness of a Mefp-1 Protein Film during Adsorption and Cross-Linking: A Quartz Crystal Microbalance with Dissipation Monitoring, Ellipsometry, and Surface Plasmon Resonance Study. Anal. Chem. 2001; 73: 5796-5804.

[68] Hook F, Kasemo B, Nylander T, Fant C, Sott K, Elwing H. Variations in Coupled Water, Viscoelastic Properties, and Film Thickness of a Mefp-1 Protein Film during Adsorption and Cross-Linking: A Quartz Crystal Microbalance with Dissipation Monitoring, Ellipsometry, and Surface Plasmon Resonance Study. Anal. Chem. 2001; 73: 5796-5804.

[69] Caruso F, Furlong DN, Kingshott P. Characterization of Ferritin Adsorption onto Gold. Journal of Colloid and Interface Science 1997; 186: 129-140.

[70] Weber N, Pesnell A, Bolikal D, Zeltinger J, Kohn J. Viscoelastic properties of fibrinogen adsorbed to the surface of biomaterials used in blood-contacting medical devices. Langmuir 2007; 23: 3298-3304.

[71] Hovgaard M, Rechendorff K, Chevallier J, Foss M, Besenbacher F. Fibronectin adsorption on tantalum: the influence of nanoroughness. Journal of Physical Chemistry B 2008; 112: 8241-8249.

[72] Lassen B, Malmsten M. Competitive protein adsorption studied with TIRF and ellipsometry. Journal of Colloid and Interface Science 1996; 179: 470-477.

[73] Ying PQ, Yu Y, Jin G, Tao ZL. Competitive protein adsorption studied with atomic force microscopy and imaging ellipsometry. Colloids and Surfaces B-Biointerfaces 2003; 32: 1-10.

[74] Elwing H. Protein absorption and ellipsometry in biomaterial research. Biomaterials 1998; 19: 397-406.

[75] Jenkins TE. Multiple-angle-of-incidence ellipsometry. Journal of Physics D Applied Physics 1999; 32: R45-R56.

[76] Norde W, Rouwendal E. Streaming Potential Measurements As A Tool to Study Protein Adsorption-Kinetics. Journal of Colloid and Interface Science 1990; 139: 169-176.

[77] Kondo A, Murakami F, Higashitani K. Circular dichroism studies on conformational changes in protein molecules upon adsorption on ultrafine polystyrene particles. Biotechnology and bioengineering 1992; 40: 889-894.

[78] Lenk T, Horbett T, Ratner BD. Infrared spectroscopic studies of time-dependent changes in fibrinogen adsorbed to polyurethanes. Langmuir 1991; 7: 1755-1764.

[79] Lee J, Saavedra S. Molecular orientation in heme protein films adsorbed to hydrophilic and hydrophobic glass surfaces. Langmuir 1996; 12: 4025-4032.

[80] Garcia AJ, Boettiger D. Integrin-fibronectin interactions at the cell-material interface: initial integrin binding and signaling. Biomaterials 1999; 20: 2427-2433.

[81] Tougaard S. Accuracy of the non-destructive surface nanostructure quantification technique based on analysis of the XPS or AES peak shape. Surface and interface analysis 1998; 26: 249-269.

[82] Hayakawa T, Yoshinari M, Nemoto K. Quartz-crystal microbalance-dissipation technique for the study of initial adsorption of fibronectin onto tresyl chloride-activated titanium. Journal of Biomedical Materials Research Part B-Applied Biomaterials 2005; 73B: 271-276.

[83] Matsuura T, Hosokawa R, Okamoto K, Kimoto T, Akagawa Y. Diverse mechanisms of osteoblast spreading on hydroxyapatite and titanium. Biomaterials 2000; 21: 1121.

[84] Voinova M, Jonson M, Kasemo B. 'Missing mass' effect in biosensor's QCM applications. Biosensors & Bioelectronics 2002; 17: 835-841.

[85] Erickson HP, Carrell N, McDonagh J. Fibronectin molecule visualized in electron microscopy: a long, thin, flexible strand. The Journal of Cell Biology 1981; 91: 673-678.

[86] Williams EG, Janmey PA, Ferry JD, Mosher DF. Conformational states of fibronectin. Effects of pH, ionic strength, and collagen binding. The Journal of Biological Chemistry 1982; 257: 14973-14978.

[87] Benecky MJ, Kolvenbach CG, Wine RW, DiOrio JP, Mosesson MW. Human plasma fibronectin structure probed by steady-state fluorescence polarization: evidence for a rigid oblate structure. Biochemistry 1990; 29: 3082-3091.

[88] Khan MY, Medow MS, Newman SA. Unfolding transitions of fibronectin and its domains. Stabilization and structural alteration of the N-terminal domain by heparin. Biochemical Journal 1990; 270: 33-38.

[89] Benecky MJ, Wine RW, Kolvenbach CG, Mosesson MW. Ionic-strength- and pH-dependent conformational states of human plasma fibronectin. Biochemistry 1991; 30: 4298-4306.

[90] Rechendorff K, Hovgaard M, Foss M, Zhdanov V, Besenbacher F. Enhancement of protein adsorption induced by surface roughness. Langmuir 2006; 22: 10885-10888.

[91] Hook F, Kasemo B, Nylander T, Fant C, Sott K, Elwing H. Variations in coupled water, viscoelastic properties, and film thickness of a Mefp-1 protein film during adsorption and cross-linking: a quartz crystal microbalance with dissipation monitoring, ellipsometry, and surface plasmon resonance study. Anal. Chem. 2001; 73: 5796-5804.

[92] Otzen DE, Oliveberg M, Hook F. Adsorption of a small protein to a methyl-terminated hydrophobic surfaces: effect of protein-folding thermodynamics and kinetics. Colloids and Surfaces B-Biointerfaces 2003; 29: 67-73.

[93] Dolatshahi-Pirouz A, Rechendorff K, Hovgaard M, Foss M, Chevallier J, Besenbacher F. Bovine serum albumin adsorption on nano-rough platinum surfaces studied by QCM-D. Colloids and Surfaces B: Biointerfaces 2008; 66: 53-59.

[94] Rodahl M, Höök F, Fredriksson C, Keller C, Krozer A, Brzezinski P, Voinova M, Kasemo B. Simultaneous frequency and dissipation factor QCM measurements of biomolecular adsorption and cell adhesion. Faraday Discussions 1997; 107: 229-247.

[95] Hook F, Kasemo B, Nylander T, Fant C, Sott K, Elwing H. Variations in Coupled Water, Viscoelastic Properties, and Film Thickness of a Mefp-1 Protein Film during Adsorption and Cross-Linking: A Quartz Crystal Microbalance with Dissipation Monitoring, Ellipsometry, and Surface Plasmon Resonance Study. Anal. Chem. 2001; 73: 5796-5804.

[96] Hook F, Kasemo B, Nylander T, Fant C, Sott K, Elwing H. Variations in Coupled Water, Viscoelastic Properties, and Film Thickness of a Mefp-1 Protein Film during Adsorption and Cross-Linking: A Quartz Crystal Microbalance with Dissipation Monitoring, Ellipsometry, and Surface Plasmon Resonance Study. Anal. Chem. 2001; 73: 5796-5804.

[97] Dillman WJ, Miller IF. On the adsorption of serum proteins on polymer membrane surfaces. Journal of Colloid and Interface Science 1973; 44: 221-241.

[98] Nyilas E, Chiu TH, Herzlinger GA. Thermodynamics of native protein/foreign surface interactions. I. Calorimetry of the human gamma-globulin/glass system. Transactions - American Society for Artificial Internal Organs 1974; 20B: 480-490.

[99] Mitra SP, Chattoraj DK. Some thermodynamic aspects of expanded & condensed films of BSA adsorbed at the alumina-water interface. Indian Journal of Biochemical and Biophysics 1978; 15: 147-152.

[100] Hummel SP, Anderson BS. Ribonuclease adsorption on glass surfaces. Archives of Biochemistry and Biophysics 1965; 112: 443-449.

[101] Yang YZ, Cavin R, Ong JL. Protein adsorption on titanium surfaces and their effect on osteoblast attachment. Journal of Biomedical Materials Research Part A 2003; 67A: 344-349.

[102] do Serro APVA, Fernandes AC, Saramago BDV, Norde W. Bovine serum albumin adsorption on titania surfaces and its relation to wettability aspects. Journal of Biomedical Materials Research 1999; 46: 376-381.

[103] Miller R, Treppo S, Voigt A, Zingg W, Neumann AW. Contact angle kinetics of human albumin solutions at solid surfaces. Colloids and Surfaces 1993; 69: 203-208.

[104] Jung S, Lim S, Albertorio F, Kim G, Gurau MC, Yang RD. The Vroman effect: a molecular level description of fibrinogen displacement. Journal of American Chemical Society 2003; 125: 12782-12786.

[105] Vroman L, Adams AL. Findings with the recording ellipsometer suggesting rapid exchange of specific plasma proteins at liquid/solid interfaces. Surface Science 1969; 16: 438-446.

[106] Brash JL, Lyman DJ. Adsorption of plasma proteins in solution to uncharged, hydrophobic polymer surfaces. Journal of Biomedical Materials Research Part A 1969; 3: 175-189.

[107] Noh H, Vogler EA. Volumetric interpretation of protein adsorption: competition from mixtures and the Vroman effect. Biomaterials 2007; 28: 405-422.

4. Development of early fibronectin matrix and adhesion of MG63 osteoblasts-like cells on c.p. rough Ti coated with different biological pre-coatings

4.1. Introduction

The development of bone-implant interfaces depends on the direct interactions of osteoblasts and the subsequent deposition of bone matrix. Therefore, proper cell adhesion and the formation of osteoblast extracellular matrix (ECM) are essential steps for successful osseointegration of biomaterials [1;2]. Cell adhesion on 2D surfaces constrains natural interaction with the ECM to a certain extent. It starts with the adsorption of adhesive matrix proteins from the surrounding medium, followed by recognition of these proteins by the cells [3;4], which triggers specific cellular responses [5;6]. Fibronectin (Fn) is one of the earliest proteins to be laid down in the ECM [7] and its distribution in the areas of skeletogenesis suggests that it is involved in the early stages of bone formation [8;9]. Fn has also been shown to play a critical role in osteoblast differentiation and survival [10]. Several studies have suggested that Fn is required for the recruitment of growth factors [11] and for the assembly of multiple ECM proteins,

including collagen [12], fibrinogen [13] and thrombospondin [14]. Fn is a soluble matrix protein that is particularly important for the initial cellular interaction with foreign materials, as it is uniformly available in most biological fluids [7;15] and readily adsorbs to the surfaces. Together with other ECM proteins, Fn is recognized by specific cell surface receptors from the integrin family [5;16;17], which guide the initial adhesion and subsequent behaviour of the adhering cells [17]. Bovine serum albumin (BSA) is a globular protein and the most abundant component of many biofluids serving the transport of various metabolites and the regulation of the osmotic pressure [18;19]. Fibrinogen (Fbg) is believed to be central to surface-induced thrombus formation by directly participating in the coagulation cascade [20]. Moreover, Fbg adsorption plays a very important role in governing inflammatory responses [21] and positively related to platelet adhesion [22].

Early *in vitro* studies of osteoblast behaviour focused essentially on the involvement of materials associated with biologically active molecules, but paid less attention to their surface characterization [23;24]. It is now well documented that surface properties, such as wettability [25], charges [3;26] and chemistry and surface topography [27], play a critical role in the establishment of cell-biomaterial contacts [17;28]. Although Richards found that surface roughness had no influence on the total area of adhered fibroblasts [29], the fact that surface topography strongly influences the behaviour of adhering cells is widely accepted in the literature [23;27;28] particularly for Ti surfaces [26;30]. For example, fibroblasts that adhered to a ground Ti surface extended their body in the direction of the surface grooves. These aligned cells attached better than spherical ones [31]. Osteoblasts were oriented in a similar way on grooved surfaces [32]. On smooth substrate, they were randomly oriented, whilst on grooved surfaces they lined up in parallel to the 5μm deep grooves. However, attempts to quantitatively characterize roughness are rather weak in many of these studies. Indeed, it is now increasingly admitted that roughness has to be considered in terms of not only the vertical dimensions of the topographical features, but also their distribution, organization and frequency on the surfaces under study [17;28;33;34].. All these factors influence osteoblast behaviour.

The removal of material from dental-implant surfaces by means of grit-blasting, etching or a combination of both methods is a well-documented example of the beneficial effects of surface topography modifications on the *in vitro* and *in vivo* implant response that is already used in treatments [35;36]. The vertical dimensions of the randomly-distributed topographical features range from micrometre to nanometre level, depending on the applied treatment and conditions. However, the optimal values of the amplitude-roughness parameters (R_a, S_a,) for these surfaces are still disputed. In fact, beneficial effects have been correlated between surfaces with R_a in the range 0,5-8,5 μm and *in vivo* histomorphometric results [37]. Moreover, surface topography and surface physicochemical properties are intrinsically intertwined. Consequently, surface topography is not the only variable controlling the biological response [38]. Among other

factors, surface energy has recently been studied as a very influential property in the biological response of these surfaces, specifically in the early events that occur when proteins adsorb and cells are recruited and adhered to the substrate.

However, the mechanisms that underscore such topographical and physicochemical responses are still poorly understood and are the focus of the work presented here.

Specifically, another factor that is important for successful cellular interaction is the ability of adhering cells to remodel adsorbed and secreted matrix proteins, which may be supported by the material's surface properties. For example, Fn is significantly remodelled by the adhering cells, such as fibroblasts [39-42] and endothelial cells [43]. This process is strongly dependent on the material surface properties, such as its wettability [40] and chemistry [44]. It has further been demonstrated that the remodelling of both adsorbed (early matrix) and secreted (late matrix) Fn are guided by the coordinated function of integrins [45], which presumably reflects an attempt by the cells to develop their own provisional ECM on the biomaterial interface [41].

Although Anselme et al. showed that the organization of provisional ECM by osteoblasts is better organized on smooth than on rough surfaces [28], the role of topographical features on the behaviour of Fn adsorption has not been studied.

Consequently, the hypothesis that the organization of the Fn matrix at the material interface will be strongly influenced by the surface roughness and its parameters, which in their complexity may resemble the natural organization of ECM to a certain extent is tested here.

4.2. Objectives

The main objectives of the present chapter are:

1. To characterize the observed amount of fluorescent BSA, Fn and Fbg and Fn distribution onto smooth and rough titanium surfaces.

2. To study the influence of Fn pre-coating and surface parameters, i.e. surface energy and roughness, on MG63 osteoblasts-cells-like adhesion.

3. To investigate the spatial organization of Fn fibrils within the secreted extracellular matrix on grit-blasted Ti surfaces that is already known that had led to a beneficial *in vitro* and *in vivo* biological response [46-48].

4.3. Materials and Methods

4.3.1. Materials

4.3.1.1. Surfaces

8 mm in diameter and 2 mm thick disks of c.p. Titanium Grade II (c.p. Ti) were used for the experiments. Seven different series of Ti surfaces were obtained by blasting at 0,25 MPa-pressure during the time required for roughness saturation. Depending on the nature of the blasting parameters the samples were divided as A for Al_2O_3 and S for SiC particles. Moreover, by the different particles size the following codification was used: 3 for 212-300 μm mean particle size, 6 for 425-600 μm and 9 for 1000-1400 μm. The obtained surfaces finishes were A3, A6, A9, S3, S6, S9, respectively, and a Smooth surface was used as control.

Smooth   Polished c.p. Ti. The samples were abraded subsequently with 400, 600 and 1200 grit silicon carbide abrasive paper and finally polished with a water suspension of 1 μm alumina powder

A3   c.p. Ti blasted with Al_2O_3-particles of 212–300 μm in size

A6   c.p. Ti blasted with Al_2O_3-particles of 425–600 μm in size

A9   c.p. Ti blasted with Al_2O_3-particles of 1000–1400 μm in size

S3   c.p. Ti blasted with SiC-particles of 212–300 μm in size

S6   c.p. Ti blasted with SiC-particles of 425–600 μm in size

S9   c.p. Ti blasted with SiC-particles of 1000–1400 μm in size

After blasting the samples were cleaned by sonication in acetone for 15 min, followed by sonication in distilled water for 15 min. Finally, all samples were steam-sterilized at 121 ⁰C for 30 min and kept under vacuum. .

4.3.1.2. BSA, Fn and Fbg

Bovine serum albumin (BSA) (Sigma, Sant Louis, USA) and human fibrinogen (Fbg) (Sigma, Sant Louis, USA) were diluted in PBS phosphate buffered saline 1X (PBS, consisting of 140 mM NaCl; 2,7 mM KCl; 8,1mM $Na_2HPO_4 \cdot 7H_2O$; 1,5mM $KHPO_4$) to obtain a working concentration of 1 mg/ml.

Human plasma Fn was prepared by affinity chromatography on gelatin-Sepharose 4B /12/ and further purified on heparin-Sepharose 4B. Fn was eluted with 0,5 M NaCl, 50

mM Tris pH 7,3. For the experiments, Fn was diluted to concentration of 1mg/ml in PBS 1X and stored at 4 ºC for up to 1 week. Working dilutions were also done in PBS 1X.

4.3.1.3.   Cells

Human osteoblast-like MG63 cells were grown in Dulbecco's modified Eagle's medium (DMEM, Gibco) supplemented with 10% foetal calf serum (FCS), 1% penicillin/streptomycin, 1% L-glutamine, 1% pyruvate (Sigma) at 37ºC in 5%CO_2/95% air atmosphere and 100% humidity. MG63 cells were obtained from American Type Culture Collection (Rockville, MD). Culture medium was changed every two days. For the experiments, cells were harvested at 70-90% confluence by Tripsin/EDTA, centrifuged and re-suspended in serum-free medium before plating on the samples. The cells were incubated for 4h when the initial adhesion was studied, and for 4 days for the visualization of Fn matrix (see below), at 37 ºC.

4.3.2.   Methods

4.3.2.1.   Protein adsorption

4.3.2.1.1.   Fluorescent FITC- BSA, Fn, and Fbg preparation

FITC-labelled BSA (FITC-BSA), Fn (FITC-Fn) and Fbg (FITC-Fbg) were prepared as described by Faucheux et al. [39]. Briefly, 1ml of each protein solution (1mg/ml) was dissolved in 0,1 M sodium bicarbonate buffer pH 9 and than 10 µl of FITC (fluorescein isotiocianat, Sigma Chemicals Co) dissolved in DMSO (10mg/ml stock) was added. The mixture was incubated for 2 hours at room temperature and non-reacted dye was separated on Sephadex G-25 column (5 ml, flow rate of 2 ml/min) pre-equilibrated with PBS. The final protein concentration was estimated by measuring the absorbance at 280nm (UV Mini 1240 spectrophotometer, Shimadzu) and after, the labelled protein solutions stored at 4 ºC.

4.3.2.1.2.   Quantification of FITC-labelled BSA, Fn and Fbg adsorption

FITC-BSA, FITC-Fn and FITC-Fbg, at working concentrations of 100, 20 and 50 µg/ml respectively, were adsorbed on the different Ti series for 30 min at 37 ºC. The samples were then rinsed three times with PBS. The adsorbed FITC-labelled protein was eluted with 500 µl of 0,2 N NaOH for 2h.

The fluorescent intensity of the extracts was measured with a spectrofluorophotometer RF-1501 (Shimadzu). The excitation and emission wavelengths were set at 488 and 530 nm, respectively. The quantity of the protein was determined by comparison to a standard curve prepared under identical conditions with 262, 328, 410, 512, 640, 800 and 1000 ng/ml of FITC-labelled protein.

4.3.2.1.3. Visualization of adsorbed FITC-fibronectin

FITC-Fn (20 µg/ml) was adsorbed onto smooth and grit-blasted samples for 30 min at 37 ⁰C. The samples were then fixed with 3% paraformaldehyde, mounted in Moviol and examined with a fluorescence confocal laser scanning microscope, CLSM (Leica TCS SP2) using the z-stack mode. 3D images were reconstructed using the original microscope software. The CLSM settings were kept constant allowing comparative measurements at several points of the substrata.

4.3.2.2. Initial cell adhesion

Surfaces were pre-coated with 20 µg/ml Fn for 30 min at 37 ⁰C. Then the samples were washed three times with sterilized PBS 1X and the cells added. In parallel, control series without pre-coating were prepared.

The washed samples were placed into a 24-well tissue culture plates (TCPS) (Falcon, Becton Dickenson & Company, New Jersey) then, 3×10^4 cells per sample (diluted in 2ml serum free medium) were added and incubated for 4h in serum free medium. To observe cell adhesion and the overall morphology of adhering cells, the samples were stained with fluorescein diacetate (FDA) added directly to the medium to give a final concentration of 1 µg/ml (from a stock of 1mg/ml in acetone) for 3 min. The stained living cells, the only able to convert the die to a fluorescent analogue, were viewed and photographed with an inverted fluorescent microscope (Nikon, Eclipse E600) using the green channel.

The microscope settings were kept constant allowing comparative measurements at several points on the surface. Different parameters were studied by ImageJ software:

i.   Cell mean area ($µm^2$).
ii. Aspect ratio: The maximum ratio of width and height of a bounding rectangle for the cell, as a shape parameter.
iii. Maximum diameter (µm): The maximum cell length, as a cell spreading parameter.
iv. Number of cells/cm^2: The number of cells for each sample was calculated and normalized by the image area.

4.3.2.3. Fibronectin matrix

The ability of cells to secrete and organize Fn into an extracellular matrix was examined via indirect immunofluorescence. For that purpose 3×10^4 cells were incubated in 2ml of completed medium (with 10% FCS) for 4 and 7 days, in 24-well TC plates containing the different series of Ti samples. After the incubation, the cultured discs were washed and fixed with 3% paraformaldehide for 10min, then rinsed again three times with PBS before saturation with 1% albumin/PBS for 15 min. Fn matrix was stained with rabbit polyclonal anti-human Fn (1:100) primary antibody (Immunotech SA, France, lot No.0326), followed by Goat anti-rabbit Cy2 conjugated (1:500) secondary antibody (Molecular Probes A-11070). The samples were finally rinsed 3 times with PBS and once with distilled water, and then mounted on a microscope slide under glass cover slips and visualized by fluorescence confocal laser scanning microscope (CLSM). The CLSM reflection mode was used to visualize the substrate in parallel as the ECM was studied. Ten points on the substrata for each series were checked to obtain statistics results of the ECM overall thickness and the start and ending point with respect to the sample roughness.

4.3.2.4. Statistical analysis

ANOVA tables and Fisher's multiple comparisons tests were performed to assess statistically significant differences between groups (p<0,05). Each data point represents mean ± standard deviation (SD) of at least five independent experiments. These tests were carried out with Minitab™ Release 14 (Minitab Inc.,USA).

216

4.4. Results

4.4.1. Protein adsorption

The adsorption of the three fluorescent-labelled proteins on the different titanium surfaces is shown in Figure 5-1. The first row in Figure 4-1 shows the amount of FITC-BSA, FITC-Fn and FITC-Fbg absorbed per surface real area of smooth, S3, S6, A3 and A6 titanium surfaces. The second and third rows plot the values of protein absorption vs surface free energy, SFE, and mean surface roughness, R_a-parameter, respectively.

The protein adsorbed by squared centimeter of smooth and rough Ti samples is dependant on the protein of study. Blasting with SiC particles, provide conditions for increased adsorption of FITC-Fn and FITC-BSA protein compared to surfaces blasted with alumina. And the lower the particle size, the higher the amount of FITC-BSA and FITC-Fn adsorbed. No statistically significant differences were found in the Fbg adsorption values on the different surfaces except on A6, which lowered Fbg adsorption.

When adsorption values are plotted vs. the corresponding SFE values for the different titanium surfaces (Figure 4-1, 2nd row) a positive correlation between adsorbed Fn and total SFE was determined for the blasted surfaces. A value of 0,85 for the Pearson's correlation coefficient was calculated. However, the smooth samples with nanometre roughness and absence of particles on the surface did not correlated with the values for the blasted samples. Same trend was obtained for BSA protein adsorption, with a 0,91 Pearson's coefficient. Again, smooth samples did not correlate with the values for blasted samples. Interestingly, no correlation was found between Fbg adsorption and SFE.

None of the proteins tested showed adsorption values that correlated with roughness values (Figure 4-1, 3rd row). An increased roughness, i.e., the use of a higher particle size for blasting, did not influence the amount of proteins adsorbed per real surface area. Otherwise, as aforementioned and even better visualized in these plots, Fn and BSA were adsorbed in highest quantities onto SiC-blasted surfaces than on Al_2O_3-blasted ones. Again, no influence of the topographical parameter was determined on the values of Fbg adsorption.

The pattern/distribution of FITC-labelled Fn adsorption on the different rough Ti surfaces is shown on Figure 4-2. The 3D images were obtained by CLSM and presented as maximum projections from the Z stacks mode. Thus, all surface-associated Fn is visible. The main observation from these studies was the irregularity of the adsorbed Fn pattern on blasted surfaces. Overall, Fn adsorbs preferentially on peaks (arrow) than on valleys (arrowhead). Conversely, on smooth surfaces Fn was adsorbed with a typical fully-homogeneous pattern.
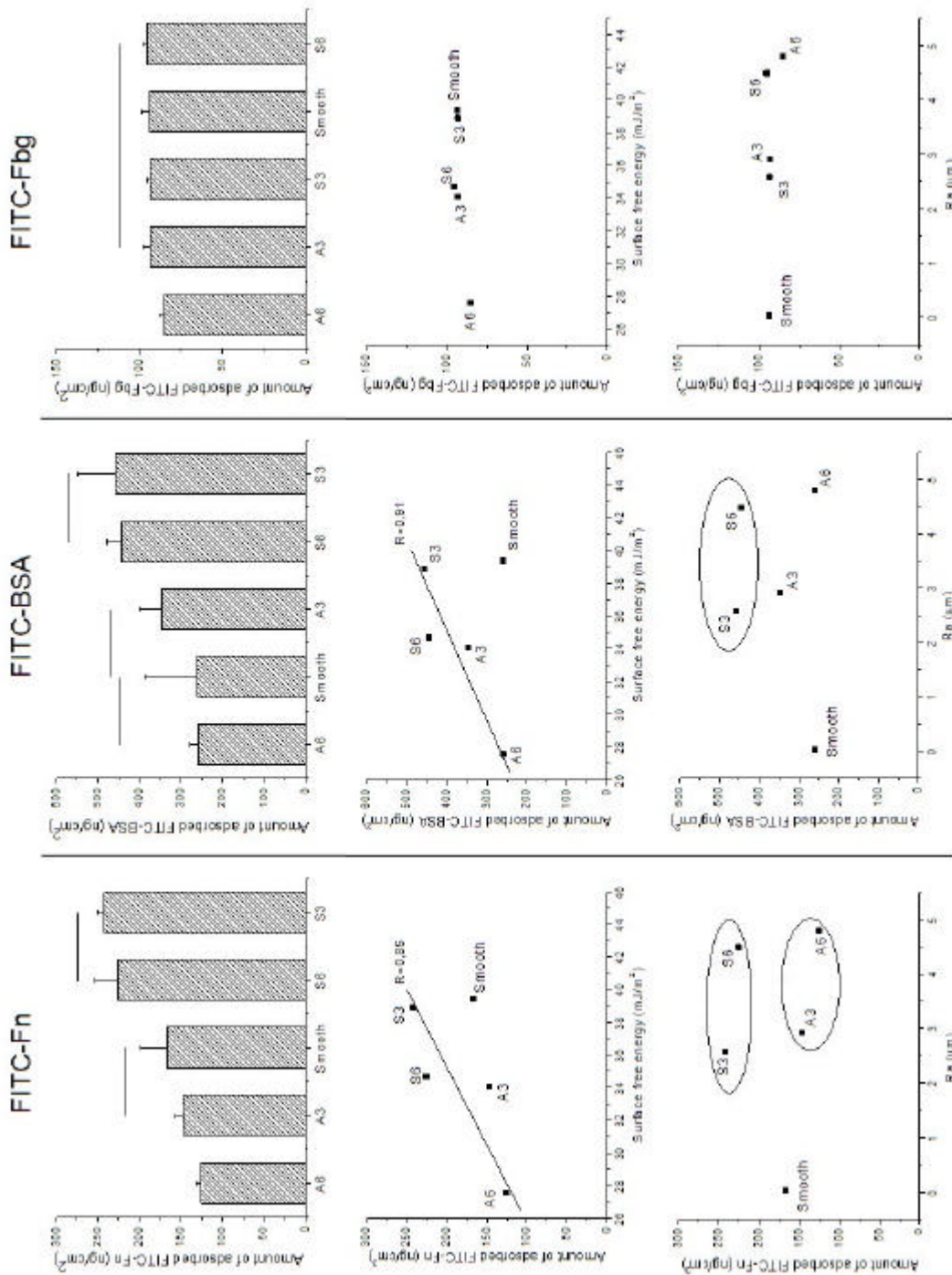
Figure 4-1 FITC- BSA, FITC-Fn and FITC-Fbg adsorption on the different titanium surfaces. First row: values of protein adsorption on the different titanium surfaces. First row: values of protein adsorption per real surface area. Second row: values of protein adsorption vs surface free energy. Third row: values of protein adsorption vs the mean roughness, Ra-parameter. Points on graphs in second and third row are mean values. Standard deviation bars are not depicted for a better visualization of the trends of the response
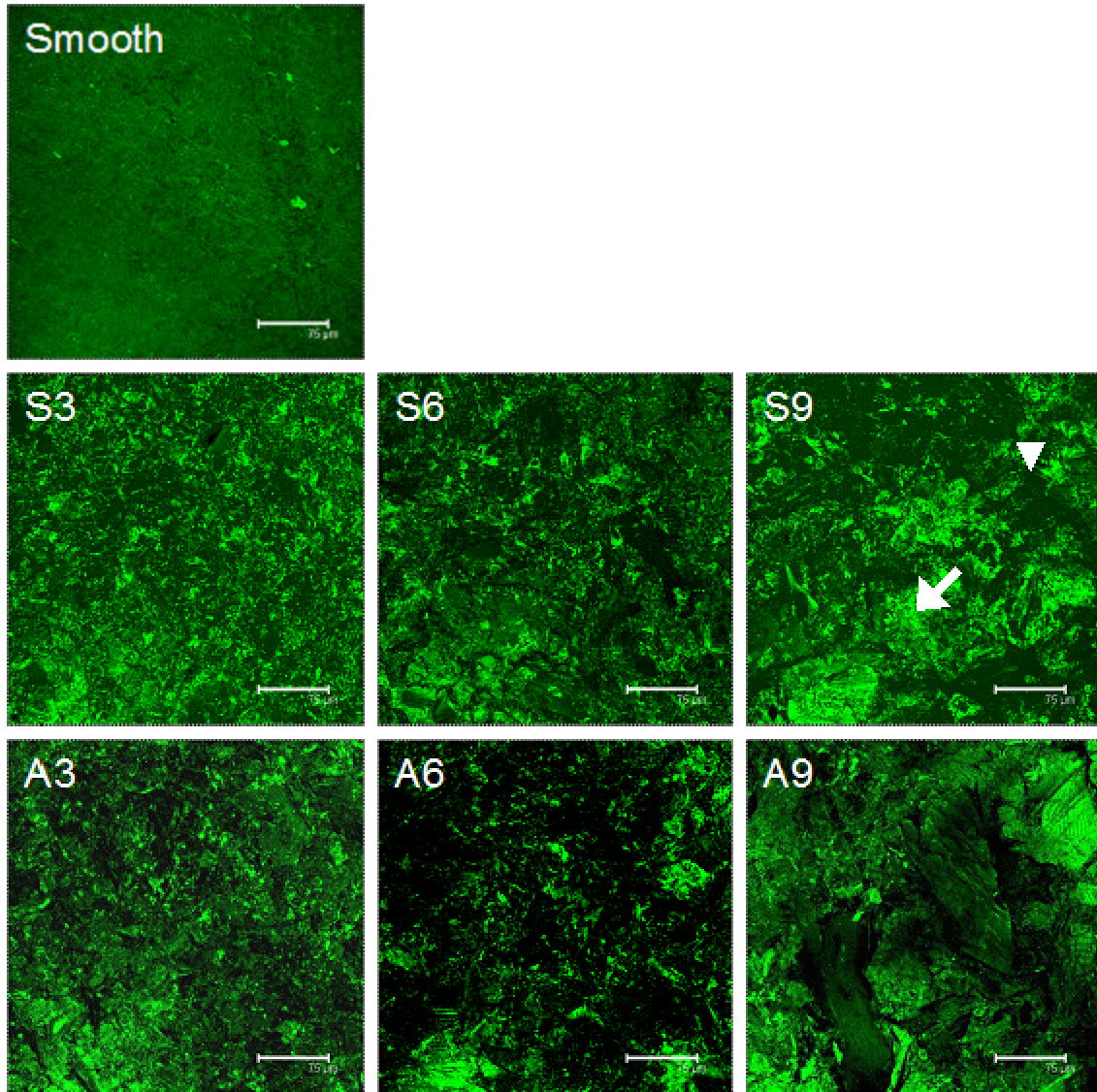
*Figure 4-2 Visualization by CLSM Distribution of adsorbed FITC-labelled fibronectin on the different Ti surfaces. All bars are 75**m**m*

4.4.2. Cell adhesion and overall morphology

Figure 4-3 shows the overall morphology of adhering MG63 cells after 4 hours in culture on Fn pre-coated and plain surfaces. The higher the surface roughness, the higher the number of adhered cells is. This effect was most pronounced on samples blasted with Al_2O_3 particles (A3, A6, A9), in which cells also tended to aggregate (A6 and A9). Pre-adsorption with Fn clearly induced cell spreading on smooth Ti surfaces. The quantification of cell adhesion (Table 4-1) confirmed an increase in the number of cells per real surface area when the size of blasting particles was increased, i.e. when the surface roughness was higher. All differences were statistically significant when tested against results for smooth titanium surfaces (p<0,05).
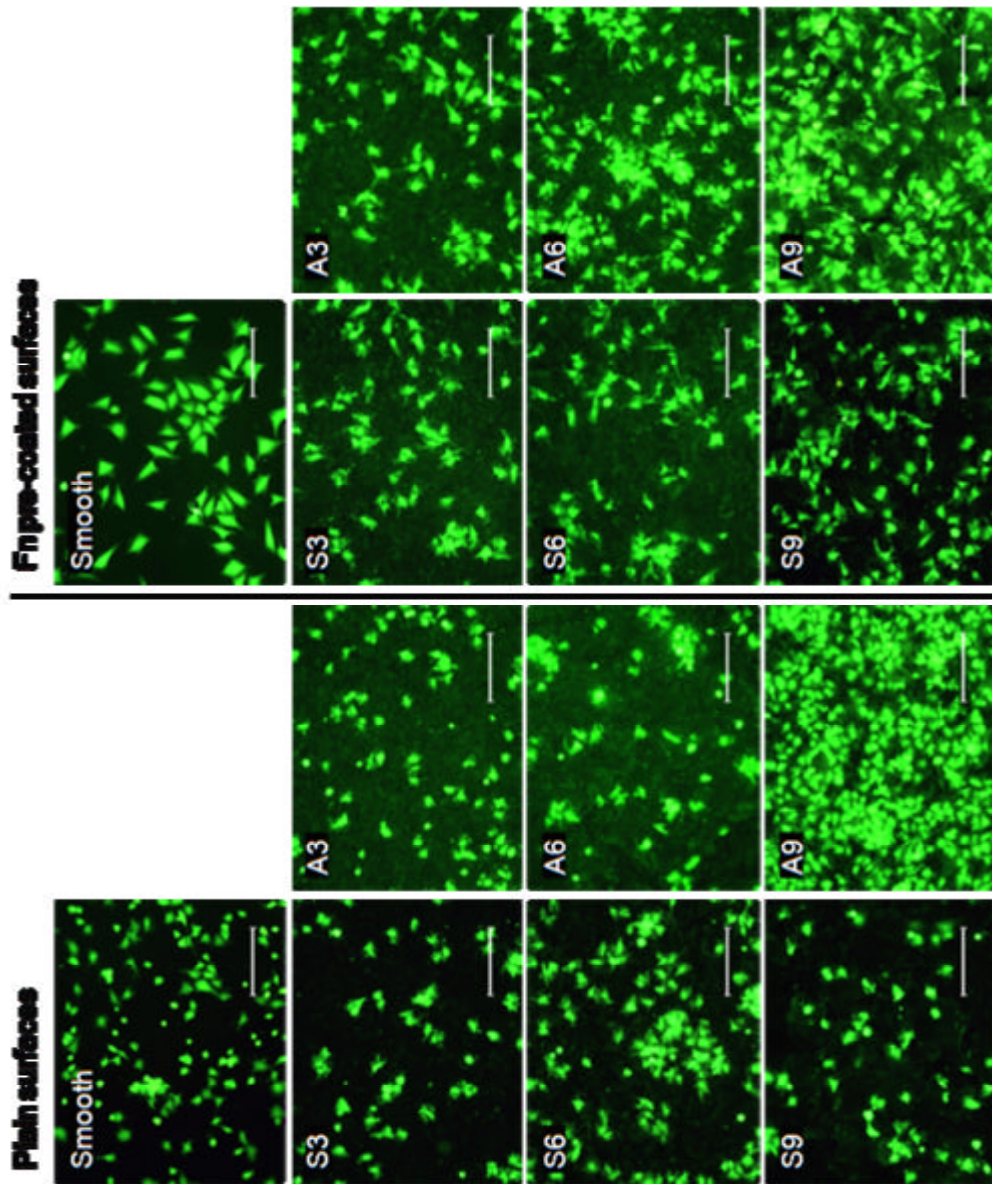
Figure 4-3 Overall morphology of adhered MG63 cells after 4h in culture on the different titanium surfaces without and with Fn pre-coatings. . All bars are 50mm

Osteoblasts spread less efficiently on rougher Ti surfaces and often showed multiple projections. Such typical cells are shown in Figure 4-4, right; and compared to the well-spread cells on smooth samples, Figure 4-4, right. The quantitative data for cell surface areas shown in Table 4-1 confirmed this fact, as a two-fold or even three-fold reduction was found, with values of around 500-800µm² (S9 and A9 samples) compared to approx. 1500µm² on a smooth Ti surface. That is approximately 3 times more spread, though it is worth mentioning that high variations of the mean values where calculated as a result of the heterogeneity in cell sizes.
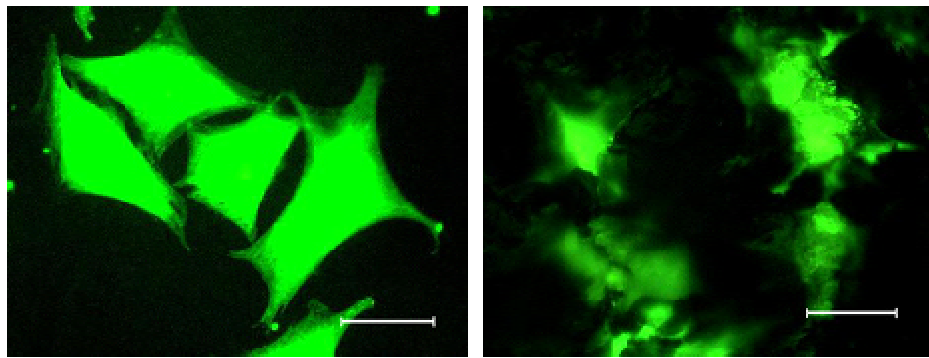
Figure 4-4 *Zoomed CLSM image showing the morphology of adhered MG63 cells on smooth and A9 surfaces pre-coated with Fn. All bars are 15**m**m*

Table 4-1 *Different cell adhesion parameters and the number of cells per squared cm were calculated from CLSM images at low magnification (100X). Each area analysed by ImageJ software was 861,46**m**m×687,55**m**m*

Samples		Area (mm²)	Aspect ratio	Ø Max (mm)	Number of particles/cm²
Serum	**Smooth**	514,00 ± 215,24	1,44 ± 0,36	35,24 ± 11,17	1257,82 ± 322,34
Fn	**Smooth**	1543,08 ± 494,88	1,81 ± 0,55	67,59 ± 14,71	1029,89 ± 23,88
	S3	574,80 ± 352,03	1,73 ± 0,47	40,55 ± 17,22	1226,86 ± 194,22
	S6	514,56 ± 388,84	1,75 ± 0,50	37,04 ± 17,31	1350,67 ± 442,53
	S9	539,62 ± 331,84	1,65 ± 0,49	36,97 ± 15,56	2235,94 ± 155,20
	A3	748,93 ± 544,62	1,73 ± 0,46	45,41 ± 23,27	1173,40 ± 226,83
	A6	869,25 ± 462,85	1,58 ± 0,40	48,09 ± 16,62	2068,22 ± 513,35
	A9	504,36 ± 274,05	1,65 ± 0,51	35,58 ± 11,94	3781,89 ± 501,41

4.4.3. Fibronectin matrix formation

After 4 days of incubation the samples were fixed and the newly produced Fn matrix visualized by immunofluorescence. As shown in Figure 4-5, MG63 osteoblasts deposited Fn fibrils in a specific "facet-like" pattern following the organization of the cell layer, which was rather dense and randomly dispersed on the smooth Ti surface. The rough topography visibly affected the organization of the osteoblast matrix. Fn fibrils became irregularly dispersed and tended to organize into focal structures that were more expanded when the roughness increased. Fn matrix was not present in these foci. Its absence was not due to an out-of-focus device, as the maximum projection mode of at least 15 z-stacks of CLSM was used to visualize the samples. Figure 4-6 shows 3D reconstituted images of the Fn network. The Fn was mostly on the peaks of the surface topographic features. Matrix fibrils were almost absent in the valleys.
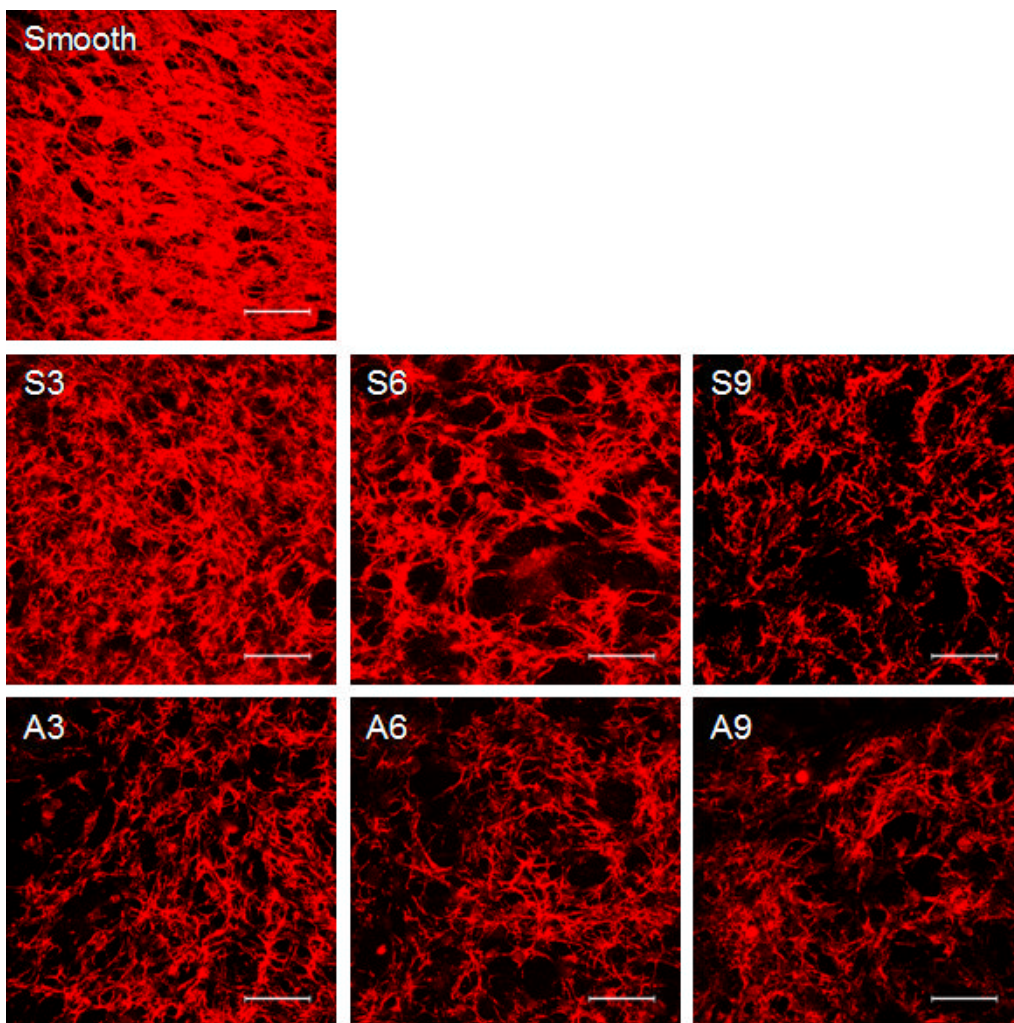
Figure 4-5 Extracellular fibronectin matrix produced by MG63 cells after 4 days culturing on the different Ti samples. Fibronectin is visualized via immunofluorescence. All bars are 20 mm

To learn more about the spatial organization of the Fn matrix, the fluorescent images were reconstituted simultaneously with the topography viewed in the CLSM reflection mode (Figure 4-7). These samples were cultured with cells for a longer period of 7 days. Figure 4-7 shows that on rough Ti surfaces, the Fn matrix appeared to be much thicker and did not follow the unevenness of the underlying topography. Instead, the Fn matrix seemed to overlie the top of the rough Ti surface, and therefore did not enter the valleys beneath. Quantitative measures show that the thickness of this Fn-containing matrix layer significantly increased when the vertical amplitude of the roughness increased (Table 4-2). However, this layer did not penetrate the topography by more than half of the maximum peak-to-valley distance, i.e. it only reached the "cross point" depicted on the graph inserted in Table 4-2.
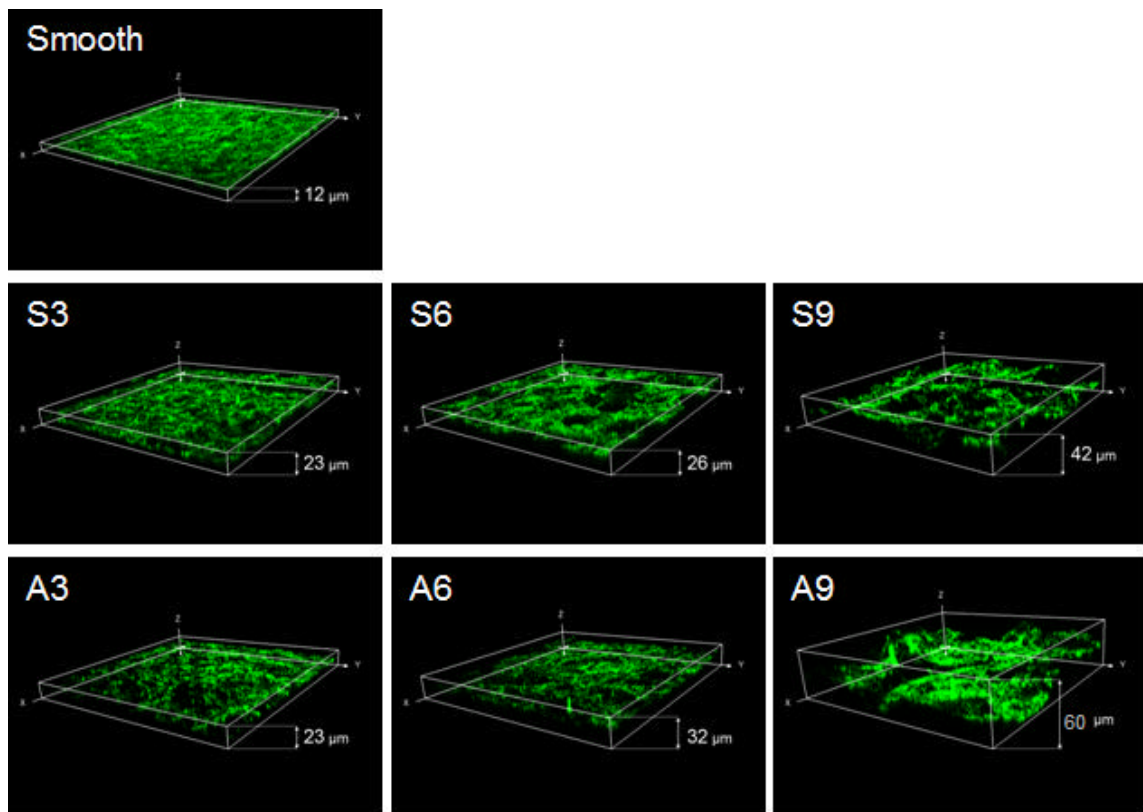
Figure 4-6 3D organization of the extracellular fibronectin matrix formed by MG63 culturing cells after 7days on different Ti samples. Images were obtained by CLSM (Z stack mode) and viewed by the corresponding software
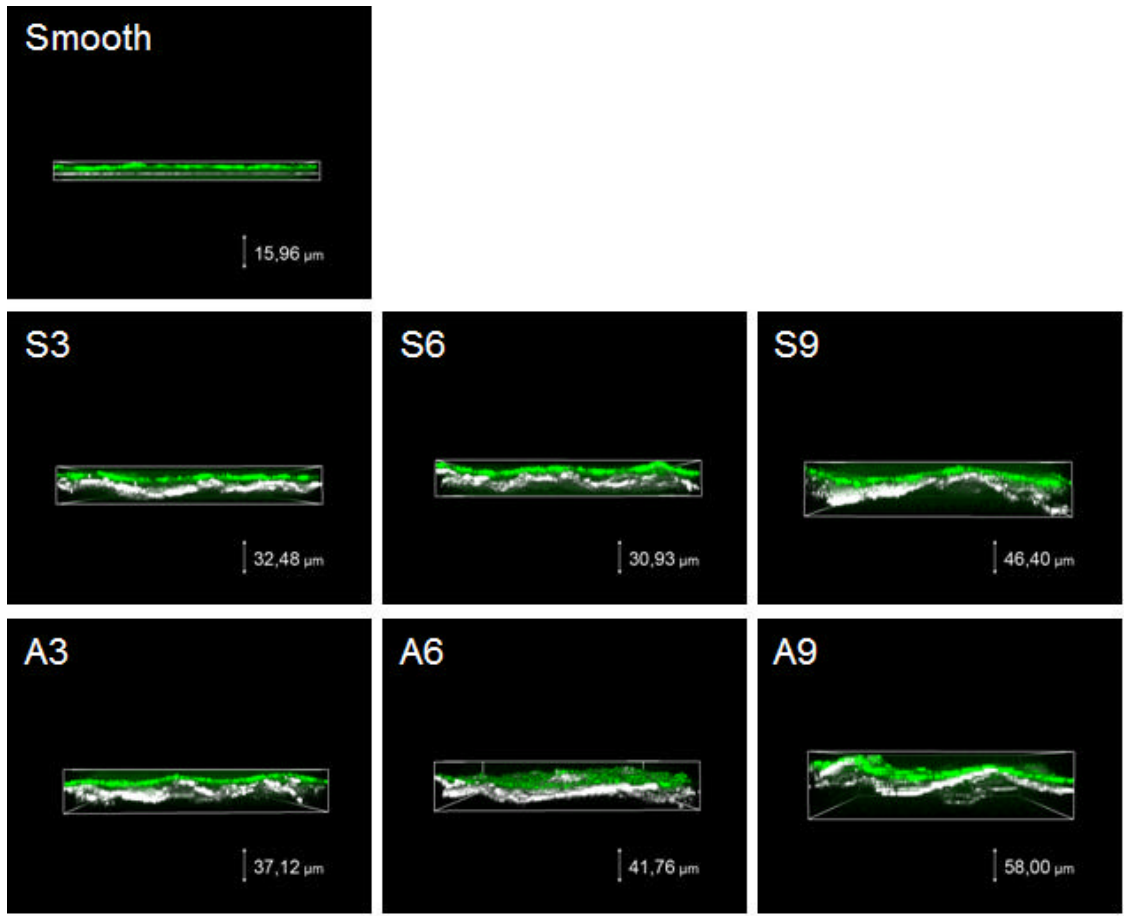
Figure 4-7 *Confocal Z-stack mode images of Fn organization of the ECM, the fluorescent images were reconstituted simultaneously with the topography which was viewed at the CLSM reflection mode*

Table 4-2 *Roughness and distance parameters obtained by confocal microscopy measurements from the visualization of the ECM at the same time as the substrate by the reflection mode. Ry corresponds to the distance, ECM is the extracellular matrix thickness, the Cross point is the distance where the ECM starts to appear and Above ECM is the matrix above of the sample*

Samples	Ry (nm)	ECM (nm)	Cross point (nm)	Above ECM (nm)	Graph parameters
Control	Ø	$11{,}295 \pm 0{,}666$	Ø	Ø	
Smooth	$15{,}267 \pm 2{,}678$	$11{,}255 \pm 1{,}367$	$5{,}682 \pm 1{,}592$	$1{,}670 \pm 1{,}707$	
S3	$25{,}691 \pm 2{,}336$	$16{,}379 \pm 2{,}109$	$12{,}194 \pm 1{,}405$	$2{,}882 \pm 1{,}417$	
S6	$29{,}339 \pm 3{,}529$	$18{,}397 \pm 2{,}311$	$16{,}265 \pm 2{,}684$	$5{,}323 \pm 1{,}449$	
S9	$48{,}768 \pm 6{,}864$	$27{,}503 \pm 3{,}233$	$24{,}630 \pm 3{,}769$	$3{,}365 \pm 2{,}575$	
A3	$35{,}436 \pm 2{,}011$	$18{,}215 \pm 1{,}353$	$20{,}396 \pm 2{,}253$	$3{,}175 \pm 1{,}885$	
A6	$41{,}518 \pm 5{,}433$	$23{,}052 \pm 4{,}413$	$19{,}150 \pm 1{,}948$	$0{,}684 \pm 0{,}920$	
A9	$50{,}955 \pm 7{,}028$	$26{,}206 \pm 3{,}529$	$24{,}953 \pm 4{,}421$	$0{,}204 \pm 0{,}645$	

4.5. Discussion

The present study describes an *in vitro* approach to studying the early events of bone matrix formation that characterizes the initial osteoblasts interaction and the spatial organization of provisional Fn matrix on different rough Ti surfaces. This model reflects the relatively early cellular events of confluent osteoblasts cultures when no osteogenic differentiation factors have been added.

It is generally agreed that topography affects the cellular interaction, which influences the orientation, migration, growth and differentiation of adhering cells [17;23]. Several *in vivo* studies have shown that surface roughness improves the osseointegration of Ti implants [49;50] but the mechanisms involved in this biological response [25-28;30;31] are still not thoroughly understood [51]. Therefore, the present work is a continuation of these earlier investigations. Its aim is to better the understanding and characterization of the quality of early osteoblast interaction with rough Ti surfaces. More specifically, in our view this interaction is strongly influenced by the organization of surface-associated adhesive proteins such as Fn [40;41;43;44;52], which in turn are expected to be dependent on the roughness, its parameters, and other associated physicochemical properties, such as wettability, surface energy and surface charge. We anticipate that the third dimension of topography, which will affect the distribution of Fn, may resemble the natural organization of ECM to a certain extent, and will thus constrain the biological response.

The Fn, BSA and Fbg protein adsorbed by squared centimeter was calculated by fluorescence. The objective was to find correlations between the quantity of protein adsorbed and relevant physical-chemical properties of the tested surfaces, such as the surface free energy or surface roughness. As concluded in Chapter 2, both grit-blasting particle size and its chemical nature changed SFE of blasted Ti. In fact, the chemical nature of the particle was found the most influencing parameter. In this way, grit-blasting influences surface free energy which in turn influences directly the adsorbed Fn and BSA protein on rough surfaces. Michiardi et al., [53], also found albumin adsorption directly related to the surface energy, on smooth NiTi surfaces, indicating that BSA adsorption is directly influenced by SFE of the metal. On the contrary, Michiardi et al. did not assess any correlation between adsorbed Fn and SFE. In the present work; FITC-Fn was positively correlated to SFE of the titanium surfaces tested, this difference might be due to the prevalence of surface chemistry. While no correlation between the adsorbed Fbg and surface parameters was found indicating that adsorption could have other preferential parameters such as surface charges and/or chemical composition.

Fn is one of the key proteins involved in cell-biomaterial interaction [6;15], and has also been shown to play a distinct role in early bone development [7-9] and osteoblast differentiation [10]. In this study, we demonstrate that Fn adsorbs irregularly on a rough Ti surface in a quantity that is relatively independent of the roughness values. Instead,

Fn adsorption correlates better with the increase in wettability and its associated SFE. Conversely, cellular interaction seems to be more dependent on the roughness parameters. The observation that Fn accumulated on peaks rather than on valleys of microrough Ti surfaces was an unexpected phenomenon that was revealed by 3D reconstruction of CLSM images. This phenomenon was confirmed when the patterns of both FITC-Fn and topography were reconstituted simultaneously (Figure 4-7). The differences in morphology between peaks and valleys may explain the heterogeneous distribution of this protein on the studied surfaces. As Fn adsorption is mainly guided by the energetic and wettable properties on blasted microrough surfaces, a difference in the density of the polar/charged groups on the titanium surface, which depends on the concavity/convexity of the topographical feature, could lead to this different affinity for Fn binding. Therefore, concave valleys on a titanium surface will accumulate a higher density of hydroxil (negative/highly polar) groups than convex peaks [54;55]. The possibility of air pockets at the bottom of the topography in the early stages of contact with the protein solution, due to dynamic effects during wetting, is also a possible explanation for the preferential accumulation of the protein on the top of the topographical features. Consequently, the SFE values must be put into perspective and considered only for comparative purposes between surfaces with similar topographical characteristics, i.e. those that are grit-blasted. Additionally, some of the blasting particles remain adhered to the surface after the mechanical treatment, as demonstrated and calculated in a previous study [56]. Their composition was confirmed with the EDS-spectra by the existence of high alumina and silicon peaks. These remaining particles influence SFE but they were not heterogeneously distributed along the surfaces, so they probably did not influence Fn distribution on the blasted surfaces. However, they may have affected the total amount of protein adsorbed through their influence on the wettability and SFE. A similar pattern of adsorption was observed for other proteins, such as albumin and fibrinogen, i.e., one globular and one fibrillar protein, in a limited set of surfaces. This means that the heterogeneity of adsorption has nothing to do with the protein structure. Moreover, there was no correlation between the blasting particle size, i.e. the surface roughness, and the corresponding changes in SFE. All these factors lead to the conclusion that the observed heterogeneity in protein adsorption must be attributed to a property or feature of the blasted Ti surface, regardless of the protein structure or the way the roughness is formed. The detailed mechanism of this effect is still not clear and is currently under investigation. However, it indicates that prevalent Fn adsorption on the tips will probably accumulate more osteoblasts, which may provoke their homotypic association, as seen on some blasted samples. Consequently, the increased adhesion on the roughest Ti surfaces may be explained in part by facilitated cell aggregation. Indeed, such aggregates can be easily distinguished, particularly on surfaces blasted with higher particle size.

Consistent with the considerable body of work [23;25-28;30;31;47], our data suggest that a certain degree of roughness improves *in vitro* osteoblast interaction. A long-term *in*

vitro experiment showed that the roughness of Ti positively influenced adhesion and expression of adhesive molecules, such as Fn, type I collagen and osteopontin [28], but had no effect on the initial osteoblast adhesion. Our system evaluated the specific cell-to-Fn interaction (as serum free conditions and single protein adsorption were used), which to our knowledge has not been studied until now. The results showed that Fn adsorption on rough Ti increased the initial osteoblast adhesion, also confirmed by the increased cell area and maximum diameter of smooth and Fn pre-coated samples compared to smooth and non-coated ones after 4h of incubation (Table 4-1). This effect did not depend on the increase of substratum wettability and energetic properties or on the amount of Fn adsorbed. Instead, it depended mostly on the roughness parameters. From a morphological point of view, it is interesting to note that on rough Ti surfaces the cells represented multiple projections resembling stellate morphology, as noted by Anselme et al. [28]. However, such morphology is typical for cells residing in a 3D environment [57]. The different cell adhesion parameters, Table 4-1, are affected by the 3D cell structure of cells on rough surfaces since a lower values of cell area, aspect ratio and maximum diameter are found for all the rough series compared to smooth both of them Fn pre-coated. Therefore, we speculate that when adhering on rough Ti substrata the osteoblasts recognize their 3rd dimension, and sense the organization of adsorbed Fn within the pattern of topography. In this respect, the intriguing observations of Anselme et al. [58] are of particular relevance. These authors found that the cellular adhesive response depends not only on the amplitude but also on the organization of underlying topography of a rough Ti surface. How the topography affects the organization of substratum-associated Fn has not been systematically studied so far.

The stepwise assembly of Fn proceeds from the initiation, through the elongation, to the stabilization of Fn fibrils [59], and each step involves multiple Fn interactions with cells (e.g. integrin receptors) and with other Fn molecules. Therefore, the initial binding of Fn to the substratum could play a significant role in the development of matrix [40;41;52]. Indeed, the newly synthesized Fn was not observed in the depth of the micro-topography. The existing dark zones on rough Ti surfaces may only be interpreted as an absence of Fn matrix on the bottom of the valleys, presumably because Fn adsorbs less there, Thus, the newly synthesized Fn fibrils followed the initial affinity for Fn adsorption. However, secreted Fn tended to organize into a distinct focal pattern, following the organization of adhering cells. As these structures expand in size on rougher surfaces, the surface might work as a template for the future organization of bony matrix, which appears *in vitro* through the formation of distinct alveolar structures [60]. Thus, the observed micro-compartmentalization of the adjacent living stroma could be an explanation for the improved osseointegration of rough Ti implants [25-28;30;31;47]..

The formation of newly Fn produced by cells as an ECM was studied a higher periods of time, 7 days of incubation. To learn more about the overall organization of the Fn matrix, the 3D immunofluorescence images were viewed on CLSM and further reconstructed for

quantitative analyses. The main observation from this study was that on rough Ti surfaces the Fn matrix appears thicker and does not follow the unevenness of the Ti surface topography. Indeed, the 3D images of the Fn layer reconstituted with the underlying surface topography show that it overlies only the upper part of the rough Ti surface. Quantitative measurements revealed that this Fn-containing matrix did not penetrate by more than half of the maximum peak-to-valley distance, which indicates that cells interact with only part of the available rough surface and ignore the rest of it.

Systematic studies by Boyan's group [25-28;30] have shown that cells cultured on microrough Ti exhibited reduced proliferation and enhanced differentiation when compared with smooth Ti substrates. This was also confirmed in our previous study [47]. Further studies are underway to evaluate the strength of Fn matrix interaction with rough Ti interfaces and how it relates to the functional performance of osteoblasts, which will be a direct link to their osseointegration.

4.6. Conclusions

❖   Fn and BSA adsorbed on blasted micro-rough surfaces was positively correlated with the surface energy of the blasted-rough titanium surfaces. No correlation was found between the size of the grit particles, i.e. the surface roughness and the adsorbed BSA or Fn per surface area.

❖   Blasting treatment did not influence the amount of Fbg adsorbed on titanium surfaces.

❖   The adsorption of fibronectin from solution on shot-blasted rough titanium surfaces results in an irregular pattern of adsorption with a higher amount of protein adsorbed on peaks than on valleys of the topography.

❖   Fn adsorption on rough Ti increases the initial osteoblast adhesion. Cells sensed the 3D topography by adhering at the surface with morphologically multiple projections resembling stellate morphology.

❖   Osteoblast-like cells deposit Fn- fibrils in a specific facet-like pattern that is organized within the secreted total matrix, which appears as a film overlying the top of the different rough titanium surfaces. The thickness of this layer increases with the roughness of the underlying topography, but no more than half of the total maximum peak-to-alley distance is covered.

4.7. Bibliography

[1] Jayaraman M, Meyer U, Buhner M, Joos U, Wiesmann HP. Influence of titanium surfaces on attachment of osteoblast-like cells in vitro. Biomaterials 2004; 25: 625-631.

[2] Lange R, Luthen F, Beck U, Rychly J, Baumann A, Nebe B. Cell-extracellular matrix interaction and physico-chemical characteristics of titanium surfaces depend on the roughness of the material. Biomolecular Engineering 2002; 19: 255-261.

[3] Wilson CJ, Clegg RE, Leavesley DI, Pearcy MJ. Mediation of biomaterial-cell interactions by adsorbed proteins: A review. Tissue Engineering 2005; 11: 1-18.

[4] Puleo DA, Nanci A. Understanding and controlling the bone-implant interface. Biomaterials 1999; 20: 2311-2321.

[5] Siebers MC, ter Brugge PJ, Walboomers XF, Jansen JA. Integrins as linker proteins between osteoblasts and bone replacing materials. A critical review. Biomaterials 2005; 26: 137-146.

[6] Garcia AJ. Get a grip: integrins in cell-biomaterial interactions. Biomaterials 2005; 26: 7525-7529.

[7] Lebaron RG, Athanasiou KA. Extracellular matrix cell adhesion peptides: Functional applications in orthopedic materials. Tissue Engineering 2000; 6: 85-103.

[8] Nordahl J, Mengarelliwidholm S, Hultenby K, Reinholt FP. Ultrastructural Immunolocalization of Fibronectin in Epiphyseal and Metaphyseal Bone of Young-Rats. Calcified Tissue International 1995; 57: 442-449.

[9] Vogel V, Baneyx G. The tissue engineering puzzle: A molecular perspective. Annual Review of Biomedical Engineering 2003; 5: 441-463.

[10] Globus RK, Doty SB, Lull JC, Holmuhamedov E, Humphries MJ, Damsky CH. Fibronectin is a survival factor for differentiated osteoblasts. Journal of Cell Science 1998; 111: 1385-1393.

[11] Dallas SL, Sivakumar P, Jones CJP, Chen Q, Peters DM, Mosher DF, Humphries MJ, Kielty CM. Fibronectin regulates latent transforming growth factor-beta (TGF beta) by controlling matrix assembly of latent TGF beta-binding protein-1. Journal of Biological Chemistry 2005; 280: 18871-18880.

[12] Velling T, Risteli J, Wennerberg K, Mosher DF, Johansson S. Polymerization of type I and III collagens is dependent on fibronectin and enhanced by integrins alpha(11)beta(1) and alpha(2)beta(1). Journal of Biological Chemistry 2002; 277: 37377-37381.

[13] Pereira M, Rybarczyk BJ, Odrljin TM, Hocking DC, Sottile J, Simpson-Haidaris PJ. The incorporation of fibrinogen into extracellular matrix is dependent on active assembly of a fibronectin matrix. Journal of Cell Science 2002; 115: 609-617.

[14] Sottile J, Hocking DC. Fibronectin polymerization regulates the composition and stability of extracellular matrix fibrils and cell-matrix adhesions. Molecular Biology of the Cell 2002; 13: 3546-3559.

[15] Garcia AJ, Boettiger D. Integrin-fibronectin interactions at the cell-material interface: initial integrin binding and signaling. Biomaterials 1999; 20: 2427-2433.

[16] Stephansson SN, Byers BA, Garcia AJ. Enhanced expression of the osteoblastic phenotype on substrates that modulate fibronectin conformation and integrin receptor binding. Biomaterials 2002; 23: 2527-2534.

[17] Anselme K. Osteoblast adhesion on biomaterials. Biomaterials 2000; 21: 667-681.

[18] Renner L, Pompe T, Salchert K, Werner C. Fibronectin displacement at polymer surfaces. Langmuir 2005; 21: 4571-4577.

[19] Ramsden JJ. Experimental Methods for Investigating Protein Adsorption-Kinetics at Surfaces. Quarterly Reviews of Biophysics 1994; 27: 41-105.

[20] Fuss C, Palmaz J, Sprague E. Fibrinogen: structure, function, and surface interactions. Journal of Vascular and Interventional Radiology 2001; 12: 677-682.

[21] Tang L, Eaton JW. Fibrin(ogen) mediates acute inflammatory responses to biomaterials. The Journal of Experimental Medicine 1993; 178: 2147-2156.

[22] Bai Z, Filiaggi MJ, Dahn JR. Fibrinogen adsorption onto 316L stainless steel, nitinol and titanium. Surface Science 2009; 603: 839-846.

[23] Boyan BD, Lohmann CH, Dean DD, Sylvia VL, Cochran DL, Schwartz Z. Mechanisms involved in osteoblast response to implant surface morphology. Annual Review of Materials Research 2001; 31: 357-371.

[24] Vrouwenvelder WCA, Groot CG, Degroot K. Histological and Biochemical Evaluation of Osteoblasts Cultured on Bioactive Glass, Hydroxylapatite, Titanium-Alloy, and Stainless-Steel. Journal of Biomedical Materials Research 1993; 27: 465-475.

[25] Ponsonnet L, Reybier K, Jaffrezic N, Comte V, Lagneau C, Lissac M, Martelet C. Relationship between surface properties (roughness, wettability) of titanium and titanium alloys and cell behaviour. Materials Science & Engineering C-Biomimetic and Supramolecular Systems 2003; 23: 551-560.

[26] Boyan BD, Batzer R, Kieswetter K, Liu Y, Cochran DL, Szmuckler-Moncler S, Dean DD, Schwartz Z. Titanium surface roughness alters responsiveness of MG63 osteoblast-like cells to 1 alpha,25-(OH)(2)D-3. Journal of Biomedical Materials Research 1998; 39: 77-85.

[27] Schwartz Z, Martin JY, Dean DD, Simpson J, Cochran DL, Boyan BD. Effect of titanium surface roughness on chondrocyte proliferation, matrix production, and differentiation depends on the state of cell maturation. Journal of Biomedical Materials Research 1996; 30: 145-155.

[28] Anselme K, Bigerelle M, Noel B, Dufresne E, Judas D, Iost A, Hardouin P. Qualitative and quantitative study of human osteoblast adhesion on materials with various surface roughnesses. Journal of Biomedical Materials Research 2000; 49: 155-166.

[29] Richards RG. The effect of surface roughness on fibroblast adhesion in vitro. Injury-International Journal of the Care of the Injured 1996; 27: 38-43.

[30] Martin JY, Schwartz Z, Hummert TW, Schraub DM, Simpson J, Lankford J, Dean DD, Cochran DL, Boyan BD. Effect of Titanium Surface-Roughness on Proliferation, Differentiation, and Protein-Synthesis of Human Osteoblast-Like Cells (Mg63). Journal of Biomedical Materials Research 1995; 29: 389-401.

[31] Eisenbarth E, Linez P, Biehl V, Velten D, Breme J, Hildebrand HF. Cell orientation and cytoskeleton organisation on ground titanium surfaces. Biomolecular Engineering 2002; 19: 233-237.

[32] Chesmel KD, Clark CC, Brighton CT, Black J. Cellular-Responses to Chemical and Morphologic Aspects of Biomaterial Surfaces .2. the Biosynthetic and Migratory Response of Bone Cell-Populations. Journal of Biomedical Materials Research 1995; 29: 1101-1110.

[33] Wieland M, Hanggi P, Hotz W, Textor M, Keller BA, Spencer ND. Wavelength-dependent measurement and evaluation of surface topographies: application of a new concept of window roughness and surface transfer function. Wear 2000; 237: 231-252.

[34] Bigerelle M, Anselme K. Statistical correlation between cell adhesion and proliferation on biocompatible metallic materials. Journal of Biomedical Materials Research Part A 2005; 72A: 36-46.

[35] Bagno A, Di Bello C. Surface treatments and roughness properties of Ti-based biomaterials. Journal of Materials Science-Materials in Medicine 2004; 15: 935-949.

[36] Schliephake H, Scharnweber D. Chemical and biological functionalization of titanium for dental implants. Journal of Materials Chemistry 2008; 18: 2404-2414.

[37] Shalabi MM, Gortemaker A, Van't Hof MA, Jansen JA, Creugers N. Implant surface roughness and bone healing: a systematic review. Journal of Dental Research 2006; 85: 496-500.

[38] Morra M, Casinelli C, Bruzzone G, arpi A, i Santi G, iardino R, Fini M. Surface chemistry effects of topographic modification of titanium dental implant surfaces: 1. Surface analysis. International journal of oral and maxillofacial implants 2003; 18: 40-45.

[39] Faucheux N, Tzoneva R, Nagel MD, Groth T. The dependence of fibrillar adhesions in human fibroblasts on substratum chemistry. Biomaterials 2006; 27: 234-245.

[40] Altankov G, Groth T. Fibronectin matrix formation by human fibroblasts on surfaces varying in wettability. Journal of Biomaterials Science-Polymer Edition 1996; 8: 299-310.

[41] Altankov G, Groth T. Fibronectin matrix formation and the biocompatibility of materials. Journal of Materials Science-Materials in Medicine 1996; 7: 425-429.

[42] Altankov G, Groth T, Krasteva N, Albrecht W, Paul D. Morphological evidence for a different fibronectin receptor organization and function during fibroblast adhesion on hydrophilic and hydrophobic glass substrata. Journal of Biomaterials Science-Polymer Edition 1997; 8: 721-740.

[43] Tzoneva R, Groth T, Altankov G, Paul D. Remodeling of fibrinogen by endothelial cells in dependence on fibronectin matrix assembly. Effect of substratum wettability. Journal of Materials Science-Materials in Medicine 2002; 13: 1235-1244.

[44] Altankov G, Richau K, Groth T. The role of surface zeta potential and substratum chemistry for regulation of dermal fibroblasts interaction. Materialwissenschaft und Werkstofftechnik 2003; 34: 1120-1128.

[45] Faucheux N, Schweiss R, Lutzow K, Werner C, Groth T. Self-assembled monolayers with different terminating groups as model substrates for cell adhesion studies. Biomaterials 2004; 25: 2721-2730.

[46] Aparicio C, Gil FJ, Fonseca C, Barbosa M, Planell JA. Corrosion behaviour of commercially pure titanium grit blasted with different materials and sizes of grit particles for dental implant applications. Biomaterials 2003; 24: 263-273.

[47] Aparicio C, Gil FJ, Planell JA, Engel E. Human-osteoblast proliferation and differentiation on grit-blasted and bioactive titanium for dental applications. Journal of Materials Science-Materials in Medicine 2002; 13: 1105-1111.

[48] Aparicio C, Gil FJ, Thams U, Munoz F, Padros A, Planell JA. Osseointegration of grit-blasted and bioactive titanium implants: Histomorphometry in minipigs. Key engineering materials 2004; 254-2: 737-740.

[49] Larsson C, Esposito M, Liao H, Thomsen P. The titanium-bone interface in vivo. In: Springer (ed.), Titanium in Medicine. Berlin: 2001: 588-633.

[50] Buser D, Schenk RK, Steinemann S, Fiorellini JP, Fox CH, Stich H. Influence of surface characteristics on bone integration of titanium implants. A histomorphometric study in miniature pigs. Journal of Biomedical Materials Research 1991; 25: 889-902.

[51] Zinger O, Zhao G, Schwartz Z, Simpson J, Wieland M, Landolt D, Boyan BD. Differential regulation of osteoblasts by substrate microstructural features. Biomaterials 2005; 26: 1837-1847.

[52] Altankov G, Grinnell F, Groth T. Studies on the biocompatibility of materials: Fibroblast reorganization of substratum-bound fibronectin on surfaces varying in wettability. Journal of Biomedical Materials Research 1996; 30: 385-391.

[53] Michiardi A, Aparicio C, Ratner BD, Planell JA, Gil J. The influence of surface energy on competitive protein adsorption on oxidized NiTi surfaces. Biomaterials 2007; 28: 586-594.

[54] Wang X-X, Hayakawa S, Tsuru K, Osaka A. A comparative study of in vitro apatite deposition on heat-, H2O2-, and NaOH-treated titanium surfaces. Journal of Biomedical Materials Research Part A 2001; 54: 172-178.

[55] Aparicio C, Manero JM, Conde F, Pegueroles M, Planell JA, Vallet-Regí M, Gil FJ. Acceleration of apatite nucleation on microrough bioactive titanium for bone-replacing implants. Journal of Biomedical Materials Research Part A 2007; 82: 521-529.

[56] Pegueroles M, Gil FJ, Planell J, Aparicio C. The influence of blasting and sterilization on static and time-related wettability and surface-energy properties of titanium surfaces. Surface and coatings technology 2008; 202: 3470-3479.

[57] Grinnell F. Fibroblast biology in three-dimensional collagen matrices. Trends in Cell Biology 2003; 13: 264-269.

[58] Anselme K, Bigerelle M, Noel B, Iost A, Hardouin P. Effect of grooved titanium substratum on human osteoblastic cell growth. Journal of Biomedical Materials Research 2002; 60: 529-540.

[59] Schwarzbauer JE, Sechler JL. Fibronectin fibrillogenesis: a paradigm for extracellular matrix assembly. Current Opinion in Cell Biology 1999; 11: 622-627.

[60] Ahmad M, McCarthy M, Gronowicz G. An in vitro model for mineralization of human osteoblast-like cells on implant materials. Biomaterials 1999; 20: 211-220.

5. Effect of blasting-treatment and Fn pre-coating on MG63 adhesion and differentiation on c.p. Ti. A gene expression study using qRT-PCR

5.1. Introduction

The biological processes that play a role when cells come in contact with a material surface involve initial focal adhesion formation, cell adhesion, and extracellular matrix formation and reorganisation. The quality of the cell-material interaction will influence the cell's capacity to proliferate and differentiate [1]. Cells bind to surfaces indirectly by binding to attachment proteins [2], such as fibronectin and vitronectin among others [3], through cytoskeletal associated transmembrane receptors of which integrins are the most important [4;5]. Biomaterial surface properties, via alterations in adsorbed protein structure, and the presence of specific functional groups, may influence integrin binding specificity, thus modulating signalling and expression of differentiated phenotypes [6-10].

The use of human cells lines such as MG63 is providing a useful tool both to investigate the effects of biomaterials and to understand the mechanisms of cell response. To

understand the mechanisms of bone formation at the implant surface, the effects of the material on the surrounding cells must be understood. *In vitro* studies support the hypothesis that implant surface may have direct effects on osteoblast migration, attachment, proliferation, and differentiation by showing that increased surface roughness stimulates osteogenesis [11-13]. In addition to cellular characteristics associated with osteogenic differentiation, surface roughness has also been demonstrated to alter integrin and growth factor expression [14]. In sum, it could be shown that phenotypic expression of the osteoblasts is sensitive to the topography and topology of titanium surfaces [15]. MG63 osteoblast-like osteosarcoma cells cultured on Ti roughness have shown different osteoblastic differentiation expression depending on the roughness level. While the R_a values of the micro-rough implant surfaces ranging from 3-5 μm, the MG63 cells are favoured in *in vitro* and *in vivo* experiments [12;15;16]. Cells cultured on Ti discs with an average roughness >6 μm present a lower cell differentiation compared to smooth (<0,1 mm) surfaces. Since the increase of real surface area implies a lower cell confluence at the measured time, resulting in reduced ALP activity [17]. Furthermore, the effect of surface roughness on cells can be the result of the surface roughness itself or the result of the protein layer adsorbed, also dependant of surface characteristics, which occurs as the material surface is conditioned by the media and serum. This initial interaction produces a layer of macromolecules that modify the behaviour of the cells.

Fibronectin is an adhesive protein which mediates cell adhesion and the only protein that activates $\alpha_5\beta_1$ integrins [2;18]. α_5 is an integrin subunit specific for fibronectin protein [18]. Many studies demonstrated that on titanium and Ti alloys surfaces, osteoblasts have shown to express α_5 integrin subunits among others [18;19]. The effect of Fn pre-coating has been added as a variable of this study since human fibronectin is a glycoprotein that promotes attachment of cells [20] to the biomaterial surface through its central-binding domain arginine-glycine-aspartic acid, RGD, sequence. Also, in Chapter 4, differences on the adsorbed fibronectin on rough surfaces due to the substrates properties were found. Thus the study of the effect of Fn pre-adsorption on biomaterials is of research relevance.

In previous works, an optimized shot-blasted titanium (c.p. Ti) dental implant was developed [21]. The optimal roughness and the appropriate abrasive particles for a better *in vitro* response and an earlier *in vivo* osseointegration were determined [11]. However, the first biological events that lead to this successful response and how the surface properties influence are still poorly understood. As a first step, a thorough topographical and surface free energy characterization of these optimized surfaces was carried out (see Chapter 2 and [22]), and it was correlated with the protein adsorption behaviour (amount, kinetics, and competition) on them (see Chapters 3 and 4). Studies of fibronectin adsorption on the different roughened surfaces revealed differences on the adsorbed fibronectin due to the substrates properties. Then, as a further step, α_5 integrin expression involved in adhesion processes has been studied in this work, using the real

time or quantitative reverse transcription-polymerase chain reaction (qRT-PCR) technique, which allows a reliable gene expression study. Finally the cellular response, adhesion and differentiation steps, without and with Fn pre-coatings, have also been investigated.

5.1.1. Cell adhesion

Cell adhesion to the extracellular matrix involves integrins, which are transmembrane receptors that bind to specific extracellular matrix components and the cytoskeleton. Through these interactions, integrins can regulate many cellular functions, like cell adhesion, motility, shape, growth, and differentiation. Integrins do not bind non-specifically to extracellular matrix (ECM) proteins, but to specific binding sites, within the ECM protein. The most common binding site is RGD. This sequence is present in most of the ECM proteins, like fibronectin and vitronectin. The fact that many integrins recognize this RGD sequence is probably the explanation for the overlap in specificity [18].

Cell adhesion can be divided into two phases: the attachment phase and the adhesion phase. Cellular attachment takes place rapidly with short-term events, like physicochemical linkages between the cell and the material. The adhesion phase occurs in a longer term, involving three types of proteins: ECM proteins, cell membrane proteins, and cytoskeletal proteins [1]. As explained before, integrins are the primary family of cell membrane proteins that mediate the adhesion of cells to substrates; they provide tissue structure and integrity. After the binding of a ligand, the integrins will cluster together into focal contacts. After clustering, cytoskeletal and signalling molecules will be recruited and activated. The signalling pathway inside the cell is complex, and involves the accumulation of several proteins. Besides the recruitment of signalling molecules and signalling, integrin activation also results in changes in the organization of the cytoskeleton, subsequently affecting cell adhesion and motility [23;24].

Several characteristics of the substrate have been shown to influence protein adsorption and integrin expression [1;18]. Evidently, differences in protein adsorption will result in differences in the interaction with integrins, and subsequently trigger different signals, influencing the regulation of cell survival, proliferation, and differentiation [8;24].

5.1.2. Osteogenic cell differentiation markers

The formation of bone that is required for biomaterials osseointegration relies on the presence of undifferentiated mesenchymal cells with the ability to proliferate and

differentiate along an osteogenic pathway. Mesenchymal tissues such as bone, cartilage and muscle are thought to be derived from a common precursor cell that proliferates and commits to specific lineages under the guidance of environmental influences and molecular signals which initiate a cascade of gene activities [25]. Ultimately, a non-dividing mature cell, osteoblast for bone, is produced, and will be responsible for the generation of a specific tissue.
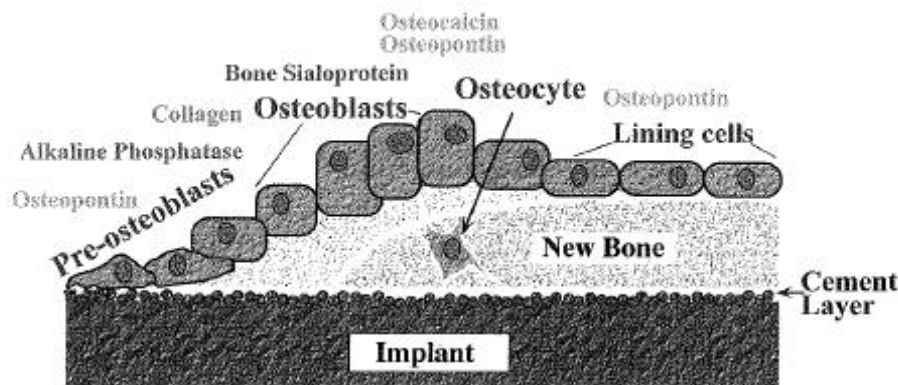

Figure 5-1 *Schematics of bone formation on implant surfaces. The temporal expression of bone-matrix proteins is shown in context with osteogenic differentiation and the formation of mineralized tissue matrix on the surface of an implant. Early expression of osteopontin associated with the initial deposition of a cement layer on the implant surface. The collagenous matrix, which is laid down on the cement layer, is mineralized in the presence of alkaline phosphatase and bone sialoprotein. Osteocalcin and osteopontin are expressed following the initial formation of mineral, the osteopontin being a prominent component of the organic matrix formed on the bone surface beneath the lining cells and surrounding the osteocytes [25]*

Bone-matrix proteins have proven to be particularly useful osteogenic markers, especially for the later stages of differentiation. These proteins are present in the mineralized matrix of bone; their expression is regulated in an apparently defined temporal-spatial manner as osteogenic differentiation takes place (Figure 5-1). Alkaline phosphatase, ALP, and collagen Type I, COL I, expression are characteristic of the osteogenic lineage [25]. The emergence of osteoblasts is first indicated by the induced expression of bone sialoprotein, BSP, which correlates with the initiation of mineralization *in vitro* and *in vivo*. Osteocalcin, OC, expression is increased following BSP expression. In comparison, the expression of ostepontin, OP, fluctuates throughout osteogenic differentiation. OC and OP are expressed at high levels after mineralization has been initiated, with high levels being maintained as osteoblasts differentiate further into osteocytes and lining cells [26].

5.1.3. Cell line

An enormous number of studies investigated variations in titanium surface topographies but there are still open questions about their behaviour in a biological environment. Cell culture studies provide a useful tool for investigations because cell and matrix interactions with material surfaces can be evaluated in detail. Processes, such as cell attachment, motility, proliferation, differentiation, and protein adsorption and conformation can be evaluated. Human osteoblast-like MG63 cell line (American Type Culture Collection (ATCC), Rockville, MD, USA) has often been used to evaluate the effects of different implant surface topographies. This well-characterized cell line was originally isolated from a human osteosarcoma. MG63 exhibit many osteoblastic traits which are characteristic for bone forming cells, they are believed to be relatively immature osteoblasts. However they can exhibit a number of osteoblast-like phenotypic markers such as ALP and OC.

MG63 osteoblast- like cells are widely used and studied for *in vitro* tests [12;15;17;27;28], in part because they are an excellent model to study the influence of the morphology of the surface of a substrate on the cell adhesion, proliferation and differentiation.

5.2. Objectives

The main objectives of the present chapter are:

4. To evaluate the influence of surface properties, i.e., surface energy and roughness, and Fn pre-coating of c.p Ti. on the gene expression of α_5 integrin subunit during human osteoblasts adhesion.

5. To evaluate the influence of surface properties, i.e., surface energy and roughness, and Fn pre-coating of c.p Ti. on human osteoblasts differentiation by analysing the osteocalcin and alkaline phosphatase gene expression as well as the corresponding protein synthesis.

5.3. Materials

5.3.1. Surfaces

The studied surfaces were disks of c.p. Titanium Grade II (c.p. Ti) roughened using the grit-blasting method described in detail in Chapter 2 and 4. Seven different series of Ti surfaces were obtained by blasting at 0,25 MPa-pressure during the time required for roughness saturation. Depending on the nature of the blasting parameters the samples were divided as A for Al_2O_3 and S for SiC particles. Moreover, by the different particles size the following codification was used: 3 for 212-300μm mean particle size, 6 for 425-600μm and 9 for 1000-1400μm. The obtained surfaces finishes were A3, A6, A9, S3, S6, S9, respectively, and a polished Smooth surface was used as control.

For qRT-PCR experiments only Smooth, A6 and S6 surfaces finishes were tested. Tissue culture polystyrene (TCPS) was studied as a control.

After blasting the samples were cleaned by sonication in acetone for 15min, followed by sonication in distilled water for 15min. Finally, all samples were steam-sterilized at 121ºC for 30min and kept under vacuum.

5.3.2. Fn pre-coating

Two series of the different surface finishes were performed in parallel for all the studies: a) fibronectin (Fn) pre-coated surfaces; or b) non-coated/plain surfaces. The former were pre-coated with Fn, 20μg/ml during 30min at 37ºC; and the later were not coated previously to the *in vitro* cell assays.

5.3.3. Cells

Human osteoblast-like MG63 cells were grown in Dulbecco's modified Eagle's medium (DMEM, Gibco) supplemented with 10% foetal calf serum (FCS), 1% penicillin/streptomycin, 1% L-glutamine, 1% pyruvate (Sigma) at 37ºC in 5%CO_2/95% air atmosphere and 100% humidity. MG63 cells were obtained from American Type Culture Collection (Rockville, MD). Culture medium was changed every two days. For the experiments, cells were harvested at 70-90% confluence by Tripsin/EDTA, centrifuged and re-suspended in serum-free medium before plating 2×10^4 MG63 cells per sample.

For the differentiation studies, after 7 days of incubation, the time course of mineralization was accelerated by the change to an osteogenic media which consists of a completed medium supplemented with 10^{-8}M dexamethasone, 100μM acide ascorbique 2-phosphate, 10mM β-glycerolphosphate.

5.4. Methods

5.4.1.   Real time qRT-PCR technique

The polymerase chain reaction (PCR) is a technique widely used in molecular biology for amplifying the amount of DNA present in a sample. Consequently, PCR is the technique used when comparison and assessment of the most abundant of two samples of DNA is pursued.

Initially RNA is extracted after cell lysis; then, RNA strand will be reverse transcribed (RT) into its DNA complement and finally amplified with PCR technique. That's why the overall process is called, reverse transcription polymerase chain reaction, RT-PCR, technique.

Quantitative qRT-PCR is identical to a simple RT-PCR except that the progress of the reaction is recorded in real-time. RT-PCR quantifies DNA because of the amplification of the target DNA sequence which allows a greater sensitivity of detection. In an optimized reaction, the target quantity will approximately double during each amplification cycle. The amount of amplified product is linked to fluorescence intensity using a fluorescent reporter molecule, SYBR green. The point at which the fluorescent signal is measured in order to calculate the initial template quantity can either be at the end of the reaction (endpoint RT-PCR) or while the amplification is still progressing (real-time quantitative qRT-PCR).

In the endpoint RT-PCR, fluorescence data are collected after the amplification reaction has been completed, moment at which the reaction efficiency can decrease as reagents are consumed. When identical samples are being amplified the amplification plots, after the reaction is completed, are generally non uniform (Figure 5-2, endpoint detection). At the endpoint detection, PCR are no longer exponential at the plateau stage, which means that the association of a two-fold increase in quantity from one cycle number to the next has come to an end. Then, in the endpoint technique the data measured following the amplification are not reproducible enough to be useful for the precise measurements required for gene expression analysis.

The real time technique is the more sensitive and reproducible method, where the fluorescence at each cycle as the amplification progresses is measured. The fluorescence intensity increases proportionally with each amplification cycle. Then, the first cycle at which the instrument can distinguish the amplification generated fluorescence as being above the ambient background signal is called the threshold cycle (Figure 5-2). The greater the amount of initial DNA template in the sample, the earlier the threshold value for that sample. This value can be directly correlated to the starting target concentration for the sample.
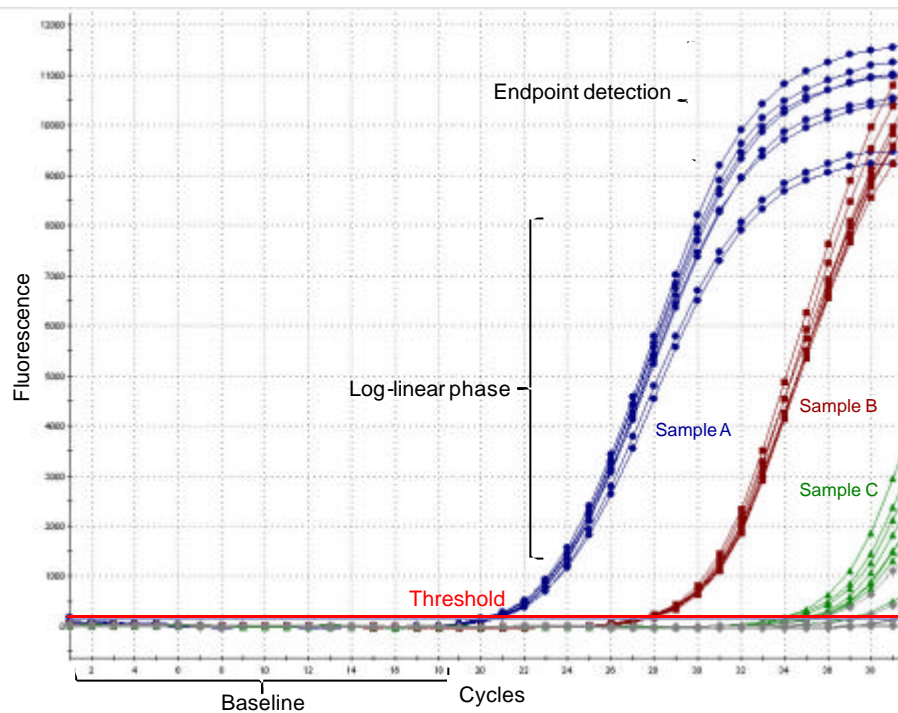
Figure 5-2 *SYBR Green real time RT-PCR amplification plot (Adapted from Cultek)*

In qRT-PCR experiments, especially those based in comparative quantification, it is important to include a normalizer, reference or control gene. It is essential to quantify the normalizer gene side by side with the gene of interest. The normalizing gene is typically a housekeeping gene whose expression should be constant under the experimental conditions of the assay. This constant level must be verified experimentally. The most common housekeeping genes used are GAPDH, β-actin and β2-μglobulin. Because the expression level of the normalizer is constant, any variation in the C_t (threshold) of the normalizer can be attributed to other sources of variation, such as efficiency of the reverse transcription reactions or yield of the RNA purification. These sources of variation will affect the normalizer and the gene of interest equally, so differences in the C_t of the normalizer from sample to sample can be used to correct for any variation in the C_t of the gene of interest that is not due to changes in the expression level.

Moreover negative controls are also performed during the PCR process. "No template controls" (NTC), and "No reverse transcription controls" (No RT) provide a mechanism to control for external contamination or other factors that can result in a non-specific increase in the fluorescence signal.

In this study, the following protocol was performed: (1) mRNA extraction; (2) Spectrophotometric quantification of RNA; (3) Reverse transcription, RT; and (4) Polymerase chain reaction, PCR.

To extract the mRNA from the cell pellets a kit (RNeasy Minikit, QIAGEN, Germany) was used and quantification was accomplished by measuring the absorbance with the NanoDrop Spectrophotometer ND-100 (Thermo Scientific, USA) using the ND-1000 V 3.5.2 software (Thermo Scientific, USA). The NanoDrop® ND-1000 is a full-spectrum (220-750nm) spectrophotometer that measures 1μl samples with high accuracy and reproducibility. During the reverse transcription, the enzyme reverse transcriptase is used to make a double-stranded cDNA copy of the mRNA molecules (QuantiTect Reverse Transcription kit, QIAGEN, Germany). The resulting cDNA is then amplified using a SYBR Green method. This requires a double-stranded DNA dye in the PCR reaction which binds to newly synthesized double-stranded DNA and gives fluorescence (QuantiTect SYBR Green kit, QIAGEN, Germany).

It should be noted that the real-time qRT-PCR assay requires expensive, special equipment and additional reagents compared with conventional RT-PCR. Consequently, only a reduced set with the most significant and representative surfaces have been tested (TCPS, Smooth, S6 and A6 series).

5.4.1.1. Gene expression of integrin subunit α_5, ALP and OC protocol

Integrin gene expression of subunit α_5 (α_5 mRNA), alkaline phospatase (ALP mRNA) and osteocalcin (OC mRNA) were obtained using qRT-PCR. Cell culture was completed after 30min and 4h incubation as adhesion time for α_5 mRNA integrin studies (QT00080871, QIAGEN, Germany). For cell differentiation studies, cell cultured was prolonged up to 7 and 14 days of incubation for ALP mRNA (QT00012957, QIAGEN, Germany) and OC mRNA studies (QT00232771, QIAGEN, Germany). β_2-μglobuline (QT00088935, QIAGEN, Germany) was used as normalizer. Negative controls, NTC and No RT have been included with each real time assay. For each series and controls, three samples were tested.

The primers used were those corresponding to α_5 integrin subunit, ALP, OC and β_2-μglobuline (QIAGEN, Germany). Then, repeated heating-cooling cycles up to 94ºC to separate the DNA strands, and down to around 55 ºC to allow the oligonucleotide primers to specifically bind were performed. This was followed by incubation at 72ºC, which activated the DNA polymerase to copy the DNA. Up to 35 cycles were carried out to amplify the signal.

5.4.2.   Cell differentiation markers

Cell differentiation was also monitored by measuring the ALP activity and OC production by cells after 14 and 21 days of cell culture for Fn-coated and non-coated series. Measurements after 3 days for non-coated series were performed as a control.

Both ALP and OC activity were normalised with the total protein concentration readings explained below.

5.4.2.1.   Total Protein Concentration

The total protein concentration was measured with a BCA Protein Assay kit (Pierce). This method combines the reduction of Cu^{2+} to Cu^{1+} by protein in an alkaline medium with the selective colorimetric detection of the cuprous cation using a reagent containing bicinchoninic acid (BCA). The reaction product of the assay, formed by the chelation of two molecules of BCA with one cuprous ion, is purple-coloured and can be read at 562 nm.

The samples were rinsed twice in phosphate buffered saline (PBS 1X), and soaked in 500 µl of Mammalian Protein Extraction Reagent (MPER), in order to detach the cells from the studied surfaces. The test was performed by adding 25 µl of the MPER supernatant to 200 µl of the kit's Working Reagent. The working reagent was composed of 50 parts of Reagent A (sodium carbonate, sodium bicarbonate, bicinchoninic acid and sodium tartrate in 0,1M sodium hydroxide) with 1 part of Reagent B (4% cupric sulphate). The mixture was incubated for 30 minutes at 37 °C and read at 562 nm. The calibration curve proposed by the assay kit was used to calibrate the absorbance corresponding to bovine serum albumin concentrations ranging between 0–2,000 µg/ml. The total protein concentration was measured at days 3 (only for non-coated series surfaces), 14 and 21 of culture in triplicate.

5.4.2.2.   Alkaline phosphatase activity

ALP activity was measured with a Phosphatase, Alkaline Acid, Prostatic Acid assay kit (SIGMA Diagnostics). The measurements with this kit depend on the hydrolysis of p-nitrophenyl phosphate by the alkaline phosphatase enzyme obtaining p-nitrophenol. As the name suggests, alkaline phosphatases are most effective in an alkaline environment and then, p-nitrophenol (pNPP) is converted to a yellow complex which can be read at 400-420 nm. The intensity of the colour formed is proportional to the phosphatase activity.

ALP was measured at days 3 (only for non-coated series surfaces), 14 and 21 of culture in triplicate. Ti samples were rinsed twice in PBS 1X, soaked in 500 µl of MPER. The MPER is meant to detach the cells from the surfaces and lysate them because ALP is hosted on the cell membrane. The assay was performed by mixing 100 µl of the MPER supernatant with 50 µl of substrate solution (p-nitrophenyl phosphate, disodium) and 50 µl of alkaline buffer solution (2-Amino-2- methyl-1-propanol). The MPER supernatant was centrifuged prior to the mixture in order to eliminate debris which could hamper spectrophotometric readings. The mixture was then incubated at 37°C. The reaction was stopped after 30 minutes with 100 µl of 0,01 N NaOH solution and read at 405 nm on a PowerWaveX Bio-Tek Instruments Spectrophotometer. The results were normalised to the total protein concentration as given by the BCA readings.

5.4.2.3. Osteocalcin production

Osteocalcin, OC, concentration was measured by means of a Metra® Osteocalcin kit (Roche). This assay is a competitive immunoassay. It uses OC coated multiwell strips, a mouse anti-osteocalcin antibody, an anti-mouse IgG- alkaline phosphatase conjugate and pNPP substrate to quantify osteocalcin concentration. The cell culture supernatant (which contains the OC released by the cells) is added to the coated multiwells and incubated with the antibody. After incubation, the wells are thoroughly washed and the conjugate is added. The conjugate will attach to the antibodies which have not latched on to the OC on multiwells. Next, the pNPP substrate is added which reacts with the ALP conjugate creating the colouring which can be read on a spectrophotometer.

OC was measured at days 3 (only for non-coated series surfaces), 14 and 21 of culture in triplicate. 1ml of supernatant from the samples culture wells was centrifuged to avoid debris. The supernatant was then analysed as described above. The results were normalised to the total protein concentration as given by the BCA readings.

5.4.3. Statistical analysis

ANOVA tables and Fisher's or Tukey's multiple comparisons tests were performed to assess statistically significant differences between average values for different samples. Tukey's test was used, instead of that of Fisher, for the comparison of several groups of samples when samples had different sizes. A p-value=0,05 was chosen to determine significance. These tests were carried out using Minitab™ Release 14 software (Minitab Inc.,USA).

5.5. Results

5.5.1. Cell adhesion

5.5.1.1. α_5 integrin subunit gene expression

α_5 integrin subunit (α_5 mRNA) gene expression of cells increased with time on all surfaces except on the smooth ones (Figure 5-3). After 30min in culture, cells on smooth Ti surfaces showed the higher levels of α_5 mRNA expression. However, after 4h of cell culture, cells on rough Ti surfaces expressed higher levels of α_5 mRNA than on smooth Ti samples.

Osteoblastic cells on Fn pre-coated surfaces show a lower level of α_5 mRNA expression compared to non-coated surfaces. This effect is more noticeable for the expression of this gene when cells were on TCPS series, whereas the gene expression by cells cultured on smooth surfaces was the least sensitive to the presence of the Fn coating. Fn delayed the expression of α_5 mRNA of cells on all the studied surfaces after 4h in culture, except for those on smooth surfaces.
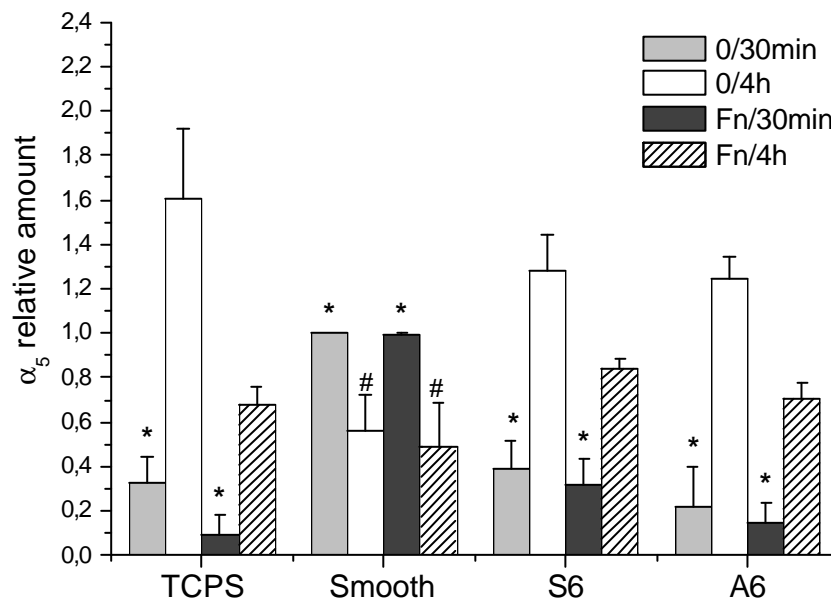
Figure 5-3 *Gene expression of a_5 integrin-subunit of cells on Ti surfaces with (Fn) or without (0) Fn pre-coating by qRT-PCR after 30min and 4h of cell culture. Ratios of target genes relative to housekeeping gene -microglobulin- were expressed as a percentage relative to non-coated smooth surfaces after 30min of cell culture. Bars with same symbols (*,#) indicate that differences are not statistically significant between them when compared in the same group of surface finishing*

5.5.2. Cell differentiation

5.5.2.1. Alkaline phosphatase gene expression

ALP mRNA gene expression of MG63 osteoblast-like cells increased with time on all the studied surfaces.

Rough and non-coated samples expressed higher levels of ALP mRNA expression compared to smooth and TCPS surfaces.

After 7 days of cell culture Fn-coatings had a non prevalent effect on the ALP expression. Whereas after 14 days in culture, cells on Fn-coated surfaces expressed lower levels of ALP mRNA compared to those on non-coated surfaces in all cases. That result indicated a delay in the ALP mRNA expression due to the presence of the Fn-coating (Figure 5-4).
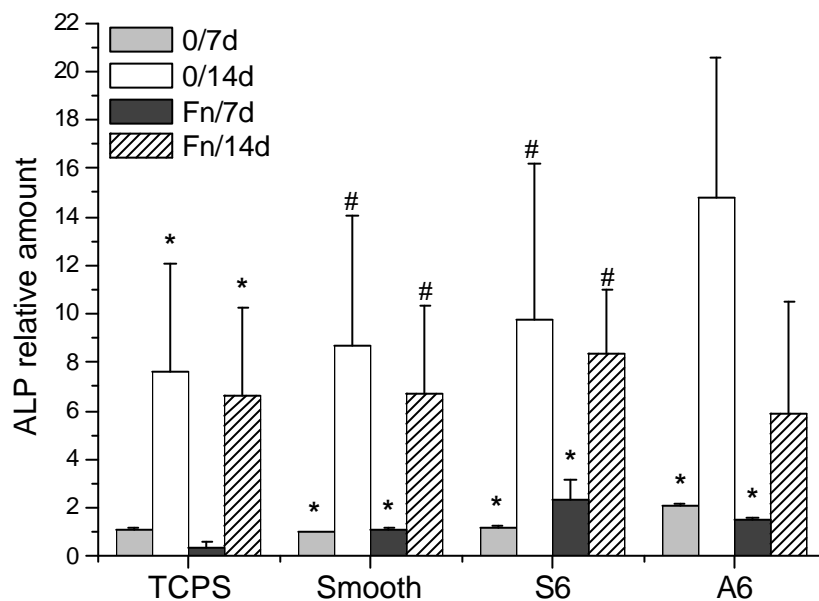
Figure 5-4 ALP gene expression of MG63 osteoblast-like cells on Ti surfaces with (Fn) or without (0) Fn pre-coating by qRT-PCR after 7 and 14days of cell culture. Ratios of target genes relative to housekeeping gene -microglobulin- were expressed as a percentage relative to non-coated smooth surfaces after 7days of cell culture. Bars with same symbols (*,#) indicate that differences are not statistically significant between them when compared in the same group of surface finishing

5.5.2.2. Alkaline phosphatase activity

The ALP results were normalised to the BCA readings. Figure 5-5 shows the results of the ALP/total protein ratio for cells on all smooth and rough Ti series. ALP activity of

cells increased with time on all studied surfaces. Differences were statistically significant when comparing results after 3 days.

Roughness did not influence ALP activity of cells after 14days in culture. On the contrary, the effect of roughness was detected on ALP activity after 21 days of cell culture, which was generally higher than on smooth surfaces (Figure 5-6). This trend was more noticeable for non-coated surfaces compared to the Fn-coated ones.

After 14 days of cell culture, Fn did not have a significant influence on ALP activity, whereas after 21 days in culture cells showed lower levels of ALP activity on Fn pre-coated series compared to on non-coated ones (Figure 5-5).
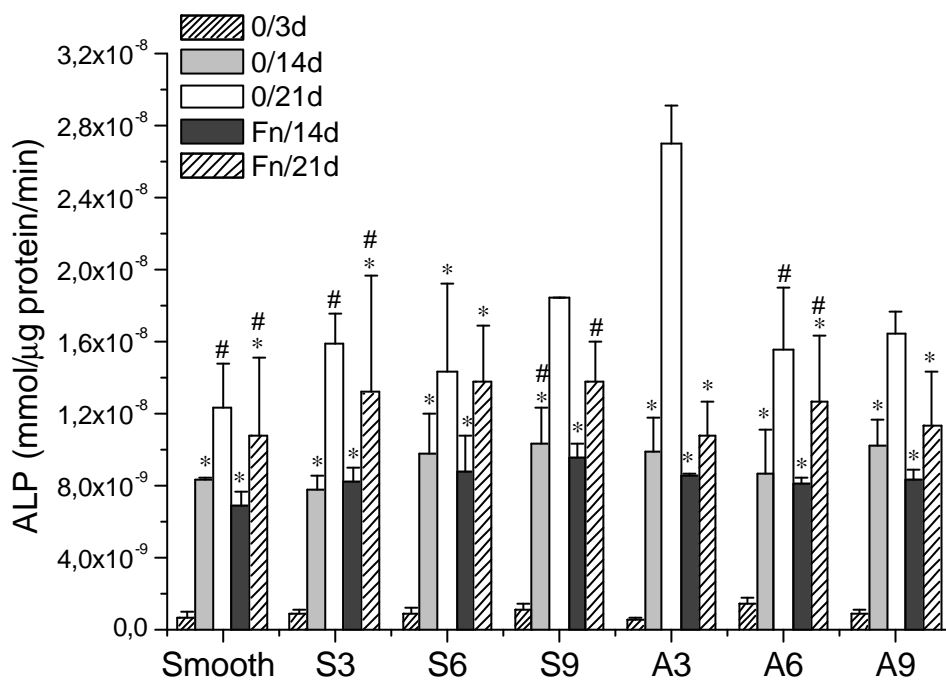
Figure 5-5 *ALP activity of MG63 cells after 3, 14 and 21 days in culture on different rough Ti surfaces, with (Fn) and without (0) Fn pre-coating. Bars with same symbols (*,#) indicate that differences are not statistically significant between them when compared in the same group of surface finishing*
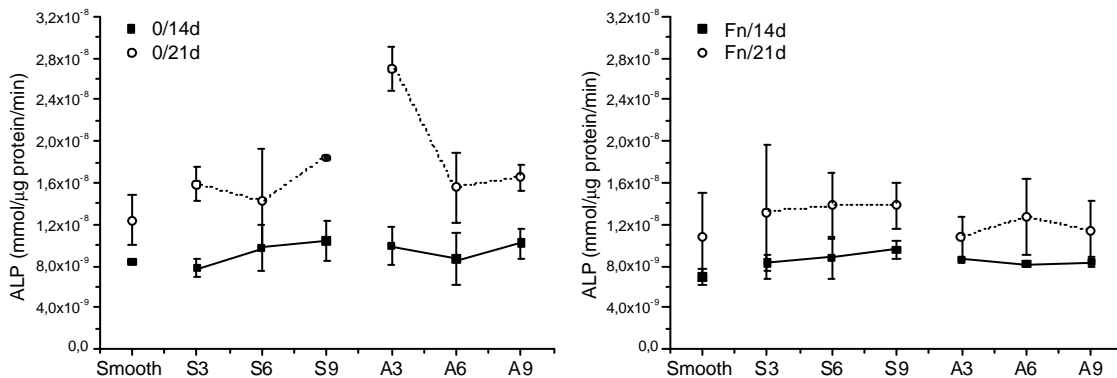
Figure 5-6 *ALP activity of MG63 cells after 14 and 21 days in culture on different rough Ti surfaces. The depicted values are the same depicted in Figure 5-5, but non-coated (left) and Fn-coated (right) series are separated and ALP activity after 3 days non included*

5.5.2.3. Osteocalcin gene expression

MG63 osteoblasts-like cells increased their OC mRNA expression with time for all the studied surfaces (Figure 5-7), but not in the case of those cultured on alumina-blasted non-coated Ti surfaces.

The effects of roughness and Fn-coating on OC mRNA gene expression were unclear. However, blasting particles had a noteworthy influence on it. OC mRNA expression on alumina-blasted surfaces was higher than on SiC-blasted surfaces.
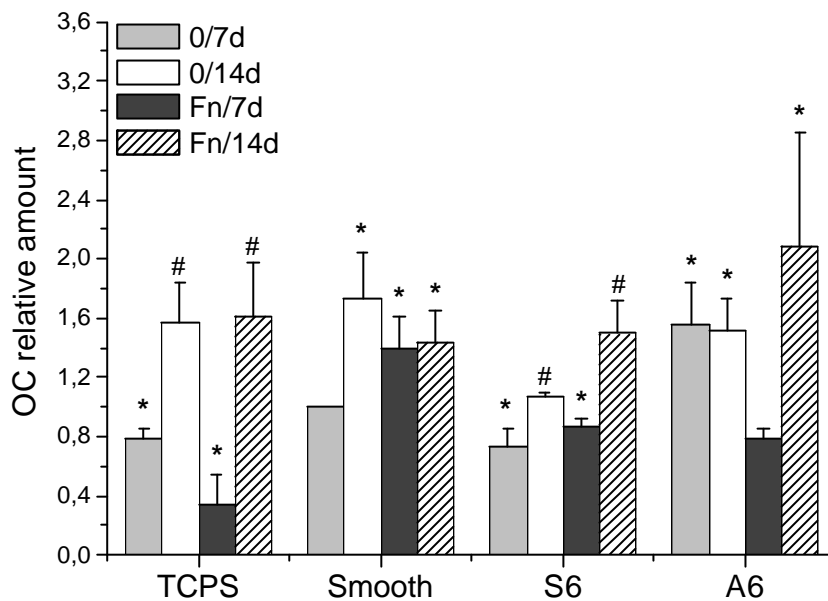
Figure 5-7 *Gene expression of OC of MG63 cells after 7 and 14days in culture on blasted Ti surfaces with (Fn) or without (0) Fn pre-coating by qRT-PCR. Ratios of target genes relative to housekeeping gene - microglobulin- were expressed as a percentage relative to non-coated smooth surfaces after 7days in culture. Bars with same symbols (*,#) indicate that differences are not statistically significant between them when compared in the same group of surface finishing*

5.5.2.4. Osteocalcin production

Figure 5-8 shows the results of OC production of osteoblast-like cells cultured on all the studied surfaces.

Cells on non-coated surfaces showed a decrease of the level of OC production with time (Figure 5-9, left graph). Whereas cells on Fn-coated samples expressed a slightly increase of OC production with time (Figure 5-9, right graph).

Cells on rough surfaces showed a higher OC production compared to those on smooth surfaces. That effect was more pronounced in non-coated samples than in Fn-coated.

Concerning to the chemical composition of the blasting particles used to rough the surfaces, cells on Al_2O_3-blasted surfaces increased OC production compared to on SiC-blasted surfaces after the same time in culture.

No correlation was found between OC production and the nature of the blasting particles for cells on Fn-coated surfaces.

On non-coated series, alumina blasted surfaces induced cells to produce higher levels of OC with increasing roughness. However, cells on SiC-blasted surfaces peaked OC production on S6-surfaces (Figure 5-9, left graph). Interestingly, Fn pre-coating reversed those trends.
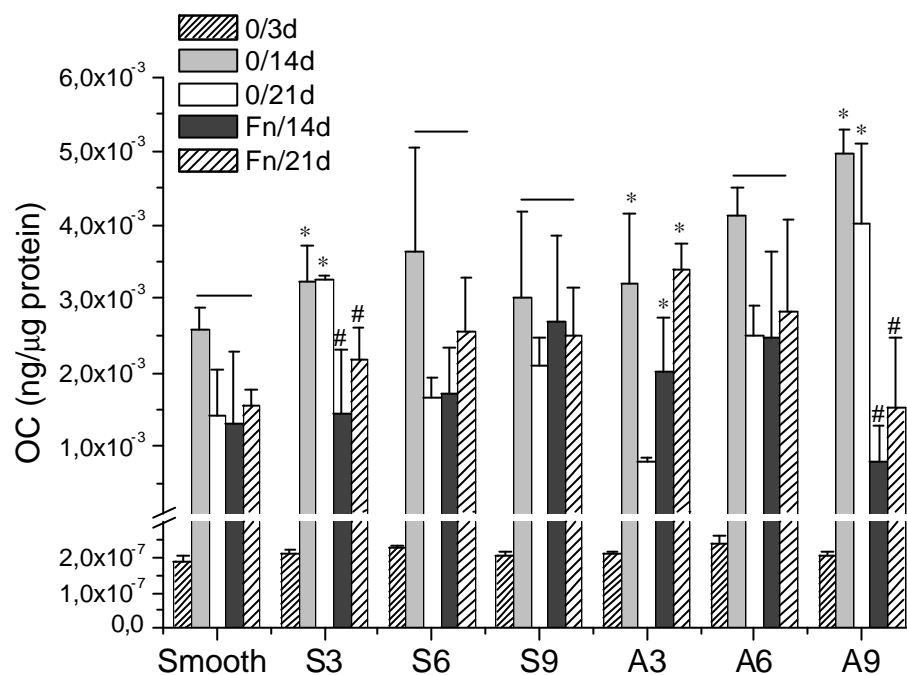
Figure 5-8 *Osteocalcin production of MG63 cells after 3, 14 and 21 days in culture on different rough Ti surfaces, with (Fn) and without (0) Fn pre-coating. . Bars with same symbols (*,#) indicate that differences are not statistically significant between them when compared in the same group of surface finishing*
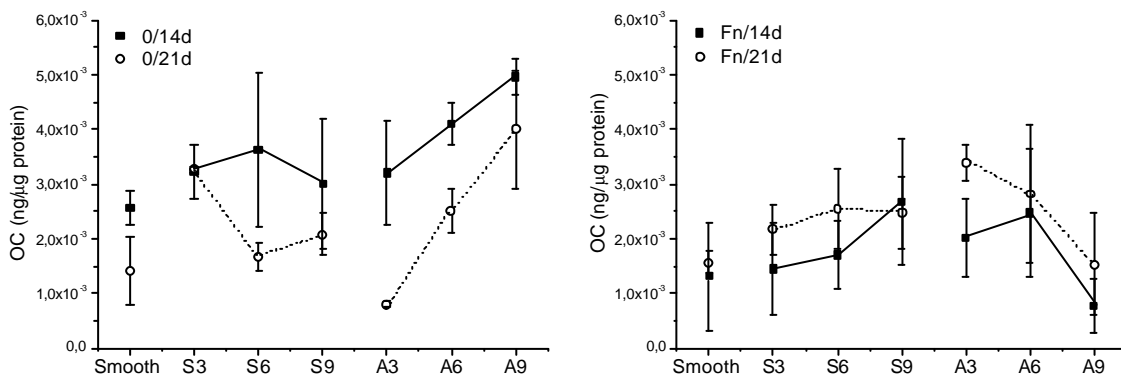

Figure 5-9 *OC production of MG 63 cells after 14 and 21 days in culture on different rough Ti surfaces. The depicted values are the same depicted in Figure 5-8 but non-coated (left) and Fn-coated (right) series are separated and OC production after 3 days non included*

5.6. Discussion

The influence of surface properties and fibronectin coatings on smooth and rough Ti samples on MG63 osteoblasts-like cell adhesion and differentiation has been studied. This will allow gaining knowledge on their possible effect on cell osteogenic processes. α_5 mRNA integrin subunit expression has been investigated since its specificity to fibronectin makes it a good indicator of the quality of cell adhesion for these experiments. Cell differentiation has been studied not only by analysing differentiation markers -alkaline phosphatase activity and osteocalcin production- using traditional techniques, but also by investigating the alkaline phosphatase and osteocalcin mRNA gene expression using the more reliable qRT-PCR technique.

5.6.1. Cell adhesion

α_5 mRNA expression was considered a good indicator of the adhesion response for osteoblastic cells because of the previous knowledge on the selectivity of integrin receptor $\alpha_5\beta_1$ for fibronectin. $\alpha_5\beta_1$ binding to fibronectin has been shown to be necessary for bone-like nodule formation *in vitro* when osteoprogenitor cells are grown on tissue culture plastic and other synthetic biomaterials [29].

The quantitative results of α_5 mRNA gene expression indicated that the values of α_5 mRNA expression increased with time of cell culture, except for cells cultured on smooth Ti surfaces (Figure 5-3). After 30 min in culture, cells on smooth Ti surfaces significantly increased the expression of the gene compared to all the rest of the series. Conversely, after 4h in culture, cells on smooth Ti surfaces showed the lowest values of gene expression, whereas cells on all the rest of the samples maximized the gene expression differences between them. From all those results, it can be concluded that 30min of culture is a short time for cells to develop the appropriate biological mechanisms to adhere onto surfaces, especially on those where they will be eventually better adhered. Based on that, it is not recommended to discriminate effects of the relevant surface treatments on osteoblasts adhesion response at 30min of cell culture.

Osteoblasts interact with the substrate through integrin receptors. The type of substrate determines which integrins and ECM proteins are expressed. After 4h of cell culture, cells on rough blasted Ti surfaces expressed higher levels of α_5 mRNA than on smooth samples (Figure 5-3). Others have reported similar results on MG63 cultured on titanium that increased the expression of integrin subunits α_2, α_3, α_5, β_1, and β_3 on rougher surfaces compared to polished ones [30].

Although cells on SiC-blasted Ti surfaces expressed higher amounts of the α_5 mRNA gene than on Al_2O_3-blasted Ti surfaces, the differences were not statistically significant. Those differences, which are also found after 30 min of cell culture, may be caused by the higher amount of Fn that is absorbed on SiC-blasted surfaces, as determined previously in this work. The higher amount of adsorbed Fn, which is led by the higher surface free energy of the SiC-blasted surfaces, could provide the surface with a higher number of specific binding sites for cells. This, is turn, would resulted in an increased α_5 mRNA gene expression.

Differences detected in α_5 mRNA gene expression of osteoblasts between the different substrates of interest were statistically significant only after 4h of cell culture. This includes one of the most interesting results obtained; that is, cells on Fn-coated Ti surfaces showed lower α_5 mRNA gene expression than on the same type but uncoated surfaces. This happened no matter the type of surface analysed. This is an unexpected result. One could have speculated with an increased expression of the gene on Fn-coated surfaces due to the aforementioned specificity of the $\alpha_5\beta_1$ integrin –and so the associated α_5-expression- to bind to fibronectin.

The α_5 integrin subunit binds to β_1 forming the integrin $\alpha_5\beta_1$, and it is via $\alpha_5\beta_1$ that cells initiate the attachment to fibronectin [29;31]. One reason for cells to express less α_5 mRNA on Fn-coated surfaces could be the fact that cells express other integrins instead to $\alpha_5\beta_1$. The β_1 integrin subunit can bind to different integrins subunits, such as α_1, α_2, α_3, α_4, α_5, α_6, α_7, α_v [32]. Consequently, the presence of Fn pre-coatings on titanium surfaces could induce that cells down-regulated the production of $\alpha_5\beta_1$ integrins because they up-regulated the production of other types of integrins, such as $\alpha_2\beta_1$ or $\alpha_v\beta_3$. The fact that Fn pre-coating could provide the surface with a higher number of specific binding sites for cells to adhere could be the reason for cells to express other integrins. In this respect, cells tend to provide the necessary integrins to perform their biological activities by up- or down-regulating the demanded subunits and integrins.

Those speculations agree with Raz et al. [33] results. They found a higher β_1 integrin subunit expression along with a lower α_5 subunit expression on Ti surfaces with rough microtopographies than on smooth-ones when MG63 cells were cultured up to confluence. So, a preferential $\alpha_2\beta_1$ integrin expression by cells on rough surfaces was assessed. However, it is worth noting that $\alpha_2\beta_1$ is known to be preferentially expressed when cells reach confluence and undergo to osteoblastic differentiation [34], as in the case of Raz et al. work [33]. In fact, Anselme et al. [35] did not find any $\alpha_2\beta_1$ expression when human osteoblasts were cultured on titanium alloy surfaces for 24 h, 7 days or 14 days.

From our data an up-regulation of $\alpha_2\beta_1$ cannot be expected since the tests were performed at shorter adhesion times, when cells are far from reaching confluence. However, one could speculate with the possibility of a down-regulation of α_5 mRNA on

Fn pre-coated surfaces because of an up-regulation of other types of integrins that have been related to cell attachment on fibronectin, such as $\alpha_V\beta_3$ [36].

Knowing that both $\alpha_5\beta_1$ and $\alpha_v\beta_3$ integrins bind to the RGD site of Fn [32;36]; it is important to note that integrin binding specificity -$\alpha_5\beta_1$ vs $\alpha_v\beta_3$- have been related in the literature by the group of A. Garcia to the regulation of osteoblastic differentiation [37] and the enhancement of in vivo bone healing and implant functional osseointegration [38]. In the present study, cells were grown on rough titanium substrates, which also stimulate osteoblastic differentiation compared to smooth surfaces. This suggests that the expression of $\alpha_v\beta_3$ is probably increased by cells on rough Fn pre-coated Ti surfaces because on smooth Ti and plastic surfaces $\alpha_5\beta_1$ was underexpressed. Improved bone tissue formation and functional osseointegration may be attributed to $\alpha_5\beta_1$-specific titanium implants because it increases recruitment of osteoprogenitor cells and differentiation into osteoblasts at the tissue-implant interface. Moreover $\alpha_5\beta_1$ integrin is the central fibronectin receptor, and its expression has been associated with increased mineralization of osteosarcoma and calvarial osteoblast cells [38]. But the adsorption of RGD containing proteins such as fibronectin or vitronectin in a non-specifically way, may support $\alpha_v\beta_3$-mediated adhesion due to the conformation of the adsorbed protein. In fact the group of A. Garcia [38] grafted a specific sequence of fibronectin -9th type repeat- on titanium, which in the correct structural context exhibits high selectivity for the integrin $\alpha_5\beta_1$. They also grafted on Ti a linear RGD oligopeptide (GRGDSPC) demonstrating that primarily supports $\alpha_v\beta_3$-mediated adhesion. Keselowsky [37] and Cheng et al. [39] showed that $\alpha_v\beta_3$ mediated adhesion to surface, suppresses osteoblastic differentiation. This would agree with our results since Fn pre-coated surfaces show a low expression of α_5 mRNA integrin; and cell differentiation with a low expression of ALP mRNA and ALP activity compared to uncoated surfaces. Since $\alpha_V\beta_3$ also binds to osteopontin and bone sialoprotein [1;31], an enhancement of cell adhesion and differentiation on hypothetic osteopontin and/or bone sialoprotein pre-coated Ti surfaces may be predicted. This is an hypothesis that can be confirmed in further studies.

While these results show substrate-dependent differences in integrin subunits expression levels, the influence of surface topography on integrin functions, such as binding activity and downstream biological responses, are still unknown. Therefore, further analyses have been addressed to identify the mediation of α_5 mRNA integrin subunit expression in osteoblast differentiation in relation to surface-dependent differences.

5.6.2. Cell differentiation

In the present study, it has been shown that Fn pre-coating influenced on α_5 mRNA gene expression and so, on cell adhesion. Therefore, it seems reasonable to assume that Fn pre-coating may shift the time course of differentiation. In all types of surfaces tested, the

ALP mRNA expression (Figure 5-4) as well as the ALP activity (Figure 5-5) was lower (some of them with statistically significant differences) on Fn pre-coated samples than on non-coated surfaces after 14 and 21 days of cell culture. None of those differences between Fn-coated and non-coated series were statistically significant for ALP activity after 14 days of cell culture, though. Consequently, the decrease of MG63 α_5 mRNA expression at cell adhesion times may be related to Fn pre-coating influence on the differentiation pathway of the osteoblasts.

As expected, the increase of roughness led to an increase of ALP activity. This response was more significant for non pre-coated surfaces after 21 days of cell culture (Figure 5-4). Same trend was assessed for ALP mRNA levels after 14 days of cell culture (Figure 5-5). After shorter cell culture times, when cell differentiation is in earlier stages, no statistically significant differences were found for ALP mRNA expression (7 days) or ALP activity (14days).

Gene expression occurs at earlier times than the production and activity of the proteins tested as makers for cell differentiation. This fact explains that qRT-PCR assays for ALP mRNA and OC mRNA were performed at shorter periods than the tests for the differentiation markers. The period of cell culture at which differentiation markers should be measured is difficult to assess since many parameters can influence the results obtained, such as the cell line or the cell number seeded.

It is generally established that smooth surfaces promote early differentiation marker, ALP activity, [13;16;28], whereas rougher surfaces promote later steps in maturation of cells, such as mineralization of the ECM [13;16;17;40]. The influence of rough surfaces on ALP activity has been extensively studied. Schwartz et al, [41], concluded that rougher surfaces increased alkaline phosphatase activity and osteocalcin production by cells compared to smooth surfaces. Also reported by Martin et al. [17] where human osteoblast-like MG63 cells and normal human osteoblasts exhibited a more differentiated phenotype when grown on substrates with micro-rough surface. Orsini et al [42] observed in their study that sandblasting and acid-etching can improve cellular adhesion and proliferation of osteoblast-like MG63 cells. It is possible that some of the differences in cellular response to surface roughness may have been due to variations in the degree of cell confluence that was obtained or the studied cell line.

Differences in ALP mRNA expression and ALP activity depending on the nature of the grit-blasting particle have been found in this study. After 14 days, cells on non-coated alumina-blasted surfaces expressed higher levels of ALP mRNA gene than on non-coated SiC-blasted surfaces (Figure 5-4). And after 21 days of cell culture, ALP activity was higher for A3 and A6 compare to S3 and S6 respectively (Figure 5-6 left). The fact that SiC surfaces show a higher Fn adsorption due to its higher SFE compared to Al_2O_3 surfaces (Chapter 4), could involve a higher $\alpha_v\beta_3$ expression and then a lower cell differentiation as explained in the previous section. However, this blasting-particle effect was not shown by cells on Fn pre-coated surfaces (Figure 5-6 right).

Osteocalcin gene has been shown to be differently involved in the process of bone mineralization. OC, which is an osteoblastic-specific protein, has been demonstrated to stimulate bone mineral maturation [43]. In the present study, the expression of OC mRNA gene increased with time of cell culture (Figure 5-7). It is worth to remind that OC mRNA gene expression usually occurs as a previous event to OC production. After that, one could expect an increase of OC production with time. But this sequence of events might not occur since the gene expression of OC by cells is not directly related to the final cell protein synthesis. Different factors such as changes in the dynamic protein layer adsorbed on biomaterials surface, could lead to a change in protein synthesis by cells. In fact, no relevant differences in OC production (Figure 5-8) after 14 and 21 days of cell culture were obtained, but fluctuating results. On non-coated surfaces the OC mRNA gene expression increased with time while OC production was decreased with time. In spite of the fact that OC gene expression increased between 7 and 14 days of incubation, it might occur that after that time a significant downregulation of OC mRNA gene expression occurred, which eventually was detected as a decrease of OC production after the longest cell culture periods.

A possible explanation for those results might be the differences in the protein layer adsorbed on titanium surfaces, which would change the integrin expression. In relation to results for ALP activity, the speculated upregulation of $\alpha_v\beta_3$ expression could also decrease cell differentiation, i.e., decrease OC activity with time.

Cell maturation stage may also explain OC production decrease after 21 days of cell culture. Depending on cell confluence state and cell line, the detection periods of cell differentiation markers can change [44]. Further, the use of total protein concentration to normalize values of cell differentiation markers could not be the most appropriate. Total protein concentration is dependant on the total number of lysed cells. This number may be shielded by the extracellular matrix. Zinger et al. [45] suggested to use number of cells to normalize ALP and OC results. Cell number is obtained by trypsinization of the culture cells and then, the counting of cells is performed with a cytometer. Other methodologies such as Lactate Dehydrogenase, LDH, are not recommended since they also rely on cell lysis.

It has been shown that roughness influences cell adhesion and differentiation. In general, cells cultured on rougher surfaces tend to exhibit attributes of more differentiated osteoblasts with higher OC production, than those cells cultured on smoother surfaces for comparable periods. But Fn pre-coating affected the OC production and OC mRNA expression by cells. In the case os Fn-coated surfaces, both OC gene expression and OC production by cells increased with time during the whole experiment. This indicates that cells on those surfaces are still in a previous stage of maturation than cells on the non Fn-coated surfaces, i.e., they have not reached the mineralization stage yet.

General relationships between ALP and OC were described by Owen et al. [46], in an study of differentiation associated genes, ALP and OC, by mRNA levels expressed by

calvarial-derived osteoblasts. A model of the relationship between proliferation and differentiation was established. One of the main conclusions was that as the cultures progressed into the mineralization stage, cellular levels of alkaline phosphatase declined. Osteocalcin exhibited the opposite pattern of expression. In general, initially, there is a period of active proliferation during which cell growth and related genes are actively expressed. Then, the down-regulation of proliferation leads to a period of matrix maturation. Finally, when the alkaline phosphatase gene is maximally expressed, the extracellular matrix is competent for mineralization. In our study the results show that ALP activity by cells is either still under the maximum values or near this maximum at 21 days of culture. Consequently, OC mRNa expression and the associated OC production was measured when cells are still in an immature stage, at which their values may fluctuate.

5.7. Conclusions

❖ 30min of culture is a short time for cells to develop the appropriate biological mechanisms to adhere onto surfaces, especially on those where they will be eventually better adhered.

❖ The higher amount of adsorbed Fn, which is led by the higher surface free energy of the SiC-blasted surfaces, provide the surface with a higher number of specific binding sites for cells and so, cells on SiC-blasted Ti surfaces expressed higher amounts of the α_5 mRNA gene than on Al_2O_3-blasted Ti surfaces.

❖ Fn-coating on Ti surfaces decreased α_5 mRNA gene expression by cells, probably because other adhesion related integrins are favored against $\alpha_5\beta_1$.

❖ The changes on α_5 mRNA expression induced by the presence on Fn pre-coatings can also influence on the differentiation pathway of the osteoblasts, as Fn pre-coatings on Ti surfaces also decreased cell ALP mRNA expression as well as ALP activity after 14 and 21 days of cell culture.

❖ The increase of roughness as well as the presence of alumina particles on blasted surfaces increased ALP activity and ALP mRNA gene expression by cells at the longest periods of cell culture.

❖ No relevant differences in OC production by cells after 14 and 21 days in culture were found for all tested surfaces.

5.8. Bibliography

[1]   Anselme K. Osteoblast adhesion on biomaterials. Biomaterials 2000; 21: 667-681.

[2]   Puleo DA, Nanci A. Understanding and controlling the bone-implant interface. Biomaterials 1999; 20: 2311-2321.

[3]   Groth T, Altankov G, Klosz K. Adhesion of Human Peripheral-Blood Lymphocytes Is Dependent on Surface Wettability and Protein Preadsorption. Biomaterials 1994; 15: 423-428.

[4]   Degasne I, Basle MF, Demais V, Hure G, Lesourd M, Grolleau B, Mercier L, Chappard D. Effects of roughness, fibronectin and vitronectin on attachment, spreading, and proliferation of human osteoblast-like cells (Saos-2) on titanium surfaces. Calcified Tissue International 1999; 64: 499-507.

[5]   Lebaron RG, Athanasiou KA. Extracellular matrix cell adhesion peptides: Functional applications in orthopedic materials. Tissue Engineering 2000; 6: 85-103.

[6]   Faucheux N, Tzoneva R, Nagel MD, Groth T. The dependence of fibrillar adhesions in human fibroblasts on substratum chemistry. Biomaterials 2006; 27: 234-245.

[7]   Garcia AJ. Get a grip: integrins in cell-biomaterial interactions. Biomaterials 2005; 26: 7525-7529.

[8]   Keselowsky BG, Collard DM, Garcia AJ. Surface chemistry modulates focal adhesion composition and signaling through changes in integrin binding. Biomaterials 2004; 25: 5947-5954.

[9]   Gronthos S, Stewart K, Graves SE, Hay S, Simmons PJ. Integrin expression and function on human osteoblast-like cells. Journal of Bone and Mineral Research 1997; 12: 1189-1197.

[10]   Sousa SR, Moradas-Ferreira P, Saramago B, Melo LV, Barbosa MA. Human serum albumin adsorption on TiO2 from single protein solutions and from plasma. Langmuir 2004; 20: 9745-9754.

[11]   Aparicio C, Gil FJ, Thams U, Munoz F, Padros A, Planell JA. Osseointegration of grit-blasted and bioactive titanium implants: Histomorphometry in minipigs. Key engineering materials 2004; 254-2: 737-740.

[12]   Lincks J, Boyan BD, Blanchard CR, Lohmann CH, Liu Y, Cochran DL, Dean DD, Schwartz Z. Response of MG63 osteoblast-like cells to titanium and titanium alloy is dependent on surface roughness and composition. Biomaterials 1998; 19: 2219-2232.

[13]   Groessnerschreiber B, Tuan RS. Enhanced Extracellular-Matrix Production and Mineralization by Osteoblasts Cultured on Titanium Surfaces Invitro. Journal of Cell Science 1992; 101: 209-&.

[14]   ter Brugge PJ, Torensma R, De Ruijter JE, Figdor CG, Jansen JA. Modulation of integrin expression on rat bone marrow cells by substrates with different surface characteristics. Tissue Engineering 2002; 8: 615-626.

[15]   Kieswetter K, Schwartz Z, Hummert TW, Cochran DL, Simpson J, Dean DD, Boyan BD. Surface roughness modulates the local production of growth factors and cytokines by osteoblast-like MG-63 cells. Journal of Biomedical Materials Research 1996; 32: 55-63.

[16]   Aparicio C. Tratamientos de superficie sobre titanio comercialmente puro para la mejora de la osteointegración de los implantes dentales. Universitat Politècnica de Catalunya; 2005. Thesis.

[17] Martin JY, Schwartz Z, Hummert TW, Schraub DM, Simpson J, Lankford J, Dean DD, Cochran DL, Boyan BD. Effect of Titanium Surface-Roughness on Proliferation, Differentiation, and Protein-Synthesis of Human Osteoblast-Like Cells (Mg63). Journal of Biomedical Materials Research 1995; 29: 389-401.

[18] Siebers MC, ter Brugge PJ, Walboomers XF, Jansen JA. Integrins as linker proteins between osteoblasts and bone replacing materials. A critical review. Biomaterials 2005; 26: 137-146.

[19] Keselowsky BG, Garcia AJ. Quantitative methods for analysis of integrin binding and focal adhesion formation on biomaterial surfaces. Biomaterials 2005; 26: 413-418.

[20] Sousa SR, Moradas-Ferreira P, Barbosa MA. TiO2 type influences fibronectin adsorption. Journal of Materials Science-Materials in Medicine 2005; 16: 1173-1178.

[21] Aparicio C, Gil FJ, Fonseca C, Barbosa M, Planell JA. Corrosion behaviour of commercially pure titanium grit blasted with different materials and sizes of grit particles for dental implant applications. Biomaterials 2003; 24: 263-273.

[22] Pegueroles M, Aparicio C, Planell JA, Gil FJ. Surface-energy properties of different shot-blasted and sterilized titanium surfaces. 19th European Conference of Biomaterials (ESB2005) 2005; T98.

[23] Cowles EA, Derome ME, Pastizzo G, Brailey LL, Gronowicz GA. Mineralization and the expression of matrix proteins during in vivo bone development. Calcified Tissue International 1998; 62: 74-82.

[24] Stephansson SN, Byers BA, Garcia AJ. Enhanced expression of the osteoblastic phenotype on substrates that modulate fibronectin conformation and integrin receptor binding. Biomaterials 2002; 23: 2527-2534.

[25] Sodek J, Cheifetz S. Molecular regulation of osteogenesis. In: Davies JE (ed.), Bone Engineering. 2000: 31-44.

[26] Kartsogiannis V, Ng KW. Cell lines and primary cell cultures in the study of bone cell biology. Molecular and cellular endocrinology 2004; 228: 79-102.

[27] Bachle M, Kohal RJ. A systematic review of the influence of different titanium surfaces on proliferation, differentiation and protein synthesis of osteoblast-like MG63 cells. Clinical Oral Implants Research 2004; 15: 683-692.

[28] Zhao G, Raines AL, Wieland M, Shwartz Z, Boyan BD. Requirement for both micron- and submicron scale structure for synergistic responses of osteoblasts to substrate surface energy and topography. Biomaterials 2007; 28: 2821-2829.

[29] Keselowsky BG, Wang L, Schwartz Z, Garcia AJ, Boyan BD. Integrin α5 controls osteoblastic proliferation and differentiation responses to titanium substrates presenting different roughness characteristics in a roughness independent manner. Journal of Biomedical Materials Research Part A 2007; 80: 700-710.

[30] Lange R, Luthen F, Beck U, Rychly J, Baumann A, Nebe B. Cell-extracellular matrix interaction and physico-chemical characteristics of titanium surfaces depend on the roughness of the material. Biomolecular Engineering 2002; 19: 255-261.

[31] Luthen F, Lange R, Becker P, Rychly J, Beck U, Nebe JGB. The influence of surface roughness of titanium on beta 1-and beta 3-integrin adhesion and the organization of fibronectin in human osteoblastic cells. Biomaterials 2005; 26: 2423-2440.

[32] Hynes RO. Integrins - Versatility, Modulation, and Signaling in Cell-Adhesion. Cell 1992; 69: 11-25.

[33] Raz P, Lohmann CH, Turner J, Wang L, Poythress N, Blanchard C, Boyan BD. 1α,25(OH)2D3 Regulation of integrin expression is substrate dependent. Journal of Biomedical Materials Research Part A 2004; 71: 217-225.

[34] Jikko A, Harris SE, Chen D, Mendrick DL, Damsky CH. Collagen integrin receptors regulate early osteoblast differentiation induced by BMP-2. Journal of Bone and Mineral Research 1999; 14: 1075-1083.

[35] Anselme K, Bigerelle M, Noel B, Dufresne E, Judas D, Iost A, Hardouin P. Qualitative and quantitative study of human osteoblast adhesion on materials with various surface roughnesses. Journal of Biomedical Materials Research 2000; 49: 155-166.

[36] Garcia AJ, Vega MD, Boettiger D. Modulation of cell proliferation and differentiation through substrate-dependent changes in fibronectin conformation. Mollecular Biology of the Cell 1999; 10: 798.

[37] Keselowsky BG, Collard DM, Garcia AJ. Integrin binding specificity regulates biomaterial surface chemistry effects on cell differentiation. Proceedings of the National Academy of Sciences 2005; 102: 5953-5957.

[38] Petrie TA, Raynor JE, Reyes CD, Burns KL, Collard DM, Garcia AJ. The effect of integrin-specific bioactive coatings on tissue healing and implant osseointegration. Biomaterials 2008; 29: 2849-2857.

[39] Cheng SL, Lai CF, Fausto A, Chellaiah M, Feng X, Mchugh KP, Teitelbaum SL, Civitelli R, Hruska KA, Ross FP, Avioli LV. Regulation of alpha v beta 3 and alpha v beta 5 integrins by dexamethasone in normal human osteoblastic cells. Journal of Cellular Biochemistry 2000; 77: 265-276.

[40] Boyan BD, Lossdorfer S, Wang L, Zhao G, Lohmann CH, Cochran DL, Schwartz Z. Osteoblasts generate an osteogenic microenvironment when grown on surfaces with rough microtopographies. European cells and materials 2003; 6: 22-27.

[41] Schwartz Z, Lohmann CH, Oefinger J, Bonewald LF, Dean DD, Boyan BD. Implant surface characteristics modulate differentiation behavior of cells in the osteoblstic lineage. Advances Dental Research 1999; 13: 38-48.

[42] Orsini G, Assenza B, Scarano A, Piatelli M, Piatelli A. Surface analysis of machined versus sandblasted and acid-etched titanium implants. International journal of oral and maxillofacial implants 2000; 15: 779-784.

[43] Boskey AL, Gadaleta S, Gundberg C, Doty SB, Ducy P, Karsenty G. Fourier transform infrared microspectroscopic analysis of bones of osteocalcin-deficient mice provides insight into the function of osteocalcin. Bone 1998; 23: 187-196.

[44] Ku CH, Piolettli DP, Browne M, Gregson PJ. Effect of different Ti-6Al-4V surface treatments on osteoblasts behaviour. Biomaterials 2002; 23: 1447-1454.

[45] Zinger O, Zhao G, Schwartz Z, Simpson J, Wieland M, Landolt D, Boyan BD. Differential regulation of osteoblasts by substrate microstructural features. Biomaterials 2005; 26: 1837-1847.

[46] Owen TA, Aronow M, Shalhoub V, Barone LM, Wilming L, Tassinari MS, Kennedy MB, Pockwinse S, Lian JB, Stein GS. Progressive Development of the Rat Osteoblast Phenotype Invitro - Reciprocal Relationships in Expression of Genes Associated with Osteoblast Proliferation and Differentiation During Formation of the Bone Extracellular-Matrix. Journal of Cellular Physiology 1990; 143: 420-430.

6. Conclusions

The research developed in this PhD dissertation was designed to increase knowledge on the interactions taking place at the bio/non-bio interface between different biological components –water, proteins, cells- and a material of clinical relevance, i.e. rough titanium.

Biomaterials with well-determined and long track of clinical success do not provide with ideal substrates for isolating and studying one surface property from the others. Thus the intertwined effects of the different properties of the synthetic surfaces appear as a challenge to unravel the ultimate causes that determine the fate of cells on synthetic biomaterials.

Additionally, there are many parameters involved in cell processes; such as, protein adsorption, integrin expression, cell adhesion, proliferation and differentiation, which make of specific difficulty the understanding of the overall biological response.

Nevertheless, the results displayed and analysed in the previous chapters, which are summarized and highlighted in the following conclusions, expanded our comprehension

of the field that could lead to a more rationalized modification and design of biomaterials and implants for bone repair and regeneration.

❖ On the chemical composition of the grit-blasting particles

Chemical composition of the grit-blasting particles was the main factor influencing on wettability and surface free energy (SFE) of titanium blasted rough surfaces. Grit-blasting with SiC-particles provided with a higher SFE and wettability to commercially pure Ti (c.p. Ti) surfaces than grit-blasting with Al_2O_3-particles. Different blasted-rough surfaces showed similar electrokinetic curves and isoelectric points, which indicate that the remaining blasting particles on the titanium surfaces did not significantly alter their electrical charge. The adsorption of fibronectin (Fn) and bovine serum albumin (BSA) on blasted micro-rough surfaces was positively correlated with the SFE and wettability of the blasted-rough titanium surfaces. The higher amount of adsorbed Fn, which was led by the higher SFE of the SiC-blasted surfaces, provided the surface with a higher number of specific binding sites for cells and so, cells on SiC-blasted Ti surfaces expressed higher amounts of α_5 mRNA gene than on Al_2O_3-blasted Ti surfaces. The presence on alumina particles on blasted surfaces increased ALP activity and ALP mRNA gene expression by cells after 14 and 21 days of cell culture

❖ On the roughness of grit-blasted titanium surfaces

Grit-blasting increases roughness of Ti surface samples to the micro-level. Differences in the final surface roughness were found depending on the particle size and, also, the particle nature. The bigger the particles used, the rougher the Ti surface and the higher its real surface area. The effect of roughness on wettability depends on the dimensions of the topographical features, i.e. if evaluating nanorough or microrough surfaces. The later induced an increase in hydrophobicity of titanium surfaces. No correlation was found between the size of the grit particles, i.e. the surface roughness, and the adsorbed BSA or Fn per surface area. The adsorption of fibronectin from solution on shot-blasted rough titanium surfaces results in an irregular pattern of adsorption with a higher amount of protein adsorbed on peaks than on valleys of the topography. This behaviour influenced the osteoblast-like cells deposition of Fn- fibrils. The Fn-fibrils were deposited in a specific facet-like pattern that was organized within the secreted total matrix, which appeared as a film overlying the top of the different rough titanium surfaces. The thickness of this layer increased with the roughness of the underlying topography, but most interestingly no more than half of the total maximum peak-to-alley distance was covered. The blasted-rough surfaces induced cell to increase ALP activity and ALP mRNA gene expression after 14 and 21 days of culture.

❖   On the fibronectin pre-coatings

Ti surfaces pre-coated with fibronectin decreased α_5 mRNA gene expression by cells, probably because the formation of other adhesion-related integrins was favoured against $\alpha_5\beta_1$. The changes on α_5 mRNA expression induced by the presence on Fn pre-coatings could also influence on the differentiation pathway of the osteoblasts, as Fn pre-coatings on Ti surfaces also decreased cell ALP mRNA expression as well as ALP activity after 14 and 21 days of cell culture.

❖   On protein adsorption on TiO_2 surfaces

Fn in the adlayer did not change its structure once adsorbed on TiO_2 surfaces, whereas Fbg presented two different structures/conformations during the time of analysis. The second step of adsorption was characterized by a significant increase in the rigidity of the adlayer. BSA adsorbed on TiO_2-crystals showed three different structures/conformations. Most probably, a relevant amount of water was trapped in the adlayer that contributed to a significant decrease in its rigidity during the time of analysis. When proteins were in competition during adsorption, and BSA was introduced the second in the system, BSA displaced larger proteins, such as Fn and Fb. This was a consequence of a) BSA's high affinity for TiO_2 surfaces, b) BSA lower molecular weight than Fn and Fbg, and/or c) BSA higher concentration in solution. On the contrary, when BSA was introduced before other proteins, bigger Fn or Fbg proteins adsorbed forming a layer on the top of the BSA layer. Consequently, the Brash and Lyman effect is more prevalent in these systems than the Vroman effect since a lower molecular weight and more concentrated protein in solution adsorbed preferentially to the TiO_2 surfaces.

CURRICULUM VITAE

George Altankov, M.D., Ph.D, Dr.Sci.
ICREA Research Professor
george.altankov@icrea.es

NIE/Passport   X6441288-T / 160924617

PROFESSIONAL EXPERIENCE
(Employment and Visiting Appointments)

2006 – at present
ICREA Research Professor at Institute for Bioengineering of Catalunia
Research Activities:
Conduct research line: "Molecular dynamics at cell-materials interface". Head of research group.

2005 – 2006
Visiting Professor in UPC/Laboratory of Nanobioengineering at Scientific Park of Barcelona

2004 – 2006
Professor in Cell Biology, Institute of Biophysics Bulgarian Academy of Sciences
Head of Department "Cell Adhesion"

2002-2003
Sabbatical GKSS Research Center, Institute of Chemistry, Teltow, Germany
(12 months Marie Curie Senior)

1991 - 1993
Visiting Scientist, Southwestern Medical Center, Dallas, Texas; Department of Cell Biology and Neuroscience (funded by the host)

1985 - 1991
Research Associate, Bulgarian Academy of Sciences Central Laboratory of Biophysics, Sofia

EDUCATION

1968 – 1974 Medical Doctor (M.D.)
Higher Medical Institute, Varna, Bulgaria
MD degree awarded - 09/74.

1979 -1981 Residency on " Human Physiology"
Higher Medical Institute, Varna, Bulgaria, Department of Physiology
Acknowledged Specialty in "Human Physiology" - 06/81.

1984   PhD degree
Higher Medical Institute, Varna, Bulgaria - PhD
Thesis: "Physiological aspects of lectin-induced lymphocyte adhesion to glass - effect of some biologically active substances".
Degree awarded at the Supreme Attestation Committee Sofia - 09/1984.

2003 DrSci (Habilitation) degree
Thesis: "Cellular interaction with material surfaces–dynamics, organization and signaling of integrin receptors in response to the material surface properties and the formation of extarecllular matrix"
Degree awarded at the Supreme Attestation Committee Sofia - 09/2004

INTERNATIONAL GRANTS

2005-2007 Project with the National Research Council of Bulgaria Nanotechnology Programme "Cellular interaction with nano-scale materials (non-woven nanofiber textile HT4 03-04 (Principal investigator: Prof. G. Altankov)

2006-2007 Project funded by the National Innovation Fund at Bulgarian Ministry of Industry "Development of micro and nano technologies for production of implantable devices with hard matter and polymer coatings (cooperative project involving USMA-EOOD, Sofia, Institute of Hard Matter and the Institute of Biophysics, Bulgarian Academy of Sciences. (Principal investigator for IBF: Prof. G. Altankov).

2007-2009 Research project "Materiales biofuncionalizados para la regeneración tisular" MAT2006-11516 Ministerio de Educación y Ciencia (participant)

Reviewer: J Biomater Sci Polym Edn, Biomaterials, J Biomed Mater Res, Membranes, Acta Biomaterialia

LIST OF PUBLICATIONS
(published in English from a total of 87 original papers)

1. Gugutkov D, Cristina Gonzalez-Garcia, Jose Carlos Rodriguez Hernandez, George Altanko and Manuel Salmeron-Sanchez, Biological Activity of the Substrate-Induced Fibronectin Network: Insight into the Third Dimension through Electrospun Fibers, Langmuir, 2009 (Erub ahead of print).
2. Gugutkov D, Altankov G, José Carlos Rodríguez Hernández, Manuel Monleón Pradas, Manuel Salmerón Sánchez (2009) Fibronectin activity on substrates with controlled –OH density, J Biomed Mater Res Part A Feb.2 (Erub ahead of print).
3. Kostadinova A, Seifert B, Albrecht W, Malsch G, Groth Th, Lemdlein A, Altankov G (2009) Novel polymer blends for the preparation of membranes for biohybrid organs. J Biomat Sci Polym Edn 20(5-6): p. 821-39.Impact Factor: 1.607
4. Kristin Kirchhof, Kamelia Hristova, Natalia Krasteva, George Altankov, Thomas Groth (2009) Multilayer coatings on biomaterials for control of MG-63 osteoblast adhesion and growth, Journal of Materials Science: Materials in Medicine **20**, 897-907
5. Gustavsson J, Altankov G, Errachid A, Samitier J, Planell J, Engel E (2008) Surface Modifications of Silicon Nitride Based ISFETs for Cellular Biosensor, J Mater Sci: Mater Med **19** (4) 1839-1850.

Patents:

6. Jankova K, <u>Altankov G</u>, Ulbricht M, Gunnar J and V. Thom, Biocompatible material with novel functionality, European Patent Application WO 0215955, 28/02/2002
7. <u>Altankov G</u>, Dimoudis N. "Autodegradable microcarriers and their use" European Patent Application PCT/EP98/06715, 21/10/1998.
8. Serdev N, <u>Altankov G</u>, Brodvarova I, Tomov N "Method for coverage of wounds with epithelial cells" BG Patent No 51904/1993.
9. Altankov G. Method for preparation of protein-coated gelatine microspheres, BG patent (INRA) No 83394/18/03/1988
10. Altankov G, Popdimitrov I, Camera for cell electrophoresis, BG Patent (INRA) No 4349/05/05/1979.

Melba Navarro Toro

Birthday: February 10th 1975, Caracas, Venezuela **Nationality:** Spanish, **Professional address**: Institute for Bioengineering of Catalonia (IBEC), C/Baldiri Reixac 13, 08028 Barcelona, Spain **Phone:** +34 662349923 **e-mail**: melba.navarro@gmail.com; mnavarro@ibec.pcb.ub.es

.

A. ACADEMIC TRAINING

- May 2009- at present Institute for Bioengineering of Catalonia (IBEC).

- May 2008- May 2009 University of Liverpool, UK Institute for Tissue Engineering (UKBioTEC). Supervisor: Dr. John Hunt

- April 2007- May 2008 Institute for Bioengineering of Catalonia (IBEC). Supervisor: Prof. Josep A. Planell

- March 2006-April 2007 Post-doctoral period at the MTP group, and MESA+ Institute at the University of Twente. Supervisor: Prof. Julius Vancso.

- **July 2005**- **Ph.D.** Programme: Materials Science and Metallurgical Engineering at U.P.C. (Technical University of Catalonia) Title: *"Desarrollo y caracterización de materiales biodegradables para regeneración ósea"* (**Development and Characterization of biodegradable materials for bone regeneration**). Supervisor: Dr. Maria Pau Ginebra

- **March 1998**- Diploma of **Chemical Engineer.** Title issued by the *Universidad Simón Bolívar,USB*. (Simón Bolívar University), Caracas (Venezuela).

E. PUBLICATIONS

Book chapters

- *The Challenges of Bone Repair,* JA Planell, M. Navarro in Bone Repair Biomaterials; ISBN-13: 978-1-84569-385-5 Woodhead Publishing, In Press

- *Materials Surface Effects on Biological Interactions,* M.Navarro, JA Planell, G.Altankov, C. Aparicio, E.Engel, J.Gil, MP Ginebra, D. Lacroix in NATO Science Series, Nanoengineering Systems for Regenerative Medicine, Springer, In Press

- *Developing targeted biocomposites in tissue engineering and regenerative medicine*, JA Planell, M. Navarro in Biomedical Composites; L.Ambrosio, ed. Woodhead Publishing, In Press

- *Stimuli Responsive Polymer Brushes* E. Benetti, M.Navarro, S. Zapotoczny, J.Vancso. In Surface Design: Applications in Bioscience and Nanotechnology; R.Förch, H.Schönherr, A.T.Jenkins, ed. ISBN: 978-3-527-40789-7. Wiley, 2008.

- *The Challenge of Combining Cells, Synthetic Materials and Growth Factors to Engineer Bone Tissue.* M.Navarro, A.Michiardi. In Tissue Engineering: Roles, Materials and Applications; S. J. Barnes and L. P. Harris, ed. ISBN: 978-1-60456-293-4. Novapublishers, 2008

- *Materials in Dental Implantology.* E. Fernández, F.J. Gil, C.Aparicio, M. Nilsson, S. Sarda, D. Rodríguez, M.P. Ginebra, J.M. Manero, M. Navarro, J. Casals, J.A. Planell. In Dental Biomechanics; A. Natali, ed. ISBN 0-41-5306663, Taylor and Francis, London, 2003.

-

International Journals (extract from 19 international journals)

- E.Sanzana, <u>M.Navarro</u>, F.Macule, S.Suso, J.A.Planell, M.P.GInebra **"Comparison of the in vivo behaviour of calcium phosphate cements and glasses as bone substitutes"** *Acta Biomaterialia*, 4:1924-1933 (2008)

- <u>M.Navarro</u>, A.Michiardi, O.Castaño, J.A.Planell **"Biomaterials in orthopaedics"** *Interface* 5(27):1137-1158 (2008)

- <u>M.Navarro</u>, E.M.Benetti, S. Zapotoczny, J.A.Planell, J. Vancso **"Buried, covalently attached RGD peptide motifs in poly(methacrylic acid) brush layers: The effect of brush structure on cell adhesion"** *Langmuir,* 24 (19):10996-11002 (2008)

- M.Charles-Harris, <u>M.Navarro</u>, M.Koch, E.Engel, D.Lacroix, JA. Planell **"A PLA/Calcium Phosphate degradable composite material for bone tissue engineering: an in vitro study"** *J.Mater.Sci.Mat.Med.* 19(4): 1503-1513 (2008)

- <u>M. Navarro</u>, E. Engel, J.A. Planell, I.Amaral, M. Barbosa, M.P. Ginebra **"Biological response and surface characterization of a PLA/CaP glass biodegradable composite material"** *J. Biomed. Mater. Res.,* 85A (2): 477-486 (2008)

- E.Engel, A.Michiardi, <u>M.Navarro</u>, D.Lacroix, J.A.Planell **"Nanotechnology in regenerative medicine: The materials side"** *Trends in Biotechnology,* 26 (1): 39-47 (2007)

- E.S. Sanzana, M.P. Ginebra, P.A.Torres, J.A.Planell, <u>M.E. Navarro</u> **"Experimental study of the bone substitution with ceramic biomaterials formulated as bone cements | [Estudio Hฬฝฝฝฬฝฬฝฝ ฬฝฝฝ Rฝฝฝฝฝฝฝฝฝฝฝฝฝฝฝฝฝฝฝฝฝฝฝฝฝฝฝฝฝฝฝฝฝฝฝ]** *"Archivos de Medicina Veterinaria* 39 (2): 129-134 (2007)

Conference Proceedings and Books of Abstracts (extract from 17 conference proceedings

-<u>M.Navarro</u>, E.Benetti, S.Zapotoczny, J.A.Planell, G.J.Vancso World Biomaterials Congress, **"Chemically structured bio-interfaces for controlling cell/biomaterial interactions"** Amsterdam, The Netherlands, May 2008

-<u>M.Navarro</u>, E.Benetti, S.Zapotoczny, J.A.Planell, G.J.Vancso ESF-EMBO Conference on Biological Surfaces and Interfaces, Sant Feliu de Guixols, Spain, July 2007

F. REVIEWER

- Biomaterials
- Journal of Materials Science: Materials in Medicine
- Journal or Biomedical Materials Research

G. FELLOWSHIPS

- **Ramón y Cajal post-doctoral fellowship**
- **Marie Curie Intra-European individual post-doctoral fellowship meant to perform a post-doctoral stay** awarded by the European Commission. May 2008-May 2009
- **NANO-Post-doctoral fellowship meant to perform a post-doctoral stay** awarded by the Catalan Government. March 2006-March 2007
- **Post-graduate fellowship meant to follow Ph. D. studies** awarded by the Catalan Government. February 2001-December 2004.
- **Summer fellowship at the Universidad Complutense de Madrid** meant to take part in the Bioceramics for Health course.
- **Summer fellowship at the Menéndez Pelayo International University** meant to take part in the Nanobiomaterials course.

CURRICULUM VITAE

PEDRO LOPES GRANJA

Born on March 11, 1970, in Porto, Portugal.

CONTACT

NEWTherapies Group
Biomaterials Division
INEB - Instituto de Engenharia Biomédica, University of Porto
Rua do Campo Alegre, 823, 4150-180 Porto, Portugal
Phone: + 351 226074900 / 86 (direct); Fax: + 351 226094567
E-mail: pgranja@ineb.up.pt
Homepage: www.pedrogranja.net

ACADEMIC QUALIFICATIONS

? PhD in Engineering Sciences. Faculty of Engineering of the University of Porto (FEUP), January 2001.

? Metallurgical Engineer. FEUP, September 1993.

PRESENT POSITIONS

? Principal Investigator at the Associate Laboratory IBMC-INEB (Institute for Molecular and Cell Biology-Institute for Biomedical Engineering; Instituto de Biologia Molecular e Celular-Instituto de Engenharia Biomédica), University of Porto, since December 2008.

? Elected member of the Council of the European Society for Biomaterials (ESB), since 2007, and Treasurer, since September 2008.

? Web Editor of the European Society for Biomaterials (ESB), since 2006.

? Auxiliary Invited Professor at FEUP, since 2005.

? Editor-in-Chief of the Biomaterials Network (Biomat.net), since 1998.

HONORS AND AWARDS

? 2006 Jean Leray Award, European Society for Biomaterials.

CO-AUTHORSHIP OF AWARDED WORKS

? Prize for best oral presentation (Maritie Grellier). Cell cooperation between osteoprogenitor and endothelial cells: Its function on bone tissue engineering. ECM VIII Bone Tissue Engineering. Davos, Switzerland: June 25-28, 2007.

? Special Oral presentation Award (Isabel F. Amaral). In vitro mineralisation of chitosan membranes carrying phosphate functionalities. 16th International Symposium on Ceramics in Medicine - Bioceramics 16. Porto: November 6-9, 2003.

ACADEMIC AND PROFESSIONAL EXPERIENCE

? 2008-2009: Principal Investigator (INEB).

? 2006-2007: Deputy Coordinator of the Biointerfaces Group.

? 2002-2008: Auxiliary Investigator (IBMC-INEB).

? 2004 (Jan/Jul): Visiting Assistant Research Scientist at Professor David Mooney's Lab (Dept. Biologic and Materials Sciences, School of Dentistry, University of Michigan, USA).

? 2002: Research training period (2 weeks) at Centro di Studio per la Chimica dei Plasmi, University of Bari (Bari, Italy) and Institute of Composite and Biomedical Materials, University of Naples (Naples, Italy).

? 2001-2002: Assistant Researcher at INEB, working on the DISC Project (Deputy Coordinator of INEB's team and member of the Steering Committee).

? 1998-2000: Post doctoral researcher at INEB, working on the CARE Project.

? 1994-2001: Researcher at INEB, working for a PhD degree, supervised by Professor Mário A. Barbosa (President of INEB) and co-supervised by Professors Charles Baquey (INSERM U.443, Institut National de la Santé et de la Recherche Médicale, Biomaterials and Tissue Repair Unit, Faculty of Medicine, University Bordeaux 2) and Bernard De Jéso (Institut du Pin, Dept. Vegetal Substances Chemistry, Faculty of Sciences, University Bordeaux 1), both Research Directors.

? 1999: Founding member of the Young Scientists Forum (YSF), integrated in the 15th

PARTICIPATION IN SCIENTIFIC PROJECTS
AS PROJECT LEADER

Pedro L. Granja ? *7/7*

? Bridging Biomaterial Research Excellence between Industry and Academia across Europe (BRIDGE). Coordinator: Hakan Engkvist (Univ. Uppsala, Sweden). Funded by the EC (Dec 2007-Nov 2009; 1919 k€ total; 200 k€ for INEB). Principal Investigator at INEB.

? Targeting nanoprobes for early detection of invasive cancer cells using Hereditary Diffuse Gastric Cancer as a model (NANOPROBE). Funded by FCT (Sep 2007-Sep 2010; 168 k€).

? Design of new gene delivery vectors based on dendrimers, alginate and the RGD sequence for bone tissue engineering (DENDRALGENE). Coordinator: Helena Tomás (Univ. Madeira). Funded by FCT (Sep 2007-Sep 2010; 175 k€). Principal Investigator at INEB.

? Bone regeneration by stimulation of angiogenesis (ANGIO). Funded by FCT (Mar 2005-Mar 2008; 95148 €).

? Microencapsulation systems for cotransplantation. Funded by Luso-American Foundation (FLAD) (Jan 2004-Dec 2004)

Resumen del curriculum – MANUEL TOLEDANO PEREZ

1. Licenciado en Medicina y Cirugía. Facultad de Medicina de Granada. 1982.

2. Médico Especialista en Estomatología. Escuela de Estomatología de la Facultad de Medicina de Granada. 1989.

3. Doctor en Medicina y Cirugía. Universidad de Granada. 1988.

4. Profesor Titular de Estomatología. Facultad de Odontología de la Universidad de Granada. 1991.

5. Catedrático de Estomatología. Facultad de Odontología de la Universidad de Granada. 2009.

6. Profesor del Master Ingeniería Tisular de la Universidad de Granada.

7. Profesor del Programa de Doctorado Investigación en Estomatología de la Universidad de Granada.

8. Profesor del Programa de Doctorado Erasmus-Mundus sobre Biomateriales en colaboración con la Universidad de Siena.

9. Autor 4 libros y 11 Capítulos de libro sobre Biomaterilaes en Odontología.

10. Director de 26 Tesis Doctorales.

11. Investigador Responsable de Proyectos de investigación obtenidos en convocatorias Nacionales Competitivas.

12. Director del Grupo de Investigación consolidado de la Junta de Andalucía: CTS-242: Biomateriales en Odontología.

13. Autor de 105 artículos científicos publicados en revistas incluídas en ISI y listadas en JCR.

14. Obtención de dos tramos de investigación por parte de la Comisión Nacional Evaluadora de la Actividad Investigadora.

15. Obtención de 15 Premios y Menciones de calidad de mi actividad investigadora.

16. Miembro del Comité Editorial: a) Revistas referidas en el *SCI*:

> *Journal of Dentistry.*
> *American Journal of Dentistry.*
> Medicina Oral Patología Oral Cirugía Bucal.
> *Journal of Applied Oral Science.*

    b) No referidas en el *SCI*:
Revista del Ilustre Consejo General de Colegios de Odontólogos y Estomatólogos de España (RCOE).
International Journal of Brazilian Dentistry.
Italian Journal of Operative Dentistry.
Internacional Dentistry of South Africa.
The Open Biomedical Engineering Journal.
The Indian Journal of Maxillofacial and Oral Surgery.
Journal of Dental Hygiene Science.

17.	Revisor científico de las siguientes revistas:

a) Revistas referidas en el *SCI*:

American Journal of Dentistry.
Journal of Biomedical Material Research.
Journal of Dentistry.
European Journal of Oral Sciences.
The Angle Orthodontist.
Journal of Oral Rehabilitation.
Boletín de la Sociedad Española de Cerámica y Vidrio.
Journal of Materials Science: Materials in Medicine.
Journal of Dental Research.
Dental Materials.
Journal of Applied Oral Science.
Operative Dentistry.
Journal of Adhesive Dentistry.
Medicina Oral Patología Oral Cirugía Bucal.

b) Revistas no referidas en el *SCI*:

International Dentistry of South Africa.
Acta Biomaterialia.
International Journal of Dental Hygiene.
Open Biomedical Engineering Reviews.
International Journal of Pediatric Dentistry.
Clinical Oral Investigations.
Indian Journal of Dental Research.
Journal of Nanoscience and Nanotechnology.
18.

Curriculum Vitae

Civility

Name : Boudeville
First name : Philippe
Born : 22-02-1947 in Saint Malo, France
Nationality: French, Maried, 2 children
Address : 9 rue des Peupliers 34830 Clapiers, France

Position

Professor (first class) in Physical and Inorganic Chemistry
Research Laboratory: « Institut des Biomolécules Max Mousseron » UMR CNRS 5247,
department: « Centre de Recherche sur le Biopolymères Artificiels »
Faculty of Pharmacy of Montpellier
University Montpellier I
15 Avenue Charles Flahault, BP 14491, 34093 Montpellier cedex 5
tel: 33+(0)4 67 54 80 78 fax: 33+(0)4 67 54 80 82
Web : www.crba.univ-montp1.fr

Diplomas
.

- Doctorat 3ème cycle Chimie option électrochimie, Université Rennes 1, 1972
- Doctorat d'état ès Sciences Physiques, Université Rennes 1, 1986
- Doctorat en Pharmacie, Université Rennes 1, 1991
- Agrégation de Pharmacie, Paris 1995
- Institut d'Administration des Entreprises, Université Rennes 1, 1971
- Diplôme d'Etude Scientifique Spécialisé d'Informatique, langages et systèmes, Université Rennes 1, 1982.

Research fields

1) Development of strontium-calcium phosphate cements (SCPC) and composites SCPS/biodegradable polymers for endodontic and orthopaedic applications.
2) Dry mechanosynthesis of pure and substituted calcium phosphates of biological interest
3) Physicochemistry in clinical preformulation (polymorphism of drug substances, drug-excipient interactions, drug/polymer solid dispersions).